Mechanisms underlying neuronal dysfunction in a mouse model of Alzheimer's disease

Dissertation

zur Erlangung des Grades eines

Doktors der Naturwissenschaften

der Mathematisch-Naturwissenschaftlichen Fakultät

und

der Medizinischen Fakultät

der Eberhard-Karls-Universität Tübingen

vorgelegt

von

Chommanad Lerdkrai

aus Bangkok, Thailand

März - 2016

Tag der münglichen Prüfung:……19.07.2016……..

Dekan der Math.-Nat. Fakultät: Prof. Dr. W. Rosenstiel

Dekan der Medizinischen Fakultät: Prof. Dr. I. B. Autenrieth

1. Berichterstatter: Prof.Dr. Olga Garaschuk

2. Berichterstatter: Prof.Dr. Robert Feil

Prüfungskommission: Prof.Dr. Thomas Euler

Prof.Dr. Philipp Kahle

Erklärung / Declaration:

Ich erkläre, dass ich die zur Promotion eingereichte Arbeit mit dem Titel:

„*Mechanisms underlying neuronal dysfunction in a mouse model of Alzheimer's disease*“

selbständig verfasst, nur die angegebenen Quellen und Hilfsmittel benutzt und wörtlich oder inhaltlich übernommene Stellen als solche gekennzeichnet habe. Ich versichere an Eides statt, dass diese Angaben wahr sind und dass ich nichts verschwiegen habe. Mir ist bekannt, dass die falsche Abgabe einer Versicherung an Eides statt mit Freiheitsstrafe bis zu drei Jahren oder mit Geldstrafe bestraft wird.

I hereby declare that I have produced the work entitled "Mechanisms underlying neuronal dysfunction in a mouse model of Alzheimer's disease", submitted for the award of a doctorate, on my own (without external help), have used only the sources and aids indicated and have marked passages included from other works, whether verbatim or in content, as such. I swear upon oath that these statements are true and that I have not concealed anything. I am aware that making a false declaration under oath is punishable by a term of imprisonment of up to three years or by a fine.

Tübingen, den 22.03.2016 Chemmanad Lerdkrai

Datum / Date Unterschrift/Signature

Abstract

Alzheimer's disease (AD) is a progressive and fatal neurodegenerative disorder that slowly destroys neurons and cognitive abilities. Familial AD is linked to mutations in a specific set of genes, most often in the genes encoding amyloid precursor protein (APP) and the presenilins 1 and 2 (PS1, PS2). Several studies have demonstrated that the missense mutations in PS genes perturb endoplasmic reticulum (ER) Ca^{2+} homeostasis. *In vitro*, such perturbations result in an increase in Ca^{2+} levels within the ER Ca^{2+} stores and in a reduction of the capacitative Ca^{2+} entry. However, little is known about the contribution of intracellular Ca^{2+} stores to network-driven neuronal activity *in vivo* and their role for AD-related neuronal dysfunction.

We studied *in vivo* functional properties of intracellular Ca^{2+} stores in cortical neurons by using two-photon Ca^{2+} imaging in 10-14-month-old transgenic APP_{swe}/PS1 G384A (AD), PS1 G384A (PS45), and age-matched wild type (WT) mice. We monitored spontaneous neuronal activity of layer 2/3 neurons in the frontal cortex and classified cells as silent, normal or hyperactive based on the frequency of their Ca^{2+} transients [Busche et al., 2008]. Compared with young adult animals, we observed a robust increase in the fraction of hyperactive cells in aged mice from all three strains, indicating an aging-mediated increase in neuronal hyperactivity. We next investigated Ca^{2+} release from intracellular Ca^{2+} stores in the intact AD and WT brain using an agonist of ryanodine receptors (RyRs) caffeine. We discovered exacerbated caffeine-induced Ca^{2+} signals in AD compared to WT mice as suggested by a prolonged decay phase of caffeine-induced Ca^{2+} transients and an increase in unitary caffeine-evoked responses. Additionally, we found that N-methyl-D-aspartate receptor (NMDAR)-mediated Ca^{2+} entry further triggers Ca^{2+} release from intracellular Ca^{2+} stores in AD mice. Interestingly, these responses are most pronounced in hyperactive cells, indicating a stronger overfilling of intracellular Ca^{2+} stores in hyperactive relative to silent and normal cells.

To decipher the contribution of Ca^{2+} release from intracellular Ca^{2+} stores to network-driven spontaneous Ca^{2+} transients, the stores were emptied by a reversible inhibitor of SERCA pumps cyclopiazonic acid (CPA). Topical CPA application normalizes pathological activity patterns by reducing neuronal hyperactivity in AD but not in WT mice. We further investigated the sole effect of PS1 G384A mutation on neuronal network activity and revealed for the first time that PS1 G384A mutation alone is sufficient to mediate neuronal hyperactivity in PS45 mice. Such perturbation occurs independently of mutant gene dosage, plaques formation, and inflammation. Furthermore, this phenomenon is already present in young adult animals (6-7 months old). Interestingly, store depletion reduces hyperactivity in PS45 mice similar to AD mice, indicating that the pathological activity patterns in both mouse strains are related to the dysfunctional of intracellular Ca^{2+} stores. We further investigated the response of presynaptic Ca^{2+} signals in PS45 mice to a depletion of intracellular Ca^{2+} stores. By imaging axonal boutons originating from layer 5/6 neurons, we found that emptying of intracellular Ca^{2+} stores affects the frequency but not the pattern of spontaneous Ca^{2+} transients in axonal boutons. Next, we tested the contribution of presynaptic glutamate release on postsynaptic spontaneous neuronal activity using the activity-dependent irreversible NMDAR blocker MK-801. Results obtained in PS45 mice showed that hyperactive cells exhibit higher open probability of postsynaptic NMDA receptors compared to normal cells, which is likely caused by increased presynaptic glutamate release. When testing the role of intracellular Ca^{2+} stores for postsynaptic dendritic Ca^{2+} signals in PS45 mice, we found that the stores are involved in controlling the frequency and synchronization of spontaneous dendritic Ca^{2+} transients in different dendritic branches.

Taken together, our data demonstrate that aging aggravates neuronal hyperactivity. Additionally, *in vivo* function of ryanodine-sensitive intracellular Ca^{2+} stores is altered in amyloid depositing mice as suggested by exaggerated caffeine-induced Ca^{2+} signals. Furthermore,

intracellular Ca^{2+} stores are critically involved in controlling the network-driven spontaneous Ca^{2+} transients in AD mice. This involvement has both pre- and postsynaptic components and is caused by the presence of mutated presenilin 1 protein. Our findings pave the way for the development of new therapeutic strategies for AD patients based on normalizing Ca^{2+} release from the intracellular Ca^{2+} stores.

Zusammenfassung

Morbus Alzheimer (*Alzheimer's disease* = *AD*) ist eine fortschreitende neurodegenerative Erkrankung, welche zu einer langsamen Degeneration von Neuronen und einem Verlust kognitiver Fähigkeiten führt. Die familiäre Form der Erkrankung lässt sich auf vor allem auf Mutationen in den Genen für das Amyloid Vorläufer Protein (*amyloid precursor protein* = *APP*) oder Präsenilin 1 bzw. Präsenilin 2 (PS1, PS2) zurückführen. Verschiedene Studien zeigen, dass Mutationen in PS1 bzw. PS2 zu Störungen der intrazellulären Ca^{2+}-Homöostase führen, welche vorrangig das Endoplasmatische Retikulum (ER) betreffen. *In vitro* resultieren diese beispielsweise in einem Anstieg der Ca^{2+}-Beladung des ER und einer Reduktion des kapazitiven Ca^{2+}-Einstroms über die Plasmamembran. Auf welche Art und Weise intrazelluläre Ca^{2+}-Speicher die neuronale Netzwerkaktivität *in vivo* beeinflussen und welche Rolle sie für AD-assoziierte neuronale Fehlfunktionen spielen ist bisher unklar.

In dieser Arbeit untersuchten wir die funktionellen Eigenschaften intrazellulärer Ca^{2+}-Speicher in kortikalen Neuronen mittels *in vivo* Zwei-Photonen-Mikroskopie in 10-14 Monate alten transgenen APP_{swe}/PS1 G384A (AD), PS1 G384A (PS45) und gleichaltrigen Wildtyp (WT) Mäusen. Zunächst ermittelten wir die spontane Aktivität von Schicht 2/3 Neuronen im frontalen Kortex und klassifizierten die einzelnen Zellen entsprechend der Häufigkeit ihrer Ca^{2+}-Transienten als ruhig, normal oder hyperaktiv [Busche et al., 2008]. Bestimmt man die Anteile dieser

drei Kategorien innerhalb der Zellpopulation, lässt sich im Vergleich zu jüngeren adulten Tieren ein deutlicher Anstieg des Anteils hyperaktiver Neuronen nachweisen. Dieser altersvermittelte Anstieg neuronaler Aktivität war in allen drei untersuchten Mausstämmen zu beobachten. Anschließend untersuchten wir die Koffein-evozierte Ca^{2+}-Freisetzung aus neuronalen intrazellulären Ca^{2+}-Speichern im intakten Gehirn von WT und AD Mäusen nach Stimulation von Ryanodinrezeptoren (RyR). Die speichervermittelten Ca^{2+}-Signale in AD Mäusen waren im Vergleich zu denen in WT Tieren verstärkt. Darüber hinaus zeigten diese Versuche, dass der N-methyl-D-aspartat Rezeptor (NMDAR)-vermittelte Ca^{2+}-Einstrom über die Plasmamembran *in vivo* eine Ca^{2+}-induzierte Ca^{2+}-Freisetzung aus den intrazellulären Ca^{2+}-Speichern hervorruft. Interessanterweise war dieser Effekt in hyperaktiven Neuronen stärker als in normalen Neuronen, was auf eine stärkere Beladung der intrazellulären Ca^{2+}-Speicher dieser Zellen schließen lässt.

Um die Bedeutung der intrazellulären Ca^{2+}-Speicher für die spontane Netzwerkaktivität von kortikalen Neuronen zu charakterisieren, wurden die Speicher durch eine reversible Blockade der SERCA Pumpe mittels Cyclopiazonsäure (CPA) entleert. Badapplikation von CPA normalisierte die pathologische Netzwerkaktivität selektiv in AD Mäusen, ohne die Aktivität in WT Mäusen zu verändern. Um herauszufinden, ob eine Mutation des PS-Gens ausreichend ist, um die erhöhte Netzwerkaktivität auszulösen, untersuchten wir auch Mäuse, welche lediglich die mutierte Variante des PS1 (G384A) exprimieren. Diese Versuche zeigten, dass das Vorhandensein dieser PS1-Mutation ausreicht, um eine neuronale Hyperaktivität auszulösen. Dieser Effekt ist unabhängig von der Gendosis, Amyloidablagerungen und Entzündungsprozessen. Außerdem lässt sich das Phänomen bereits in jungen adulten Tieren (6-7 Monate) nachweisen. Interessanterweise reduzierte eine Entleerung der intrazellulären Ca^{2+}-Speicher die neuronale Hyperaktivität in PS45 Mäusen in der gleichen Weise wie in AD Mäusen. Daraus lässt sich schlussfolgern, dass die beobachteten pathologischen Aktivitätsmuster in transgenen Mäusen auf funktionelle Veränderungen intrazellulärer

Ca^{2+}-Speicher zurückzuführen sind. Als nächstes untersuchten wir die präsynaptische Ca^{2+}-Signalgebung während einer Entleerung intrazellulärer Ca^{2+}-Speicher in PS45 Mäusen. Hierzu wurden Neuronen der kortikalen Schichten 5 und 6 mit einem Ca^{2+}-Sensor markiert und deren Axonterminalen in oberflächlichen kortikalen Schichten untersucht. Unsere Ergebnisse zeigen, dass intrazelluläre Ca^{2+}-Speicher die Frequenz spontaner Ca^{2+}-Transienten in Axonterminalen modulieren, jedoch keinen Einfluss auf das Muster der Ca^{2+}-Transienten ausüben. Außerdem untersuchten wir den Einfluss der präsynaptischen Glutamatfreisetzung auf die postsynaptische Aktivität unter Verwendung des aktivitätsabhängigen irreversiblen NMDAR Inhibitors MK-801 in PS45 Mäusen. Hyperaktive Zellen wiesen im Vergleich zu normalen Zellen eine höhere Offenwahrscheinlichkeit postsynaptischer NDMA Rezeptoren auf, was sich vermutlich auf eine gesteigerte präsynaptische Glutamatfreisetzung zurückführen lässt. Anschließend untersuchten wir die Rolle der intrazellulären Ca^{2+}-Speicher für die Ca^{2+}-Signalgebung in postsynaptischen Dornfortsätzen in PS45 Mäusen. Die Ergebnisse lassen darauf schließen, dass intrazelluläre Ca^{2+}-Speicher in diesem Kompartiment sowohl die Frequenz als auch die Synchronisation spontaner Ca^{2+}-Transienten kontrollieren.

Die vorliegende Arbeit zeigt, dass fortschreitendes Alter eine Steigerung der neuronalen Hyperaktivität hervorruft. In Mäusen mit Amyloidablagerungen ist außerdem die *in vivo* Funktion intrazellulärer Ca^{2+}-Speicher verändert, wie die Steigerung Koffein-vermittelter somatischer Ca^{2+}-Signale beweist. Intrazelluläre Ca^{2+}-Speicher kontrollieren die Frequenz netzwerkgetriebener spontaner Ca^{2+}-Transienten in AD und PS45 Mäusen. Unsere Ergebnisse legen den Grundstein für die Entwicklung neuer Behandlungskonzepte für AD-Patienten basierend auf einer Normalisierung der Ca^{2+}-Freisetzung aus intrazellulären Ca^{2+}-Speichern.

Acknowledgements

Foremost, I would like to express my sincere gratitude to my supervisor, Professor Dr. Olga Garaschuk, for the continuous support of my doctoral study and research, for her patience, motivation, and immense knowledge. Her guidance helped me in all the time of research and writing of this thesis. I must also acknowledge Dr. Bianca Brawek who patiently corrected my writing and provided valuable suggestions at all levels of the research project. I would like to thank the other members of my committee, Professor Dr. Christian Harteneck and Professor Dr. Robert Feil for the assistance they offered for this project. In addition, a very special thanks goes to all staff members of “Physiology II Team”, without their supports and persistent helps this thesis would not have been possible. I am most grateful to DAAD for financial support during my doctoral study in Germany. Finally, I dedicate this thesis to my parents, my elder brother, and sister who have given me the opportunity of an education from the best institutions and support throughout my life. They were always encouraging me with their best wishes and stood by me through the good times and bad times.

Table of contents

List of Figures

List of tables

Acronyms

AAV	adeno-associated virus
AD	Alzheimer's disease
Aβ	amyloid-β
AF	Alexa Fluor
AM	acetoxymethyl
aMCI	amnestic mild cognitive impairment
AMPA	α-amino-3-hydroxy-5-methyl-4-isoxazolepropionic acid
AP	anterior-posterior
APP	amyloid precursor protein
AUC	area under the curve
β-CTF	β-C-terminal fragment
Ca^{2+}	calcium
$[Ca^{2+}]_i$	intracellular calcium level
CaM	calmodulin
CICR	Ca^{2+}-induced Ca^{2+} release
CPA	cyclopiazonic acid
DAG	diacyglycerol
DAPI	4',6-diamidino-2-phenylindole
DMSO	dimethyl sulfoxide

EEG	electroencephalographic
ER	endoplasmic reticulum
FAD	familial Alzheimer's disease
FDA	Food and Drug Administration
fMRI	functional magnetic resonance imaging
$\Delta F/F$	relative change in fluoresence
GFAP	glial fibrillary acidic protein
GRP	glucose related protein
Iba1	ionized calcium binding adaptor molecular 1
IL-1β	interleukin-1beta
IL-6	interleukin-6
IP	intraperitoneal
IP_3R	inositol 1,4,5-trisphosphate receptor
IQR	interquartile range
KI	knock-in
LTD	long-term depression
LTP	long-term potentiation
MAOS	membrane-associated oxidative stress
MCBL	multi-cell bolus loading
ML	medio-lateral
NA	numerical aperture

Na^+	Sodium
NCX	Na^+/Ca^{2+} exchanger
NFTs	neurofibrillary tangles
NMDA	N-methyl-D-aspartic acid
OGB-1	Oregon Green BAPTA-1
PBS	phosphate buffer saline
PDI	protein disulfide isomerase
PIP_2	phosphatidylinositol-4,5 bisphosphate
PLC	phospholipase C
PM	plasma membrane
PMCA	plasma membrane Ca^{2+}- ATPase
PS1	presenilin 1
PS2	presenilin 2
ROI	region of interest
RyR	ryanodine receptor
SAD	sporadic Alzheimer's disease
SERCA	sarco-/endoplasmic reticulum calcium ATPase
SOCE	store-operated Ca^{2+} entry
STIM	stromal interaction molecule
Swe	Swedish
Syn	synapsin

TNF-α	tumor necrosis factor alpha
UPR	unfolded protein response
VGCC	voltage-gated Ca^{2+} channels

Chapter 1

Introduction

1.1 Alzheimer's disease

Alzheimer's disease (AD) is an age-related neurodegenerative disorder representing a major public health problem. AD can be classified into two categories: the sporadic and the familial form of the disease. Sporadic AD (SAD) is the most common form. Its prevalence increases with advancing age from 1% at 65-70 years to 30% after the age of 85. It is characterized by moderate to extreme severity and a late age of onset [Mayeux R, 2003; Mayeux and Stern, 2012]. Familial AD (FAD) represents some 5-10% of all AD cases. FAD is linked to mutations in a specific set of genes, most often in the genes encoding amyloid precursor protein (APP) and the presenilins 1 and 2 (PS1 and PS2, respectively) [Tabaton and Tamagno, 2007; Bertram and Tanzi, 2008]. APP is a receptor-like type I glycoprotein, with a single membrane-spanning domain, a large extracellular N-terminus, and a shorter C-terminus [Selkoe, 2004]. PSs are polytopic membrane proteins that harbor the catalytic site of the γ-secretase complex, which mediates the intramembranous cleavage of many type I membrane proteins, including APP and Notch [De Strooper et al., 2012; Ho and Shen, 2011]. In addition to PS, nicastrin, anterior pharynx defective 1, and presenilin enhancer 2 are required for the activity of the γ-secretase complex [Takasugi et al., 2003].

The histological hallmarks of SAD and FAD are the presence of extracellular deposits termed senile plaques and intracellular neurofibrillary tangles (NFTs) [Brion, 1998]. The major component of senile plaques is β-amyloid (Aβ) protein, which is produced by amyloidogenic processing of APP involving two sequential cleavage steps by the β- and γ- secretase. β- secretase cleavage of APP generates the secreted derivative, sAPP-β, and β-C-terminal fragment (β-CTF). The latter is subsequently cleaved by γ- secretase, yielding Aβ40 and Aβ42. Alternative cleavage of APP by α- secretase generates sAPP-α and α-CTF, precluding Aβ formation. Aβ40 and Aβ42 are the most common forms of Aβ, where the Aβ42 peptide is more prone to aggregate and to form soluble dimers, oligomers, protofibrills and eventually insoluble plaques [Tabaton and Tamagno, 2007; Ballard et al., 2011]. Recent studies indicate that Aβ is one of the main vicious

species in AD. It was implicated in production of reactive oxygen species, induction and release of proinflammatory cytokines, induction of endoplasmic reticulum stress, and an abnormal increase of the intracellular calcium level ($[Ca^{2+}]_i$) [Berridge, 2010; Hermes et al., 2010; Kuchibhotla et al., 2008]. Another histopathological feature of AD is the deposition of NFTs within neurons. NFTs consist of intracellular fibrillar aggregates of hyperphosphorylated forms of the microbule-associated protein tau. Under physiological conditions, normal tau protein interacts with tubulin and promotes its assembly into microtubules. Binding of tau protein to the microtubules is maintained by the phosphorylation of tau [Goedert et al., 2006; Kolarova et al., 2012]. In AD, tau exhibits an abnormal hyperphosphorylation and dissociates from microtubules. Abnormal tau redistributes from the axonal compartment to somatodendritic compartments and aggregates in the form of NFTs [Kolarova et al., 2012; Wang and Mandelkow, 2016].

1.2 Control of neuronal Ca^{2+} homeostasis

Ca^{2+} is an essential intracellular second messenger in mammalian neurons that contributes to several mechanisms, for example the modulation of membrane excitability, gene expression, metabolism, exocytosis, neurotransmission, reactive oxygen/nitrogen species formation, and apoptosis/necrosis [Supnet and Bezprozvanny, 2010; Grienberger and Konnerth, 2012]. Ca^{2+} homeostasis is attained by functional coupling between multiple Ca^{2+} channels, exchangers, and protein buffers. At the resting state, cytosolic Ca^{2+} levels are maintained between 30-100 nM and they rise transiently after activation. Activation of neurons is associated with Ca^{2+} influx through the plasma membrane (PM) and/or release from the intracellular stores, mostly the endoplasmic reticulum (ER). The Ca^{2+}- permeable channels localized in the neuronal PM can be divided into voltage-gated Ca^{2+} channels (VGCC), ligand-gated Ca^{2+} channels, e.g. N-methyl-D-aspartate (NMDA) receptors and store-operated Ca^{2+} entry (SOCE) channels [Hermes et al., 2010; Grienberger and Konnerth, 2012] (Figure 1).

Ca^{2+} can also be released from the intracellular stores of ER via two kinds of channels localized in the ER membrane, namely inositol trisphosphate receptor (IP_3R) and ryanodine receptor (RyR). The IP_3R is activated by the intracellular production of inositol 1,4,5-trisphosphate (IP_3), which is produced following activation of metabotropic receptors coupled to phospholipase C (PLC). PLC hydrolyzes a membrane phospholipid, phosphatidylinositol 4,5-bisphosphate (PIP_2), to produce the intracellular messengers diacylglycerol (DAG) and IP_3. The interaction between IP_3 and IP_3R causes a rapid efflux of Ca^{2+} from the ER and an increase of free Ca^{2+} in the cytosol [Berridge et al., 2003; Phillis and O'Regen, 2004; Mak and Foskett, 2015]. RyR is activated by the elevation of cytosolic Ca^{2+}, a process referred to as Ca^{2+}-induced Ca^{2+} release (CICR), which contributes, for example, to the amplification of the Ca^{2+} signals caused by activation of IP_3R or by a transmembrane Ca^{2+} entry [Berridge, 1998; Sandler and Barbara, 1999]. In the resting neurons the level of Ca^{2+} in the ER is approximately 1000 times higher than in the cytosol [Bojarski et al., 2008]. Such a tremendous concentration gradient is built up by the sarcoplasmic / endoplasmic Ca^{2+}-ATPase (SERCA) pump localized within the ER membrane. SERCA pump transports Ca^{2+} against its electrochemical gradient from the cytosol to the ER lumen via ATPase hydrolysis [Stutzmann and Mattson, 2011]. Additionally, the filling state of ER is modulated by SOCE (store-operated Ca^{2+} entry), a process activated upon depletion of the ER stores. The known proteins involved in this process are sensors of Ca^{2+} levels in the ER, including stromal interaction molecule 1 and 2 (STIM1 and STIM2, respectively) [Roos et al., 2005, Liou et al., 2005], and the Ca^{2+} channel-forming protein Orai in the PM [Feske et al., 2006; Zhang et al., 2006]. Upon depletion of ER Ca^{2+} stores, STIMs are activated and translocated by diffusion into ER-PM junctions, where they interact with the PM and activate Orai1 Ca^{2+} entry channels which lead to re-filling of the intracellular Ca^{2+} stores [Liou et al., 2007].

In addition, Ca^{2+} is pumped out of the cell by a plasma membrane Ca^{2+}-ATPase (PMCA) and a Na^+/Ca^{2+} exchanger (NCX). PMCA utilizes energy from ATP hydrolysis to transfer Ca^{2+} from the cytosol into the extracellular space [Strehler et al., 2007]. The main regulator of PMCA function is Ca^{2+}-calmodulin (Ca^{2+}-CaM). PMCA has an extended C-

terminal tail which forms an autoinhibitory domain. Binding of Ca^{2+}-CaM to this tail relieves the inhibition, providing a mechanism for regulation of PMCA activity by the cytosolic Ca^{2+} concentration [Zaidi et al., 2015]. NCX is a bi-directional membrane ion transporter. Using the energy of the Na^+ gradient this transporter produces an electrogenic exchange of three Na^+ for one Ca^{2+}. Under normal physiological conditions, Na^+ is transported into the cell and Ca^{2+} is extruded from the cytoplasm (termed Ca^{2+} exit mode) [Annunziato et al, 2004; Shenoda, 2015]. Furthermore, Ca^{2+} binding proteins such as parvalbumin, calbindin-D28k, or calretinin, determine the dynamics of free Ca^{2+} inside neurons [Ghosh and Greenberg, 1995; Berridge et al., 2003; Schwaller, 2010].

Mitochondria also play an important role in regulating neuronal Ca^{2+} signaling by utilizing potent mitochondrial Ca^{2+} uptake mechanisms. The primary transporter mechanism for cytosolic Ca^{2+} across the outer mitochondrial membrane is opening of voltage-dependent anion channels [Rizzuto et al., 2012]. Mitochondria accumulate Ca^{2+} in the matrix via an electrogenic mitochondrial Ca^{2+} uniporter which acts to equilibrate Ca^{2+} according the electrochemical gradient generated by the respiratory chain. The extrusion of Ca^{2+} from the mitochondrial matrix to the cytosol is mediated by mitochondrial Na^+/Ca^{2+} exchanger and H^+/Ca^{2+} exchanger [Celsi et al., 2009; Giorgi et al., 2012; Grienberger and Konnerth, 2012]. Ca^{2+} uptake into mitochondria plays an important role in neuronal physiology by stimulating mitochondrial metabolism and increasing mitochondrial energy production [Bezprozvanny and Mattson, 2008].

1.3 ER in neurons

The ER is an extensive network of interconnected membrane tubuli spread throughout the cytosol. The general structure of the ER can be divided into three domains: i) the nuclear envelope, ii) the ribosome-bound rough ER, iii) the ribosome-free smooth ER [Ramirez and Couve, 2011]. At the ultrastructural level, the neuronal ER consists of complex cisternae, flattened sheets, and tubules which resemble that of other eukaryotic cells. The neuronal ER extends from the soma to the entire

dendritic arbor, some dendritic spines, and axons. The major component of ER in the soma and proximal dendritic compartment is rough ER, while the ER distributed in distal dendrites and axons comprise mostly smooth ER [Verkhratsky and Peterson, 2002; Ramirez and Couve, 2011]. Within the soma and the proximal dendritic region, portions of ER come into close contact with the plasma membrane to form subsurface cisternae which play an important role in regulating neuronal excitability. The axonal ER network extend into the synapse where it is often closely associated with mitochondria [Berridge et al., 1998].

The ER contributes to multiple functions, including the synthesis of lipid and sterol, the regulation of intracellular Ca^{2+} dynamics, and the synthesis and post-translational modification of secretory and membrane proteins [Ramirez and Couve, 2011]. In the presynaptic compartment, ER regulates Ca^{2+}-mediated processes involved in synaptic transmission. In response to membrane depolarization, Ca^{2+} enters presynaptic terminals through VGCC and NMDA receptors [McGuinness et al., 2010; Kunz et al., 2013], which in turn may trigger CICR. Additionally, Ca^{2+} may also be released through IP_3R in response to activation of metabotropic receptors. Increased Ca^{2+} concentration near release sites triggers fusion of glutamate-containing synaptic vesicles with the plasma membrane, leading to release of glutamate into the synaptic cleft [Bardo et al., 2006; Mattson, 2010]. In the postsynaptic compartment, ER Ca^{2+} initiates gene transcription [Mellstrom and Naranjo, 2001], modulates membrane excitability, and synaptic plasticity [Stutzmann and Mattson, 2011]. Furthermore, the release of Ca^{2+} from ER has been proposed as a modulator of dendritic spine structure [Korkotian and Segal, 1998].

The ER is a highly versatile protein factory that is equipped with chaperones and enzymes essential for proper protein folding. Only successfully folded proteins are exported from the ER, while unfolded or misfolded proteins are retained and selectively degraded [Kleizen and Braakman, 2004]. Key chaperones and folding sensors in the ER include: glucose regulated protein 78 (GRP78; also known as Immunoglobulin Binding protein-BiP) and 94 (GRP94), lectin, calnexin, calreticulin, protein disulfide isomerase (PDI), and ERp57 [Brown and

Naidoo, 2012]. Perturbation of ER Ca^{2+} homeostasis lead to the accumulation of unfold proteins that trigger ER stores response or unfold protein response (UPR) [Berridge, 2002]. ER stress and activation of the UPR has been implicated in abnormal protein processing, which subsequently plays a role in the pathogenesis of AD [Salminen et al., 2009; Katayama et al., 2004].

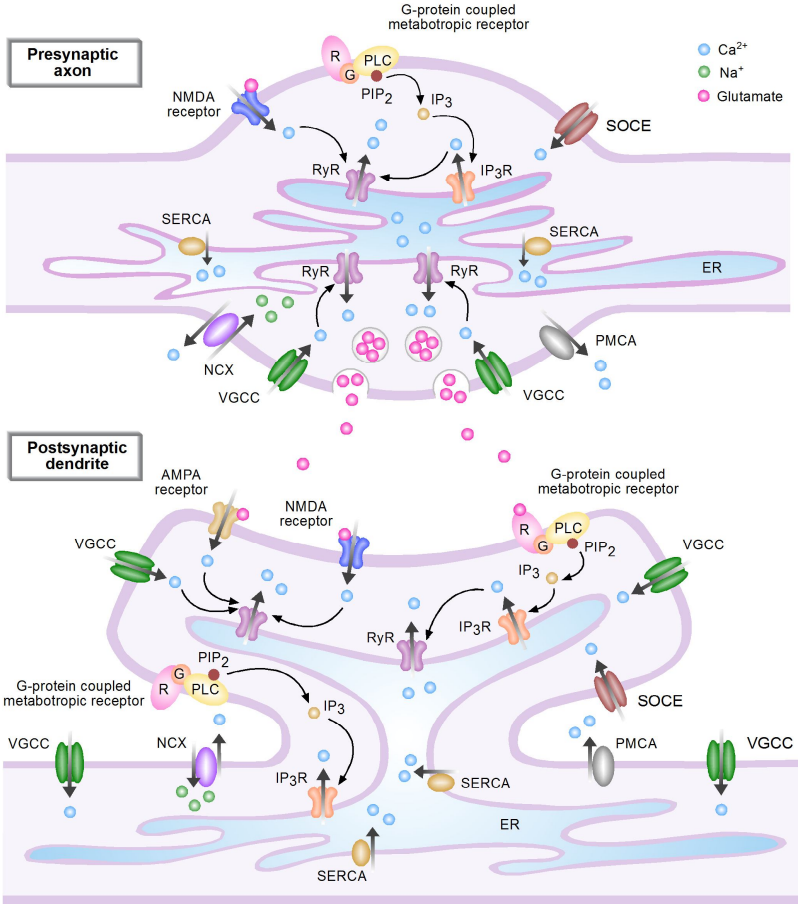

Figure 1. Schematic representation of the main Ca^{2+} homeostatic machinery components in pre-and postsynaptic compartments of neurons. Schematic representation of the key component of Ca^{2+} homeostatic mechanisms discussed in the text. Arrows indicate direction of ion flux. ER, endoplasmic reticulum; RyR, ryanodine receptor; IP_3R, inositol trisphosphate receptor; IP_3, inositol 1,4,5-trisphosphate; PIP_2, phosphatidylinositol 4,5-bisphosphate; SERCA, sarcoplasmic / endoplasmic Ca^{2+}-ATPase; NMDA, N-methyl-D-aspartate; AMPA, α-amino-3-hydroxy-5-methyl-4-isoxazolepropionic acid; VGCC, voltage-gated Ca^{2+} channels; PLC, phospholipase C; SOCE, store-operated Ca^{2+} entry; NCX, Na^{+}/Ca^{2+} exchanger; PMCA, plasma membrane Ca^{2+}- ATPase.

1.4 Ca^{2+} dysregulation in AD

In 1989, Khachaturian proposed that sustained changes in Ca^{2+} homeostasis could provide the common pathway for aging and neuropathological changes associated with AD. This hypothesis was termed *the calcium hypothesis of brain aging and AD* [Khachaturian, 1989]. Emerging evidence suggests that altered intracellular Ca^{2+} levels and/or disturbances in Ca^{2+} homeostasis affect cellular mechanisms underlying AD pathology. Previous studies have reported that the aggregation and formation of toxic Aβ oligomers disrupt Ca^{2+} homeostasis. It has been reported that Aβ oligomers can incorporate into the membrane and form ion-channel-like structures with high cation conductivity in the planar bilayer membrane [Arispe et al., 1993; Pollard et al., 1993; Quist et al., 2005] and the plasma membrane of *Xenopus laevis* oocytes [Demuro et al., 2011]. The presence of *in situ* Aβ pores has also been observed in the neuronal cell membrane derived from AD patients [Inoue, 2008]. In addition to the pore formation mechanism, Aβ oligomers have been shown to directly activate various Ca^{2+}- permeable channels. Studies in rat cultured neurons have reported that Aβ oligomers induce overactivation of NMDA and AMPA receptors, which in turn trigger mitochondrial dysfunction and neuronal apoptotic death [Alberdi et al., 2010]. Aβ peptides also enhance Ca^{2+} influx through VGCC in human neuroblastoma cells and mouse cortical neurons

[Ekinci et al., 1999]. Furthermore, Aβ oligomers can increase Ca^{2+} release from the ER stores via IP_3 and RyR receptors in cultured neurons [Ferreiro et al., 2004]. An Aβ peptide-mediated upregulation of RyR-3 expression has been described in neuronal cultures isolated from transgenic mice harboring the APP_{swe} mutation [Supnet et al., 2006, 2010]. Another mechanism by which Aβ disrupts neuronal Ca^{2+} homeostasis is Aβ-mediated production of reactive oxygen species, which may induce membrane lipid peroxidation. This results in the formation the aldehyde 4-hydroxynonenal which impairs the function of membrane transporters and ion channels leading to an elevation of $[Ca^{2+}]_i$ [Hensley et al., 1994; Keller et al., 1998; Hermes et al., 2010].

In addition to their impact on the function of γ-secretase, PS mutations were reported to have a significant impact on Ca^{2+} signaling in various AD models. Studies in *Xenopus laevis* oocytes expressing PS1-M146V, PS2-N141I, and PS2-M239V mutation have illustrated an increased in IP_3- mediated Ca^{2+} release from internal stores [Leissring et al., 1999a; 1999b]. Similar results have been observed in brain slices from knock-in (KI) mice expressing PS1- M146V mutation and from 3xTg- AD mice harboring APP_{swe}, Tau-P301L, and PS1-M146V mutation [Stutzmann et al., 2003; 2004; 2006]. A biological interaction of IP_3R with FAD mutant PS1 and PS2 have been observed in the insect Sf9 cell lines. Single-channel recordings of IP_3R have shown that the Sf9 cells expressing either different PS1 mutations or PS2-N141I mutation enhance IP_3R open probability and shift the channel gating toward a high open probability burst mode [Cheung et al., 2008; 2010]. Additionally, it has been reported that an alteration of PLC activity may be involved in FAD-linked PS mutation. The increase in basal PLC activity has been detected in the human neuroblastoma transfected PS1 exon 9 deletion (PS1deltaE9) and PS1-M146V mutation [Cedazo-Minguez et al., 2002; Popescu et al., 2004]. A PS1 mutation –mediated dysfunction of RyRs have also being described in several models. Studies in cultured neurons isolated from PS1-M146V KI mice have illustrated up-regulated RyR expression levels [Chan et al., 2000] and increased RyR-evoked Ca^{2+} release [Smith et al., 2005]. Studies in brain slices derived from PS1-M146V KI mice and 3xTg- AD mice have demonstrated increased RyR-evoked Ca^{2+} responses across neuronal compartments, including

the soma and perinuclear regions with particularly high Ca^{2+} release in dendrites and spine heads [Stutzmann et al., 2006; Goussakov et al., 2010]. In presymptomatic young 3xTg- AD mice, increased RyR-evoked Ca^{2+} responses are associated with an increase in RyR2 isoform expression [Chakroborty et al., 2009]. Consistent with these findings, the levels of RyR2 mRNA are also increased in the brain tissue samples from AD patients with mild cognitive impairment [Bruno et al., 2012].

Recent *in vitro* studies have provided evidence for a colocalization and physical interaction between PS and SERCA pump [Green et al., 2008; Jin et al., 2010]. Depletion of PS1 and PS2 results in diminished SERCA function, while the cells expressing PS1-M146V increase SERCA activity, suggesting that PS is necessary for proper functioning of SERCA [Green et al., 2008]. Furthermore, several studies have addressed the impact of PS mutations on the function of SOCE. A profound impairment of SOCE has been observed in fibroblasts isolated from PS1-M146V KI mice [Leissring et al., 2000], cell lines expressing PS1-M146L and PS2-N141I mutation, and primary cortical neurons derived from PS2-N141I transgenic mice [Yoo et al., 2000]. Additionally, studies using human B lymphocytes isolated from FAD patients with PS1 mutation have indicated an attenuated SOCE function and reduced STIM2 expression [Bojarski et al., 2009]. Furthermore, a downregulation of STIM2 protein has been reported in hippocampal cultures of PS1-M146V KI mice [Sun et al., 2014]. Moreover, recent findings have shown that wild type PS can form low-conductance divalent-cation-permeable ion channels in the ER membrane and function as passive ER Ca^{2+} leakage channels. The balance between SERCA Ca^{2+} pump activity and PS-mediated passive Ca^{2+} leak channel determines the steady-state resting ER Ca^{2+} levels [Tu et al., 2006]. Studies based on fibroblast cell lines have demonstrated that fibroblasts bearing PS1 mutations, including M146V, L166P, A246E, E273A, G384A, and P436Q lack an ER Ca^{2+} leak function, leading to ER Ca^{2+} overload and increased Ca^{2+} release from the ER [Tu et al., 2006; Nelson et al., 2007, 2010]. Similar results have also been observed in cultured hippocampal neurons from 3xTg AD mice [Zhang et al., 2010].

1.5 Synaptic dysfunction in AD

Synaptic dysfunction and synapse loss contribute to the memory impairment and cognitive deficits in AD pathogenesis [Sheng et al., 2012]. Several studies have examined the impact of Aβ oligomers on synaptic function. Studies in organotypic hippocampal slices derived from APP_{swe} mice demonstrated that Aβ oligomers selectively depress glutamatergic synaptic transmission [Kamenetz et al., 2003]. In double knock in mice carrying APP_{swe} and PS1-P264L mutation, an electrophysiological study reported a reduction in AMPA receptor function in acute hippocampal slices [Chang et al., 2006]. Consistent with this finding, a reduced expression of AMPA receptor subunit GluR1 is observed in neuronal culture derived from APP_{swe} mice treated with Aβ oligomers [Ameida et al., 2005]. The application of Aβ in cultured cortical neurons promotes endocytosis of NMDA receptors. Additionally, naturally secreted Aβ reduces the surface NR1 subunit of NMDA receptors in cultured cortical neurons derived from APP_{swe} mice [Synder et al., 2005]. Microinjection of Aβ oligomers in rat brain has been shown to inhibit hippocampal long-term potentiation (LTP) [Walsh et al., 2002] and disrupt cognitive function [Cleary et al., 2005]. An impairment of LTP and an enhancement of long-term depression (LTD) have been reported in mouse hippocampal slices treated with Aβ oligomers [Shanker et al., 2008]. Furthermore, it was found that the impairment of LTP occurs concomitantly with the appearance of intraneuronal Aβ accumulation in hippocampal CA1 neurons in 3xTg-AD mice [Oddo et al., 2003].

Recent investigations indicate the implication of dysregulated ER Ca^{2+} signaling in synaptic dysfunction. Electrophysiological studies in brain slices isolated from presymptomatic 3xTg AD mice have shown an exaggerated RyR-mediated CICR in dendritic processes and spine heads of prefrontal cortical pyramidal neurons [Goussakov et al., 2010]. Furthermore, RyR-mediated alterations in hippocampal synaptic plasticity and synaptic strength have been observed in the same mouse strain [Chakroborty et al., 2009]. These authors proposed that enhanced synaptic CICR may result in an abnormal synaptic transmission and contribute to cognitive deficits in AD. Additional evidence suggests a

contribution of FAD-linked PS mutations to cognitive dysfunction and the impairment of synaptic plasticity which can occur in the absence of amyloid and tau pathologies. Studies in PS1-M146V KI mice have demonstrated an impairment of hippocampus-dependent associative learning as measured by a contextual fear conditioning [Wang et al., 2004]. Moreover, an impairment of hippocampal spatial memory has been reported in PS1-M146V KI mice [Sun et al., 2005] and PS1-L435F heterozygous KI mice [Xia et al., 2015]. A deterioration of muscarinic modulation of LTP [Wang et al., 2009] and an impairment of the long lasting form of LTP [Auffret et al., 2010] have been described in hippocampal slices of PS1-M146V KI mice. Additionally, an adverse effect of mutant PS1 on short term plasticity and LTP at hippocampal CA1 and CA3 synapses has been reported in PS1-L435F heterozygous KI mice [Xia et al., 2015].

1.6 Aberrant neuronal network hyperactivity in AD

A growing number of studies in humans and mouse models of AD indicate that a perturbation of neuronal network activity contributes to AD pathogenesis. Aberrant excitatory network activity is observed in the brains of AD patients and may contribute to the disruption of cognitive function. It has been reported that the familial forms of AD are often associated with convulsive behavior [Palop and Mucke, 2009; Palop and Mucke, 2010; Dickerson et al., 2005; Sperling et al., 2010; Scharfman, 2012]. The incidence of seizures is increased in patients with mild-to-moderate AD. Additionally, severe AD cases are more likely to develop unprovoked seizure [Amatniek et al., 2006]. Studies in transgenic AD mice have also provided a possible connection between network hyperactivity and pathogenesis of seizures. Results from *in vivo* electroencephalographic (EEG) recordings in $APP_{swe/ind}$ mice have elucidated a pronounced epileptiform activity in cortical and hippocampal network. $APP_{swe/ind}$ mice also exhibit increased seizure acitivity induced by inhibition of $GABA_A$ receptors [Palop et al., 2007]. In APP_{swe}/PS1deltaE9 mice, electrophysiological recordings have shown increased excitability in cortical pyramidal neurons. Additionally, a high

probability of epileptic seizures has been observed in young APP_{swe}/PS1deltaE9 mice at an age when the first amyloid plaques begin to develop in the brain [Minkeviceine et al., 2009]. Recently, an *in vivo* two-photon Ca^{2+} imaging study has demonstrated an impairment of neuronal networks in double transgenic mice bearing mutant APP_{swe} and PS1-G384A mutation (APP23/PS45 mice). Measuring spontaneous Ca^{2+} transients of layer 2/3 cortical neurons *in vivo*, the authors have shown that in the vicinity of amyloid plaques only half of the neurons were active in the normal frequency range. The remaining neurons were either silent or hyperactive. The authors further demonstrated that these hyperactive neurons were found in close proximity to the plaque border, while the proportion of silent cells gradually increased at greater distances from the amyloid plaques [Busche et al., 2008]. Additionally, a deterioration of visual cortical circuit function has been reported in APP23/PS45 mice [Grienberger et al., 2012]. Interestingly, an impairment of orientation and a direction tuning property was specific to hyperactive neurons which were located in the vicinity of amyloid plaques. Furthermore, a study in CA1 region of hippocampus has shown that an increase of neuronal hyperactivity can be observed prior to plaque deposition in 1-2-month-old APP23/PS45 mice. An early occurrence of hyperactivity is causally related to the action of soluble Aβ oligomers [Busche et al., 2012].

Besides Aβ-induced network hyperexcitability, recent studies have reported the evidence of epileptic seizures in AD patients with various PS1 mutations. Early epileptic seizures have been observed in patients with the L166P and E120G mutation, while the H163R and L282R mutations have been linked to a late onset of seizures [Moehlmann et al., 2002; Gomez-Tortosa et al., 2010]. Additionally, the following mutations have been related to the epileptic seizures in AD patients: E120D, M139I, M139V, M146V, H163R, S169L, G209V, A246E, M233T, A260V, and E280A [Mann et al., 2001; Velez-Pardo et al., 2004]. Furthermore, it has been reported that also PS2 mutations might be related to epileptic seizures. The epileptic phenotype-associated with the PS2-N141I mutation has been reported in approximately 30% of 64 AD patients [Jayadev et al., 2010]. Supporting these findings, studies in transgenic mice harboring PS1-A246E and PS2-N141L mutation

exhibited a reduced seizure threshold in response to kainic acid [Schneider et al., 2001]. Collectively, these evidence raise the possibility that PS mutation may contribute to the aberrant network hyperexcitability, however, the precise mechanisms underlying this phenomenon still remain unknown.

1.7 Aim of this project

The current project aims to **understand the role of intracellular Ca^{2+} stores for *in vivo* AD-mediated neuronal network dysfunction** by

1. characterizing the ongoing neuronal activity in aged AD and WT mice by monitoring the relative proportion of silent, normal, and hyperactive neurons
2. deciphering functional properties of the intracellular Ca^{2+} stores in amyloid-depositing mice as well as their contribution to dysregulation of intracellular Ca^{2+} homeostasis
3. investigating the contribution of AD-linked PS1 mutation to the aberrant neuronal network activity

Chapter 2

Materials and Methods

All experimental procedures were conducted according to German federal and state regulations and were approved by the state government of Baden-Württemberg. The experiments were performed in anesthetized animals.

2.1 Animals

Ten- to fourteen-month-old transgenic PS45 (heterozygous, $PS45^{tg/-}$; homozygous, $PS45^{tg/tg}$), APP23xPS45 (AD), and age-matched non-transgenic (WT) mice of both sexes were used in this thesis. Additionally, 6-7-month-old $PS45^{tg/-}$ mice were used in some experiments. All transgenic lines express their transgenes under the control of Thy-1 promoter. The PS45 mice overexpress human G384A-mutated PS1. The AD mice overexpress both mutant APP with the Swedish (670/671) mutation and the human G384A-mutated PS1. In these double transgenic mice, amyloid plaque deposition in the upper cortical layers starts at approximately 2-3 months of age and the density of plaques is highest in the frontal and somatosensory cortex. Cognitive deficits in spatial learning and memory in the Morris water maze task are observed at 6 months of age [Busche et al., 2008]. Animals were housed on a 12 hours light/dark cycle with food and water available *ad libitum*.

2.2 Surgical Procedure

Acute cranial window

Mice were anesthetized using isoflurane (1-1.5% in O_2; CP-Pharma, Germany) and kept on a warming plate (37°C) to maintain body temperature. After injection of a local anesthetic (2% lidocaine; 20 mg lidocaine in 1 ml standard external saline), the skin located above the brain region of interest was removed to expose the skull. A custom-

made recording chamber with an opening in the middle (Figure 2) was then glued to the skull with cyanoacrylic glue (UHU, Buhl-Baden, Germany). The skull was thinned under a dissecting microscope using dental drills. The mouse was transferred to the recording set-up, placed onto a warming plate and continuously supplied with 0.8-1% isoflurane in pure oxygen during the experiment. The body temperature was maintained at 36-37°C and respiratory rate was continuously monitored and maintained at 80-120 bpm. The eyes were coated with Bepanthen (Bayer, Germany) to prevent dehydration. The recording chamber was perfused with warm (36-37°C) extracellular perfusion saline containing (in mM): 125 NaCl, 4.5 KCl, 26 $NaHCO_3$, 1.25 NaH_2PO_4, 2 $CaCl_2$, 1 $MgCl_2$, 20 glucose, pH 7.4, when bubbled with 95% O_2 and 5% CO_2. The position of the frontal cortex was located according to brain atlas coordinations: 3 to 3.5 mm anterior-posterior to Bregma (AP), 0.5 to 1.5 mm medio-lateral to midline (ML) [Busche et al., 2008]. A small (~ 1mm) craniotomy was performed above an area devoid of big blood vessels using a thin (30G) syringe needle. In all cases, after removing the bone flap the dura mater was left intact [Garaschuk et al., 2006].

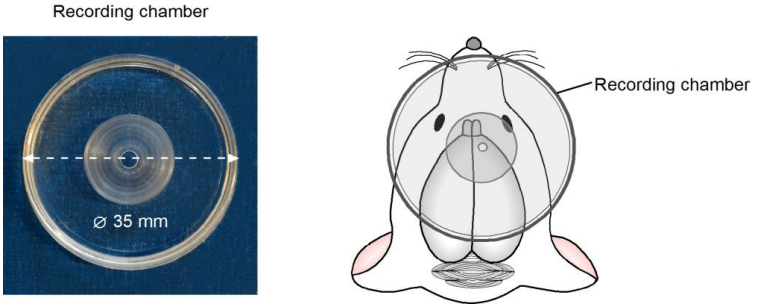

Figure 2. A custom-made recording chamber. Left panel: Photograph of custom-made recording chamber (top view) (modified from Garaschuk et al., 2006). Right panel: Schematics illustrating the recording chamber mounted on the skull.

2.3 *In vivo* two-photon imaging

2.3.1 Set up

In vivo imaging was performed with a custom-built two-photon microscope using a mode-locked Ti-Sapphire laser with a wavelength of 710-990 nm (MaiTai, Spectra Physics, Mountain View, CA) and a laser scanning system (Olympus Fluoview, Olympus, Tokyo, Japan). An upright microscope (BX51WI, Olympus, Tokyo, Japan) and a water-immersion objective (Nikon 40x, 0.8 NA, Tokyo, Japan) was attached to a laser scanning unit.

2.3.2 *In vivo* visualization of neurons

Multi-cell bolus loading technique

The cortical neurons in layer 2/3 of the frontal cortex were stained *in vivo* with a Ca^{2+} sensitive dye Oregon Green 488 BAPTA-1 AM (OGB-1 AM, Molecular Probes, Eugene, USA) using multi-cell bolus loading technique (MCBL) as previously described [Garaschuk et al., 2006]. Briefly, the fluorescent calcium indicator dye was dissolved in dimethyl sulfoxide (DMSO) plus 20% Pluronic F-127 to yield a dye concentration of 10 mM and this solution was further diluted for a final concentration of 0.5 mM with a standard pipette solution of the following composition (in mM): 150 NaCl, 2.5 KCl, 10 Hepes, pH 7.4. The dye solution was loaded in a micropipette (tip diameter 1 µm) and was pressure-ejected (2 min, 60 kPa) into the cortex ~ 200 µm below the pia. After an hour the dye was fully taken up by neurons and astrocytes. Previous studies have reported that astrocytes tend to accumulate higher concentration of indicator dyes, thus the brightly loaded cells were likely to be non-neuronal [Stosiek et al., 2003; Hirase et al., 2004; Garaschuk et al., 2006]. During the experiments astrocytes were discriminated by their bright appearance and their cell-type-specific morphology. As shown previously [Garaschuk, 2013], amyloid plaques also bind OGB-1,

therefore this labeling protocol enables visualization of the plaques during an experiment.

Two photon calcium imaging of neurons

The somata of OGB-1 labeled neurons were imaged using an excitation wavelength of 800 nm. A 40x water-immersion objective and a zoom of x4 was used throughout the recording sessions. Spontaneous somatic Ca^{2+} transients were collected at the frame rate of 7 Hz. for a 6-min-long recording period. All images shown are maximum intensity projection of ± 3 µm, taken with a 1 µm step size.

2.3.3 *In vivo* visualization of dendrites

Shadow electroporation

To investigate spontaneous Ca^{2+} transients in dendritic branches, the single-cell electroporation technique was performed as described previously [Nevian and Helmchen, 2007]. In brief, the individual pyramidal neurons in layer 2/3 of the frontal cortex were electroporated using glass pipettes with a tip diameter of < 1 µm filled with 2.5 mM Oregon Green BAPTA-1 hexapotassium salt (Life technologies, USA) dissolved in an intracellular solution containing (in mM): 175 K-gluconate, 17.5 KCl, 5 NaCl, and 12.5 HEPES. After insertion of the pipette, brief pressure pulses were applied to eject small amounts of the dye and to produce a local stain of the extracellular space. This extracellular stain caused cell bodies to appear as negatively stained objects enabling targeting of the cell membrane with the pipette. As soon as the pipette touched the cell membrane, a negative current of 500 nA was applied for 20-25 ms using a MVSC-02C iontophoresis system (NPI Electronic, Germany). After delivering the electroporation pulse, the soma and dendritic processes were rapidly loaded with dye. The pipette was then retracted slowly out of the brain. In these experiments, the pyramidal neurons were selected on the basis of their

morphological features which consist of (i) a pyramid-shaped soma, (ii) an apical dendrite extending towards the pial surface and a basal skirt, and (iii) an appearance of dendritic spines [Elston et al.,1996; Spruston, 2008] (Figure 3).

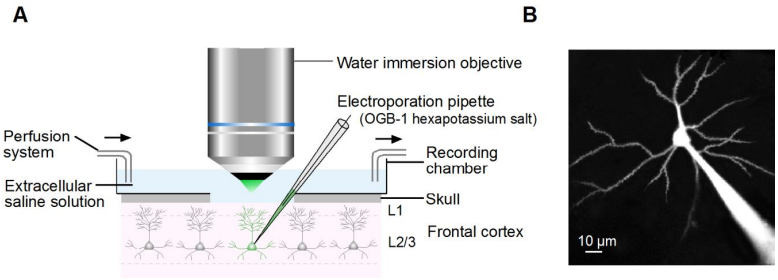

Figure 3. ***In vivo*** **shadow electroporation**. (A) Side view of the experimental arrangement. Note the position of the dye-containing (OGB-1 hexapotassium salt) electroporation pipette, water immersion objective, perfusion system, and the recording chamber glued on the skull. Layer 1 and 2/3 of the frontal cortex are indicated as L1 and L2/3, respectively. The arrows indicate the flow direction of the extracellular saline perfusing the cortical surface. (B) Maximum intensity projection (160-180 µm below the dura, step 0.5 µm) of a two-photon image stack of an electroporated pyramidal neuron in layer 2/3 of the frontal cortex in a PS45$^{tg/-}$ mouse.

Two photon calcium imaging of dendrites

Spontaneous Ca^{2+} transients in dendritic branches were recorded at least 30 minutes after electroporation to allow recovery of the cells and equilibration of the dye in the dendritic processes. Due to the technical limitations, the recordings of spontaneous Ca^{2+} transients in dendrites and their corresponding somata were taken separately for each field of view. Using an excitation wavelength of 800 nm, we first monitored the spontaneous Ca^{2+} transients in somata of electroporated neurons followed by the imaging of dendritic branches. A 40x water-immersion objective and a zoom of x4 was used throughout the recording sessions. Single and paired apical dendritic branches of normal and hyperactive cells were chosen for this study. Dendritic Ca^{2+} imaging was performed

at a frame rate of 8 Hz. for a 6-min-long recording period. Unless otherwise indicated, all images shown are maximum intensity projections of ± 2 µm, taken with a 0.5 µm step size. To determine the location of the dendritic branches of interest, a reference image was taken and compared to the images in the image stack of the soma and entire dendritic tree taken at the end of the recording. In these experiments, the apical dendrites were chosen according to the following criteria: (i) non-overlapping dendritic branches, and (ii) dendritic length within the plane of focus of more than 30-40 µm.

2.3.4 *In vivo* visualization of axonal boutons

Virus injection

Previous studies have reported that layer 2/3 pyramidal neurons receive some ascending interlaminar excitatory input from layer 5/6 pyramidal neurons [Thomson and Bannister, 2003; Shepherd et al., 2005]. To investigate spontaneous Ca^{2+} transients in ascending axons of layer 5/6 cortical neurons, we combined the viral labeling technique with the acute cranial window preparation. The viral transfection by adeno-associated virus (AAV) was used to deliver the genetically encoded Ca^{2+} indicator GCaMP6f (rAAV-synapsin*(syn)*-GCaMP6f, serotype 1, University of Pennsylvania Gene Therapy Program Vector Core) into the cortical neurons. Mice were anesthetized with a combination of medetomidine (0.5 mg/kg BW, Alfavet Tierarzneimittel GmbH, Neumünster, Germany), midazolam (5 mg/kg BW, Hameln Pharma plus GmbH, Hameln, Germany), and fentanyl (0.05 mg/kg BW, Albrecht GmbH, Aulendorf, Germany) injected intraperitoneally (IP) and transferred to a stereotaxic apparatus. Under a dissecting microscope, a high-speed drill was used to make a small hole (~0.5 x 0.5 mm) through the skull. We first attempted to label the cortical neuron in layer 5/6 of the frontal cortex, however, due to the space restriction it was difficult to cut an acute cranial window after viral injection. Therefore the nearby motor cortex was chosen for these experiments. The viral solution was injected slowly

(< 0.5 µl in 5 min) through the hole at a depth of 700-800 µm below the pia. The pipette penetration angle was set 45°- 50° from the horizontal plain to minimize the cortical tissue damage overlying the labeled neurons. The skin incision was then closed with sutures. A non-steroidal anti-inflammatory drug carprofen (5 mg/kg BW, Pfizer GmbH, Berlin, Germany), and the combination 3 antidotes atipamezole (2.5 mg/kg BW, Alfavet Tierarzneimittel GmbH, Neumünster, Germany), flumazenil (0.5 mg/kg BW, Fresenius Kabi Deutschland GmbH, Bad Homburg, Germany), and naloxone (1.2 mg/kg BW, Hameln Pharma plus GmbH, Hameln, Germany) were injected subcutaneously immediately after the surgery.

Two photon calcium imaging of axonal boutons

Preparation of acute cranial window and *in vivo* two-photon imaging were performed 14 days after virus injection. A small craniotomy was performed 0.5 – 0.7mm anterior to the injection area with the intact dura mater. Due to the limitations of our two-photon imaging setup, which allowed us only to visualize cortical layer 1-3, the recording of spontaneous somatic Ca^{2+} transients in layer 5/6 neurons was not included in this study. Axonal branches were selected on the basis of imaging characteristics, including high signal-to-noise ratio and lack of overlapping axons. Axonal boutons were identified as bright spots along the axon backbone [Shepherd et al., 2002; Stettler et al., 2006; De Paola et al., 2006]. Excitation wavelength of 920 nm was used to visualize GCaMP6f-labeled axonal boutons. A 40x water-immersion objective and a zoom of x4 to x5 was used throughout the recording sessions. The spontaneous Ca^{2+} transients in axonal boutons were collected similar to dendritic recording. All images shown are maximum intensity projection of $\pm$ 2 µm, taken with a 0.5 µm step size.

2.4 Immunohistochemistry

After *in vivo* experiments the brains were removed and fixed with 4% formaldehyde in phosphate buffer saline (PBS) for 24 hours at 4°C. The brains were then cryoprotected in 25% sucrose in PBS for 24 hours at 4°C. After cryoprotection, the brains were embedded in embedding medium (Tissue Tek®, SAKURA, USA). Embedded tissues were stored at -80°C until further use. An anti-ionized calcium binding adaptor molecular 1(Iba1) antibody (Wako, VA, USA) was used to visualize microglial morphology. An anti-CD68 antibody (Abd Serotec, Oxfordshire, UK) was used to elucidate phagocytic activity of microglia. An anti- glial fibrillary acidic protein (GFAP) antibody (Dako, USA) was used to visualize astrocytes and astrogliosis. Thioflavin-S (Sigma, USA) was used to stain amyloid plaques.

The staining procedure was performed on free-floating sagittal cryoslices (thickness 50 µm) at room temperature. The sections were incubated in a blocking solution containing 5% normal donkey serum (Jackson Immuno Research/Dianova) and 1% Triton-X 100 (Sigma, USA) in PBS for 1 hour to prevent non-specific background staining. After blocking the sections were incubated with the primary antibodies diluted in the blocking solution. The primary antibodies were used in the following concentration: anti-Iba1 (1:500), anti-CD68 (1:1000), and anti-GFAP (1:500). After incubation, the sections were rinsed in PBS three times for 10 minutes and incubated with AF 594- and AF 488-conjugated secondary antibodies (1:1000 in PBS+2% bovine serum albumin; Invitrogen) for 2 hours in the dark. Afterwards, the sections were washed three times in PBS for 10 minutes. Amyloid plaques were stained with Thioflavin-S ($1x10^{-6}$% in PBS) for 8 minutes and then washed three times in PBS for 10 minutes. Finally, the sections were

transferred to Superfrost Plus charged glass slides (Langenbrink, Emmendingen, Germany) and mounted in Vectashield Mounting Medium (Vector Laboratories, USA).

Fluorescence-stained sections were examined with a two-photon microscope. Images were acquired with a 40x water-immersion objective (Nikon 40x, 0.8 NA, Tokyo, Japan) and a zoom of x2.5. Fluorophores were excited with 800 nm. Emission wavelengths for Iba1 and Thioflavin-S were separated from each other with a 515 nm dichroic mirror. Emission wavelengths for GFAP and Thioflavin-S were separated from each other with a 570 nm dichroic mirror. All images shown are maximum intensity projection of ± 3 µm, taken with a 1 µm step size.

2.5 Drug application

NMDA (10 mM, Sigma-Aldrich, USA), caffeine (80 mM, Sigma-Aldrich, USA), cyclopiazonic acid (CPA, 400 µM, Sigma-Aldrich, USA) and MK-801 hydrogen maleate (200 µM, Sigma-Aldrich, USA) were used in these experiments. NMDA was dissolved in a solution containing (in mM): 150 NaCl, 2.5 KCl, 10 Hepes. Caffeine was dissolved in a solution containing (in mM): 120 NaCl, 4.5 KCl, 1.25 NaH_2PO_4, 10 HEPES, 1 $MgCl_2$, and 2 $CaCl_2$. NMDA and caffeine were locally applied to neurons using a pressure-application system. For improved visualization of the area subjected to the drug application and precise positioning of the pipette, the cell-impermeable fluorescent dye Alexa Fluor 594 (AF 594, 50 µM, Invitrogen, USA) was routinely added to the drug-containing solution. The application pipette (tip diameter ~1 µm) was placed 30-40 µm away from the neurons of interest. NMDA and caffeine were applied using a pressure pulse of 50-55 kPa (10-15 ms for NMDA and 40-50 ms for caffeine). CPA and MK-801 were added to the extracellular saline perfusing the recording chamber attached to the mouse's skull ('bath'

application). CPA was applied 30 minutes prior to recording the effect of the drug. MK-801 was applied for a long period of time and the recording was performed every 10 minutes for the duration of 2 hours.

2.6 Data analysis

The image analyses were performed off-line with Image J (http://rsb.info.nih.gov/ij/) and custom-made routines of the Igor Pro software (Wavemetrics, Lake Oswego, Oregon, United States). If not indicated otherwise, data were expressed as median ± interquartile range (IQR).

2.6.1 Analysis of spontaneous Ca^{2+} transients of somata, dendrites, and axonal boutons

To calculate the Ca^{2+}-dependent increase in fluorescence, regions of interest (ROIs) were drawn around individual neuronal somata, dendritic branches, and axonal boutons. After background subtraction, the values were expressed as relative change in fluorescence ($\Delta F/F$). For each ROI, a transient was accepted as a signal, when its peak amplitude was greater than three times the standard deviation of the baseline noise.

Analysis of spontaneous somatic Ca^{2+} transients

The following parameters of Ca^{2+} transients were analyzed: i) frequency, ii) amplitude, iii) T-half (duration of Ca^{2+} transients at half peak amplitude), and iv) decay time constant (tau). All recorded neurons were classified based on the frequency of their spontaneous Ca^{2+} transients as *silent* (0-0.25 transients/min), *normal* (0.26-4 transients/min), and *hyperactive* (>4 transients/min) similar to previous study [Busche et al., 2008]. The amplitudes were calculated as the difference between the peak of fluorescence and the mean baseline fluorescence immediately

before the peak. Tau values were obtained by fitting the decay of Ca^{2+} transients with an exponential function from 90% to 10% of the maximum amplitude (Figure 4).

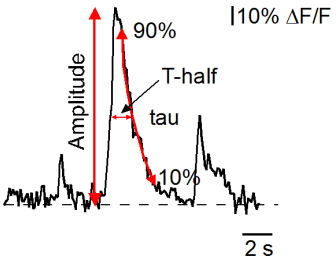

Figure 4. Representative example of spontaneous somatic Ca^{2+} transients recorded from an OGB-1 labeled neuron. Arrows indicate parameters analyzed in this study (amplitude, T-half, and tau).

Analysis of spontaneous dendritic Ca^{2+} transients

The frequency and the amplitude of spontaneous dendritic Ca^{2+} transients were analyzed similar to somatic data. Additionally, the spontaneous Ca^{2+} transients obtained from paired dendritic branches recording were classified into two groups: *local* and *synchronous transients*. The local transients invaded individual dendritic branches independently, while transients occurring simultaneously in both dendritic branches were termed synchronous.

Analysis of spontaneous Ca^{2+} transients of axonal boutons

We monitored the frequency and amplitude of spontaneous Ca^{2+} transients in individual axonal boutons. Furthermore, these transients were classified based on the number of spikes. All transients with a single peak and an immediate return to baseline

were considered as single transients whereas as series of transients showing two or more spikes without returning to baseline was considered as bursts.

2.6.2 Analysis of agonist-induced Ca^{2+} transients

We analyzed the following parameters: amplitude, T-half, tau, area under the curve (AUC) of AF 594 signals, and AUC ratio. The amplitude, T-half, and tau of agonist-induced Ca^{2+} transients were measured similar to those of spontaneous Ca^{2+} transients. The AUC of AF 594 signals is proportional to the amount of agonist applied. The AUC ratio was calculated by normalizing the AUC of agonist-induced Ca^{2+} transients to the AUC of AF 594 signals observed for the same cell. This value represents the response of a neuron per unitary stimulus (here: agonist application).

2.7 Statistical analysis

Statistical analyses were performed using the software on the VassarStats Statistical Computation Web Site (http://vassarstats.net/). Comparisons between two independent data sets were conducted with Mann-Whitney Test. Wilcoxon Signed-Rank Test was used for multiple measurements within the same data set. Chi-square test was used for comparing the fractions of silent, normal, and hyperactive cells between different data sets. Kolmogorov-Smirnov test was used for comparing the cumulative distribution of data. $P<0.05$ was considered as statistically significant.

Chapter 3

Results

3.1 Aging and ongoing amyloid deposition potentiate neuronal hyperactivity

A recent study in a mouse model of AD (APP_{swe}/PS1G384A) at 6-10 months of age demonstrated an *in vivo* impairment of neuronal network function [Busche et al., 2008]. Using 2-photon Ca^{2+} imaging, the authors measured the frequency of spontaneous Ca^{2+} transients in individual layer 2/3 neurons and observed an AD-mediated increase in the proportion of either silent or hyperactive cells in the half of neuronal population, while the remaining half of cortical neurons showed normal activity. Hyperactive cells were found in close proximity of amyloid plaques, whereas silent and normal cells were found throughout the cortex. These data provided the first *in vivo* evidence for a disturbed Ca^{2+} homeostasis in mouse models of AD, but the mechanisms underlying this disturbance as well as their relation to the function of the intracellular Ca^{2+} stores remained unknown. We conducted similar experiment in 10-14-month-old AD and WT mice to find out if the aging process *per se* affects network activity (Figure 5A). As abundant amyloid plaques were observed throughout the cortical area in AD mice of this age, only clusters of neurons in the close vicinity of amyloid plaques (10-20 µm) were analyzed. All recorded neurons were classified based on the frequency of spontaneous Ca^{2+} transients as silent, normal, and hyperactive cells according to the frequency boundaries established in the previous study [Busche et al., 2008]. Interestingly, we observed a robust increase in the fraction of hyperactive cells in WT and AD mice compared to 6-10-month-old animals analyzed previously (23.50% versus 1.2% for WT and 38.1% versus 21% for AD, $^{**}p<0.0001$; Chi-Square test; compare our Figure 5B to Figure 1 in Busche et al.,2008).

When comparing the fraction of silent, normal, and hyperactive cells between AD (n= 260 in 10 mice) and WT mice (n=226 cells in 9 mice) of the same age (Figure 5C), we found a significant increase in the fraction of hyperactive cells (38.34±11.48% in AD versus 21.74±7.78% in WT, $^{**}p=0.003$; Mann-Whitney test) and a substantial decrease in the

fraction of normal cells (44.74±8.03% in AD versus 65.22±6.73% in WT, ***p*= 0.002; Mann-Whitney test) in AD relative to WT mice. The fraction of silent cells, however, was similar in both strains (15.70±5.84% in AD versus 12.50±6.49% in WT, *p*= 0.15; Mann-Whitney test). Furthermore, we analyzed the frequency distribution of spontaneous Ca^{2+} transients using cumulative probability histograms. The frequency distribution in AD mice was significantly shifted to the right, implicating a higher frequency of spontaneous Ca^{2+} transients than in WT mice (***p*=0.006; Kolmogorov-Smirnov test) (Figure 5D).

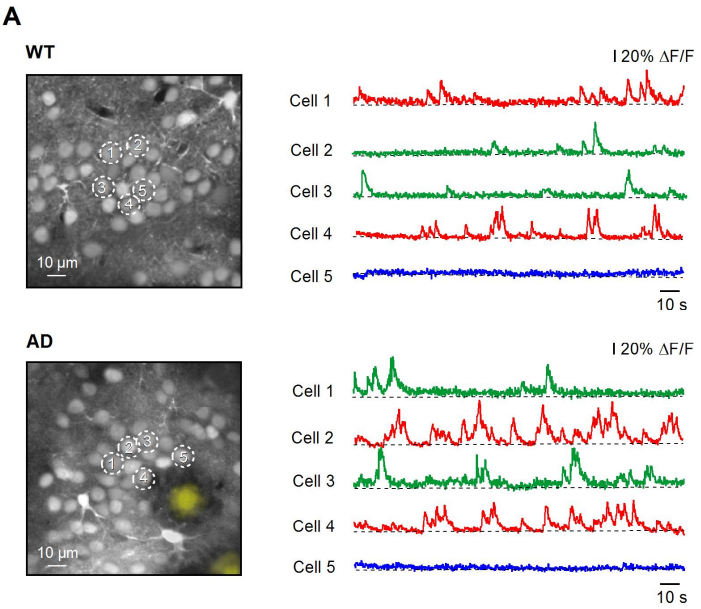

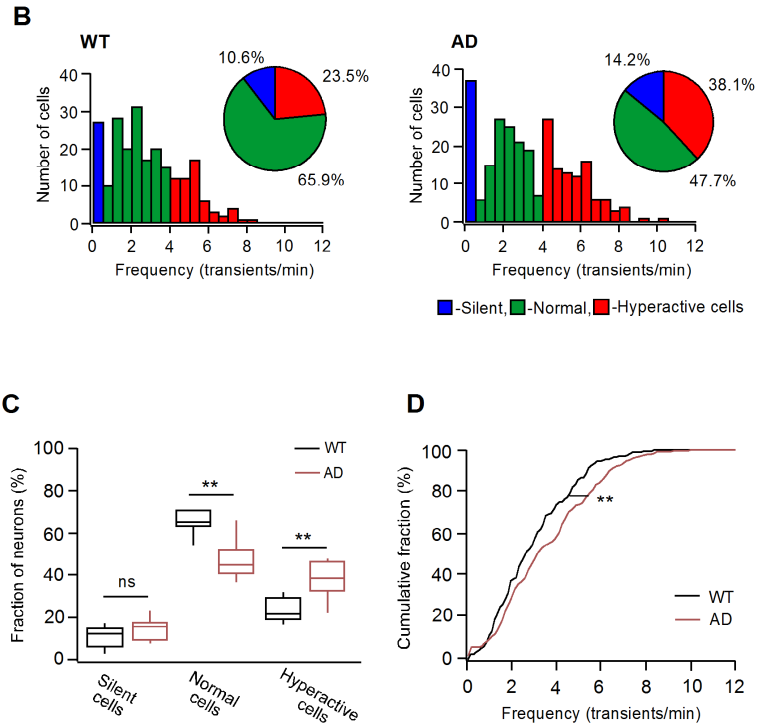

Figure 5. Altered spontaneous neuronal activity in aged amyloid-depositing mice. (A) Maximum intensity projection (167-173 µm (WT) and 172-178 µm (AD) below the dura, step 1 µm) of layer 2/3 neurons of the frontal cortex in a WT and an AD mouse. Plaques are shown in yellow. The right panel shows spontaneous Ca^{2+} transients recorded simultaneously from neurons marked with respective numbers in the left panel. Traces are color-coded to mark neurons according to their frequency: green for normal (0.26-4 transients/min), red for hyperactive (>4 transients/min), and blue for silent cells (0-0.25 transients/min). (B) Histograms showing the frequency distribution of spontaneous Ca^{2+} transients in 10-14-month-old WT (n = 226 cells in 9 mice) and AD mice (n = 260 cells in 10 mice). Insets: pie charts showing the relative proportion of silent, normal, and hyperactive cells. The proportion of the three cell types is significantly different between the two mouse strains (**p= 0.0002, Chi-square test). (C) Box-and-whisker plots illustrating the median fraction of three cell types in WT and AD mice (n= 9 mice and 10 mice, respectively). There is a significant increase in the fraction of hyperactive cells (**p=0.003; Mann-Whitney test) and a substantial decrease in the fraction of normal cells (**p= 0.002; Mann-Whitney test) in AD compared to WT mice. The fraction of silent cells is similar between the two mouse

strains (p= 0.15; Mann-Whitney test). ns= not significant. (D) The cumulative probability histograms showing a significantly higher frequency of spontaneous Ca^{2+} transients in AD relative to WT mice (**p= 0.006, Kolmogorov-Smirnov test).

In summary, these data indicate the presence of an aging-related increase in neuronal hyperactivity which is observed not only in AD but also in WT mice. Additionally, the amyloid deposition in AD mice further potentiates neuronal hyperactivity. These findings suggest that both aging and AD impair network Ca^{2+} homeostasis thus supporting Khachaturian's hypothesis that aging- and AD-related neuronal impairments may share similar mechanisms.

3.2 *In vivo* properties of somatic intracellular Ca^{2+} stores in WT and AD mice

3.2.1 Enhanced caffeine-induced Ca^{2+} release from intracellular stores in amyloid-depositing mice

Previous *in vitro* Ca^{2+} imaging studies indicated that RyR-mediated Ca^{2+} release is enhanced in cortical and hippocampal neurons from 3xTg AD mice and PS1-M146V KI mice [Smith et al., 2005; Stutzmann et al., 2006; Chakroborty et al., 2009; Chan et al., 2000]. This finding provided *in vitro* evidence that dysregulation of intracellular Ca^{2+} stores is implicated in AD pathology. However, the *in vivo* properties of the intracellular Ca^{2+} stores and their contribution to dysregulation of intracellular Ca^{2+} homeostasis in the intact AD brain remained unclear. To address this issue, we have established a technique enabling us to study the *in vivo* properties of RyRs in layer 2/3 cortical neurons. Initially we applied 80 mM caffeine (50-55 kPa for 40-50 ms) to the cells of interest by pressure application. No caffeine-induced Ca^{2+} transients were observed, probably due to a low concentration of caffeine reaching the RyRs in our application paradigm. As it was not possible to increase

the caffeine concentration in the application pipette because of solubility issues and the duration of the application due to the movement artifacts, we supported the caffeine-induced Ca^{2+} release by increasing the content of Ca^{2+} within the intracellular Ca^{2+} stores [Garaschuk et al., 1997]. Local application of glutamate receptor agonist NMDA was used to increase the Ca^{2+} content within the stores in all subsequent experiments. We first pressure-applied 10 mM NMDA (50-55 kPa for 10-15 ms) followed by 80 mM caffeine (50-55 kPa for 40-50 ms) using the 'double pipette technique' (Figure 6A and B). AF 594 (50 µM) was routinely added to the drug-containing solutions to visualize the application pipettes and the size of the drug affected area.

Cyclopiazonic acid (CPA) is a known reversible inhibitor of the SERCA pump. Because of the presence of Ca^{2+} leak channels in the ER membrane [Garaschuk et al., 1997], blockade of the pump results in the depletion of intracellular Ca^{2+} stores. To confirm that CPA effectively depleted intracellular Ca^{2+} stores in our *in vivo* conditions, the effects of CPA on caffeine-induced Ca^{2+} transients was examined in AD mice. 400 µM CPA was added to the extracellular solution superfusing the surface of the dura (so-called "bath application", Garaschuk et al., 2006) for 30 minutes and then NMDA and caffeine were applied again as described above. The caffeine-induced Ca^{2+} transients were abolished in the presence of CPA (Figure 6C, middle panel) and recovered upon wash-out of CPA (Figure 6C, right panel), demonstrating that bath-applied CPA (400 µM, 30 minutes) successfully blocks Ca^{2+} release from the intracellular Ca^{2+} stores *in vivo*.

For comparison of agonist-induced Ca^{2+} transients between WT and AD mice we used the following parameters: amplitude, T-half, tau, and AUC ratio (Figure 6D). We first assessed the amount of NMDA and caffeine released in this protocol by calculating the AUC of AF 594 signals. As shown in Figure 7 and Table 1, the AUC of AF 594 signals of NMDA and caffeine application were similar in WT (n= 63 cells in 5 mice) and AD mice (n= 51 cells in 5 mice) (p= 0.26 and p = 0.10, respectively; Mann-Whitney test), indicating that these agonists were applied in equal

amounts in both strains. Hence, this experimental protocol provided reliable data and enabled us to compare the results obtained in both strains.

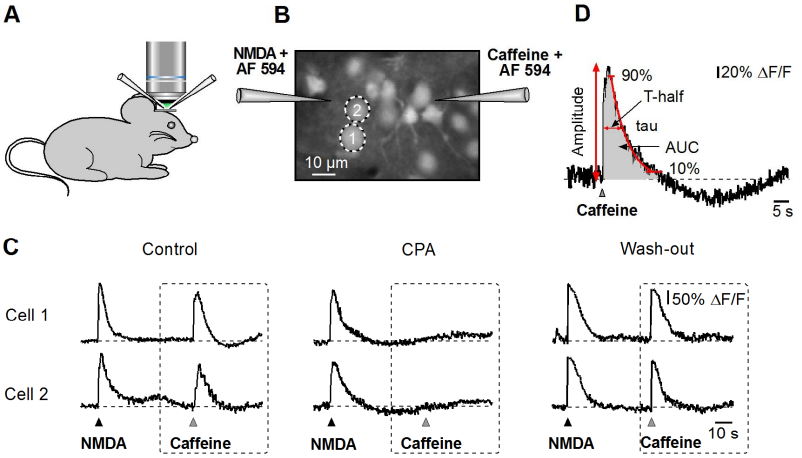

Figure 6. *In vivo* Ca^{2+} release from neuronal intracellular Ca^{2+} stores. (A) A schematic drawing illustrating the double pipette technique. (B) Maximum intensity projection (155-161 µm below the dura, step 1 µm) of layer 2/3 neurons of the frontal cortex in an AD mouse. Two pipettes containing either 10 mM NMDA or 80 mM caffeine are positioned close to cells of interest. The drugs are pressure-applied (50-55 kPa, 10-15 ms for NMDA and 50-55 kPa, 40-50 ms for Caffeine) to evoke respective Ca^{2+} transients. (C) NMDA- and caffeine-induced Ca^{2+} transients recorded simultaneously from neurons marked with respective numbers in (B) before, during, and after application of a SERCA pump inhibitor CPA (400 µM). Note that the caffeine-induced Ca^{2+} transients are abolished in the presence of CPA. Triangles indicate the time points of NMDA and caffeine applications. (D) Representative example of a caffeine-induced Ca^{2+} transient. Arrows indicate parameters analyzed in this study (amplitude, T-half, tau, and AUC).

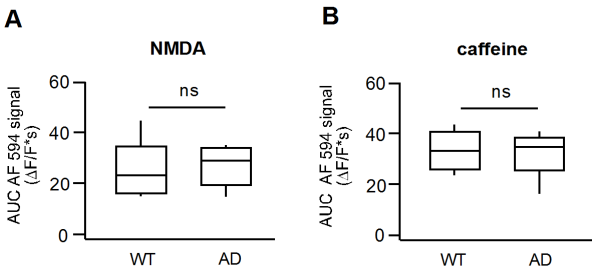

Figure 7. Similar amounts of NMDA and caffeine are applied in WT and AD mice. The distributions of median AUC of AF 594 signals of NMDA-AF 594 solution (A) and caffeine-AF 594 solution (B) in WT and AD mice (n= 5 mice per group). The AUC of AF 594 signals for both solutions are similar between WT and AD mice (p = 0.26 and p = 0.10, respectively; Mann-Whitney test). ns = not significant.

We further compared caffeine-induced Ca^{2+} transients between WT and AD mice. As illustrated in Figure 8 and Table 1, the T-half, tau, and AUC ratio of caffeine-induced Ca^{2+} transients were significantly larger in AD compared to WT mice (*p= 0.04, *p= 0.04, and *p= 0.01, respectively; Mann-Whitney test). The amplitudes of caffeine-induced Ca^{2+} transients, however, were similar in the two mouse strains (p= 0.14; Mann-Whitney test). These results indicate that Ca^{2+} release from caffeine-sensitive stores is increased in AD compared to WT mice. Next, we compared the NMDA-induced Ca^{2+} transients between the two mouse strains. We found that the amplitudes, T-half, tau, and AUC ratio of NMDA-induced Ca^{2+} transients were similar in WT and AD mice (p=0.37, p=0.41, p=0.41, and p=0.33, respectively; Mann-Whitney test) (Figure 9A-D and Table 2).

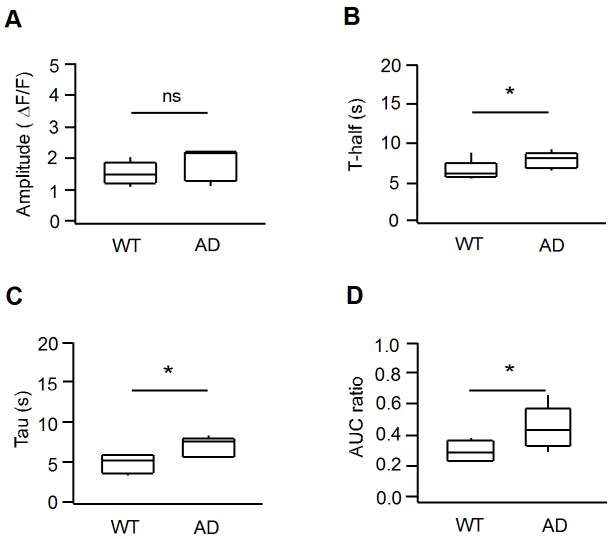

Figure 8. Caffeine-induced Ca^{2+} release from intracellular Ca^{2+} stores is stronger in AD compared to WT mice. Box-and-whisker plots illustrating the distribution of median amplitude (A), T-half (B), tau (C), and AUC ratio (D) of caffeine-induced Ca^{2+} transients in WT and AD mice (n= 5 mice per group). The T-half, tau, and AUC ratio in AD are significantly increased compared to WT mice (*p= 0.04, *p= 0.04, and *p= 0.01 respectively; Mann-Whitney test). However, the amplitudes are similar in both strains (p = 0.14; Mann-Whitney test). AUC = area under the curve; ns = not significant.

Table 1. Summary of the amplitude, T-half, tau, AUC of AF 594 signals, and AUC ratio of caffeine-induced Ca^{2+} transients in WT and AD mice. Data are presented as median ± IQR.

Parameters	caffeine-induced Ca^{2+} transients	
	WT	AD
Amplitude (ΔF/F)	1.48 ± 0.36	2.16 ± 0.73
T-half (s)	6.24 ± 0.36	7.91 ± 1.01 *
Tau (s)	5.15 ± 1.99	7.50 ± 1.93 *
AUC ratio	0.29 ± 0.10	0.44 ± 0.10 *
AUC of AF 594 signal (ΔF/F*s)	33.06 ± 0.38	34.66 ± 0.69

* Significantly different compared to the respective values in WT mice (p=0.04 for T-half and tau, p=0.01 for AUC ratio; Mann-Whitney test).

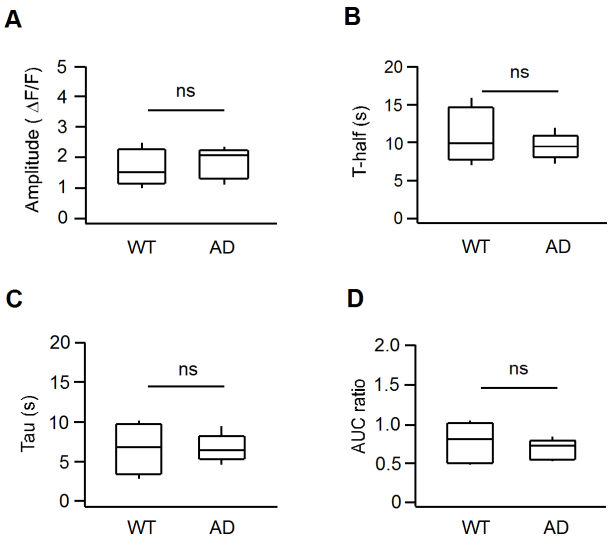

Figure 9. Similarity of NMDA-induced Ca^{2+} transients in WT and AD mice. Box-and-whisker plots illustrating the distribution of median amplitude (A), T-half (B), tau (C), and AUC ratio (D) of NMDA-induced Ca^{2+} transients in WT and AD mice (n =5 mice per group). There are no significant differences between WT and AD mice in amplitude, T-half, tau, and AUC ratio of NMDA-induced Ca^{2+} transients (p=0.37, p=0.41, p=0.41, and p=0.33, respectively; Mann-Whitney test). AUC = area under the curve; ns = not significant.

Table 2. Summary of the amplitude, T-half, tau, AUC of AF 594 signals, and AUC ratio of NMDA-induced Ca^{2+} transients in WT and AD mice. Data are presented as median ± IQR.

Parameters	NMDA-induced Ca^{2+} transients	
	WT	AD
Amplitude (ΔF/F)	1.51 ± 0.73	2.07 ± 0.65
T-half (s)	9.96 ± 5.18	9.63 ± 1.09
Tau (s)	6.86 ± 5.15	6.45 ± 0.70
AUC ratio	0.80 ± 0.43	0.74 ± 0.17
AUC of AF 594 signal (ΔF/F*s)	23.25 ± 7.64	28.99 ± 8.87

There are no significant differences in all parameters between WT and AD mice. (p>0.05 for all cases; Mann-Whitney test).

To investigate differences in the Ca^{2+} release from caffeine-sensitive stores of silent, normal, and hyperactive cells in AD mice, we compared all parameters of caffeine-induced Ca^{2+} transients (amplitude, T-half, Tau, and AUC ratio) among different cell types. Interestingly, we observed a significant increase in the T-half and tau of caffeine-induced Ca^{2+} transients in hyperactive cells (n= 17 cells in 5 mice) compared to that measured in silent (n= 13 cells in 5 mice) and normal cells (n= 21 cells in 5 mice,**p<0.01; Mann-Whitney test). Although there was a trend toward increased AUC ratios in hyperactive cells, it did not reach the level of statistical significance (p>0.05; Mann-Whitney test) (Figure

10A-D and Table 3). The amplitudes, however, were similar across the three cell types (p>0.05; Mann-Whitney test). All values measured in silent cells were indistinguishable from that measured in normal cells (p>0.05; Mann-Whitney test).

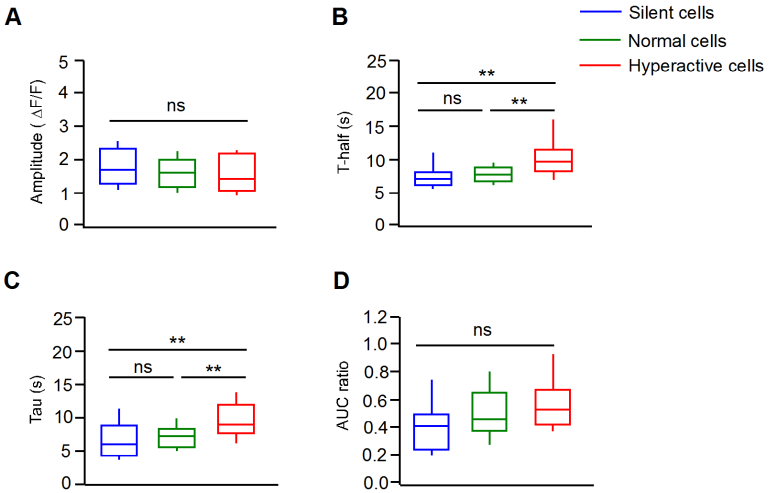

Figure 10. Larger Ca^{2+} release from caffeine-sensitive stores of hyperactive cells in AD mice. Box-and-whisker plots illustrating the distribution of amplitude (A), T-half (B), tau (C), and AUC ratio (D) of caffeine-induced Ca^{2+} transients of silent (n= 13 cells in 5 mice), normal (n = 21 cells in 5 mice), and hyperactive cells (n= 17 cells in 5 mice) in AD mice. The T-half and tau of hyperactive cells are significantly increased compared to silent and normal cells (**p<0.01 for all cases; Mann-Whitney test). There is a trend toward increased AUC ratio in hyperactive cells compared to silent and normal cells, but this does not reach the level of statistical significance (p>0.05 for all cases; Mann-Whitney test). The amplitudes, however, are similar across the three cell types (p>0.05 for all cases; Mann-Whitney test). All values measured in silent cells are not significantly different from that measured in normal cells (p>0.05 for all cases; Mann-Whitney test). ns= not significant.

Table 3. Summary of the amplitude, T-half, tau, and AUC ratio of caffeine-induced Ca^{2+} transients of silent, normal, and hyperactive cells in AD mice. Data are presented as median ± IQR.

Parameters	caffeine-induced Ca^{2+} transients		
	Silent cells	Normal cells	Hyperactive cells
Amplitude (ΔF/F)	1.71 ± 0.88	1.63 ± 0.80	1.44 ± 1.04
T-half (s)	7.09 ± 1.47	7.70 ± 1.95	9.70 ± 2.88**
Tau (s)	6 ± 3.10	7.27 ± 2.59	8.80 ± 3.97**
AUC ratio	0.41 ± 0.24	0.46 ± 0.25	0.49 ± 0.20

** Significantly different compared to the respective values measured in silent and normal cells (p<0.001 for all cases; Mann-Whitney test).

In summary, here we have established a robust protocol for functional analyses of somatic intracellular Ca^{2+} stores *in vivo*. In the intact cerebral cortex of AD mice we observed prolonged RyR-mediated Ca^{2+} release signals consistent with the overfilling of the intracellular Ca^{2+} stores and/or altered function of RyRs. When compared to silent and normal cells, the largest effects were observed in hyperactive cells.

3.2.2 NMDA receptors activation-mediated Ca^{2+} release from internal stores in amyloid-depositing mice

To find out whether the activation of NMDA receptors is able to induce CICR from the intracellular Ca^{2+} stores *in vivo* in amyloid-depositing mice, we analyzed NMDA-induced Ca^{2+} transients recorded under control conditions, during the application of CPA, and after washout of CPA (Figure 11A-B). To ensure that the obtained results are not biased by unequal agonist applications, we compared the AUC of AF 594 signals. We found that these values were similar across the three conditions (18.73±4.57 ΔF/F*s for control, 20.10±0.84 ΔF/F*s for CPA, and 22.24±2.98 ΔF/F*s for wash-out of CPA, $p>0.05$; Wilcoxon Signed-Rank test) (Figure 11C), indicating that NMDA was applied in equal amounts in all three conditions.

For comparison we normalized the amplitudes, T-half, tau, and AUC ratio of NMDA-induced Ca^{2+} transients during CPA treatment to their respective control values. As illustrated in Figure 11D and Table 4, CPA significantly reduced the amplitudes of NMDA-induced Ca^{2+} transients in hyperactive cells (n= 21 cells in 5 mice,*$p<0.05$; Wilcoxon Singed-Rank test), but not in silent and normal cells (silent, n= 6 cells and normal, n= 36 cells in 5 mice, $p>0.05$ for; Wilcoxon Signed-Rank test). Additionally, a trend toward reduction in T-half was observed in the three cell types, but it did not reach a level of statistical significance ($p>0.05$; Wilcoxon Signed-Rank test). The tau and AUC ratio, however, were not affected by CPA ($p>0.05$; Wilcoxon Signed-Rank test). Together, these results indicate that NMDA-induced Ca^{2+} transients are potentiated by CICR selectively in hyperactive cells, likely due to a stronger overfilling of their intracellular Ca^{2+} stores.

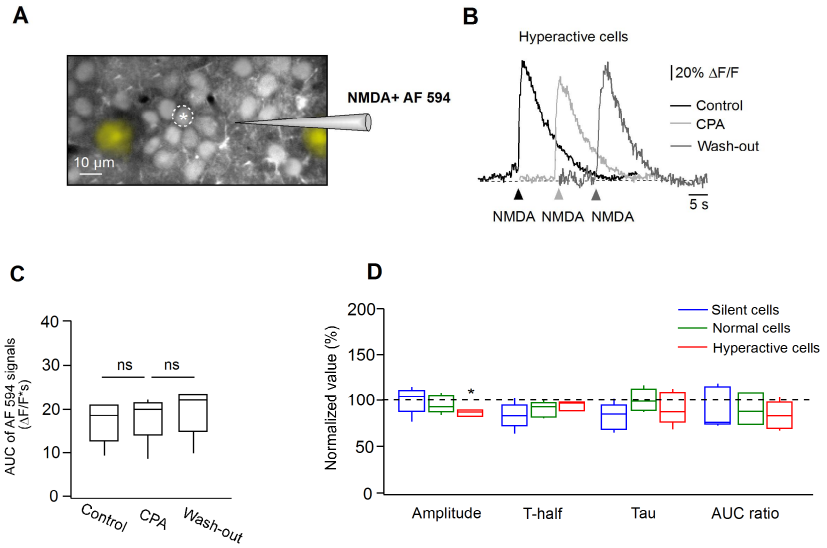

Figure 11. NMDA receptor-mediated activation of CICR in amyloid-depositing mice. (A) Maximum intensity projection (169-175 µm below the dura, step 1 µm) of layer 2/3 neurons of the frontal cortex in an AD mouse. A pipette containing 10 mM NMDA and 50 µM AF 594 is positioned close to cells of interest. The drug is pressure-applied (50-55 kPa for 10-15 ms) to evoke Ca^{2+} transients before, during, and after bath application of CPA. Plaques are shown in yellow. (B) Representative traces showing NMDA-induced Ca^{2+} transients measured in a hyperactive cell marked with a white asterisk in (A). The triangles indicate the time points of the NMDA application. Note a reduction in the amplitude of NMDA-induced Ca^{2+} transient in the presence of CPA. (C) Box-and-whisker plots illustrating the distributions of median AUC of AF 594 signals in control, CPA, and wash-out conditions (p>0.05; Wilcoxon Signed-Rank test, n= 5 mice). (D) The distribution of median normalized amplitude, T-half, tau, and AUC ratio of NMDA-induced Ca^{2+} transients measured in silent, normal, and hyperactive cells (n= 5 mice). In the presence of CPA, there is a significant decrease in the amplitude of hyperactive cells (*p<0.05; Wilcoxon Signed-Rank test), but not of silent and normal cells (p>0.05; Wilcoxon Signed-Rank test). A trend toward reduction in the T-half is observed in three cell types, but this trend does not reach the level of statistical significance (p>0.05; Wilcoxon Signed-Rank test). The tau and AUC ratio of three cell types are not affected by CPA (p>0.05; Wilcoxon Signed-Rank test). All values measured under CPA are normalized to their respective control values. A dashed help line is drawn at 100%. ns = not significant.

Table 4. Summary of the normalized amplitude, T-half, tau, and AUC ratio of NMDA-induced Ca^{2+} transients in AD mice. Data are presented as median ± IQR.

Normalized parameters (%)	NMDA-induced Ca^{2+} transients		
	Silent cells	Normal cells	Hyperactive cells
Amplitude	106 ± 7	93 ± 12	88 ± 6 *
T-half	86 ± 5	84 ± 12	85 ± 7
Tau	87 ± 15	99 ± 16	89 ± 2
AUC ratio	78 ± 36	88 ± 32	85 ± 19

* Significantly different compared to the control condition (100%) (p<0.05; Wilcoxon Signed-Rank test)

3.3 Neural network response to the empty intracellular Ca^{2+} stores

Besides the general notion that Ca^{2+} disturbances are involved in the pathogenesis of AD, very little is known about the role of the intracellular Ca^{2+} stores for dysregulation of *in vivo* neuronal network activity in AD mice. Our next aim was to elucidate the relevance of intracellular Ca^{2+} stores to the ongoing spontaneous Ca^{2+} transients in both pre- and postsynaptic compartments.

3.3.1 The effect of SERCA blocker CPA on spontaneous somatic Ca^{2+} transients in WT and AD mice

To investigate the contribution of Ca^{2+} release from intracellular Ca^{2+} stores to spontaneous neuronal activity, the effect of CPA on spontaneous Ca^{2+} transients was examined in 10-14-month-old WT and AD mice. As already noted above, bath-applied CPA reversibly inhibits Ca^{2+} uptake into the ER via inhibition of SERCA pumps and leads to store depletion. Therefore, spontaneous Ca^{2+} transients of OGB-1

labeled cortical neurons were measured before, during, and after bath application of CPA (Figure 12A-B). Following 30 min bath application of CPA, there was a dramatic decrease in the fraction of hyperactive cells and also a proportional increase in the fraction of normal cells in AD mice (*p<0.05; Wilcoxon Signed-Rank test). This effect was reversible upon wash-out of CPA (p>0.05 when compared to control conditions; Wilcoxon Signed-Rank test). The fraction of silent cells was not affected by CPA (p>0.05; Wilcoxon Signed-Rank test). In WT mice, however, the fractions of three cell types under CPA were similar across the three conditions (p>0.05; Wilcoxon Signed-Rank test) (Figure 13A-D and Table 5).

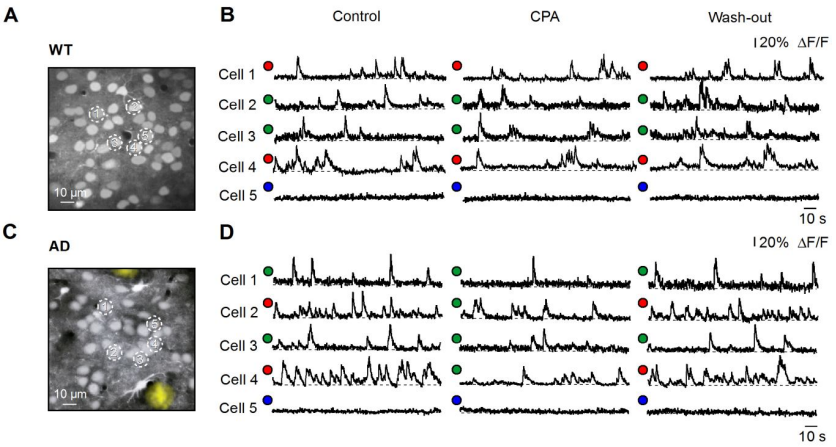

Figure 12. Effect of SERCA blocker CPA on spontaneous Ca^{2+} transients of cortical neurons in WT and AD mice. A and C, Maximum intensity projection (157-162 µm (WT) and 161-166 µm (AD) below the dura, step 1 µm) of layer 2/3 neurons of the frontal cortex in a WT and an AD mouse. Plaques are shown in yellow. B and D, Traces show spontaneous Ca^{2+} transients recorded before, during, and after bath application of CPA from neurons marked with respective numbers (A and C) in a WT and an AD mouse. The colored dots indicate the type of neuron (blue, silent; green, normal; and red, hyperactive). Note a remarkable decrease in the frequency of spontaneous Ca^{2+} transients in the presence of CPA selectively in AD mice.

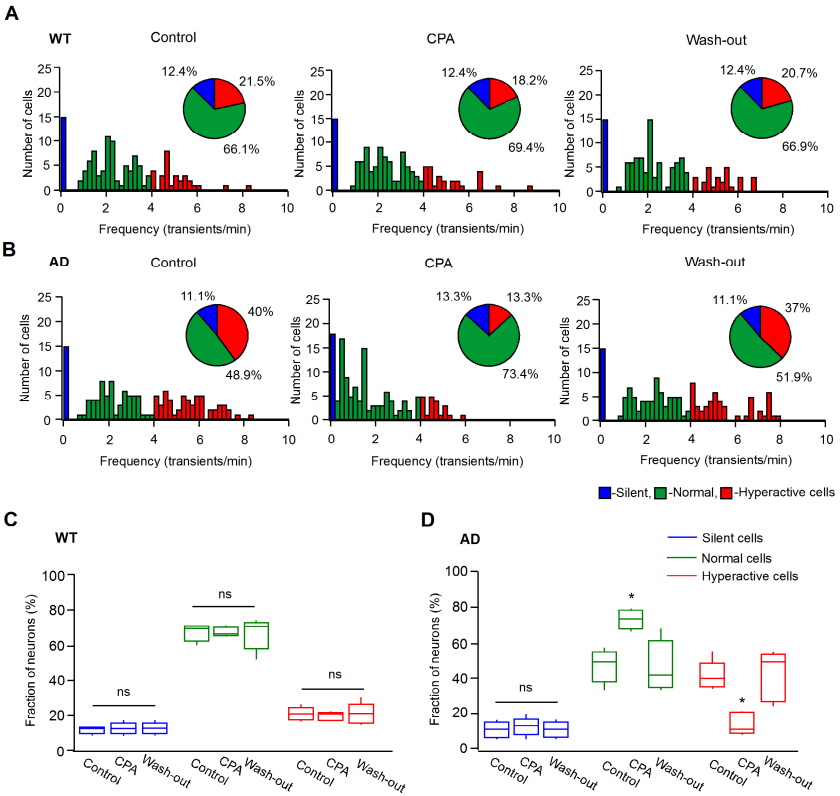

Figure 13. Store depletion normalizes pathological activity patterns in amyloid depositing mice. (A and B) Histograms showing the frequency distributions of spontaneous Ca^{2+} transients recorded before, during, and after bath application of CPA in WT (n = 121 cells in 5 mice) and AD (n = 135 cells in 5 mice) mice. Insets: pie charts showing the relative proportion of silent, normal, and hyperactive cells under respective condition (C and D) Box-and-whisker plots illustrating the median fraction of the three cell types under three conditions in WT and AD mice (n= 5 mice per group). There is a significant decrease in the fraction of hyperactive cells (*p<0.05; Wilcoxon Signed-Rank test) and a substantial increase in the fraction of normal cells (*p<0.05; Wilcoxon Signed-Rank test) in the presence of CPA in AD mice, whereas the fraction of silent cells is similar across the three conditions (p>0.05; Wilcoxon Signed-Rank test). In WT mice CPA does not affect the fraction of three cell types (p>0.05; Wilcoxon Signed-Rank test).

Table 5. Summary of the fractions of silent, normal, and hyperactive cells under control, CPA, and wash-out condition in WT and AD mice. Data are presented as median ± IQR.

Fraction of neurons (%)	Silent cells		Normal cells		Hyperactive cells	
	WT	AD	WT	AD	WT	AD
Control	12.50 ±1.9	11.10 ± 5.4	70.40 ± 5.6	50 ± 9.3	20.80 ± 3.3	40 ± 5.4
CPA	12.50 ± 1.9	13.20 ± 2.2	66.70 ± 2.9	73.70 ± 7.8 *	20.80 ± 3.3	11.10 ± 10 *
Wash-out	12.50 ± 1.9	11.10 ± 5.4	70.80 ± 5.6	42.10 ± 20	20.80 ± 5.1	50 ± 26

* Significantly different compared to their respective control and wash-out values (p<0.05; Wilcoxon Signed-Rank test).

We further normalized all values (frequency, amplitude, T-half, and tau) under CPA to their respective control values for comparison of the two conditions. There was a pronounced decrease in the frequency of both normal and hyperactive cells in AD mice (*p<0.05; Wilcoxon Signed-Rank test). Moreover, the amplitudes were significantly smaller in hyperactive cells (*p<0.05; Wilcoxon Signed-Rank test) but not in normal cells (p>0.05; Wilcoxon Signed-Rank test). There were no significant changes in neither T-half nor tau of normal and hyperactive cells (p>0.05; Wilcoxon Signed-Rank test). In WT mice, however, no significant changes in the frequency, amplitudes, T-half, and tau values were observed after depletion of Ca^{2+} stores with CPA (p>0.05 for all cases; Wilcoxon Signed-Rank test) (Figure 14 and Table 6). Collectively, these data indicate that intracellular Ca^{2+} stores influence the frequency of spontaneous activity in AD but not in WT mice. Furthermore, blocking the Ca^{2+} release from intracellular stores normalizes the aberrant network activity in AD mice by reducing neuronal hyperactivity.

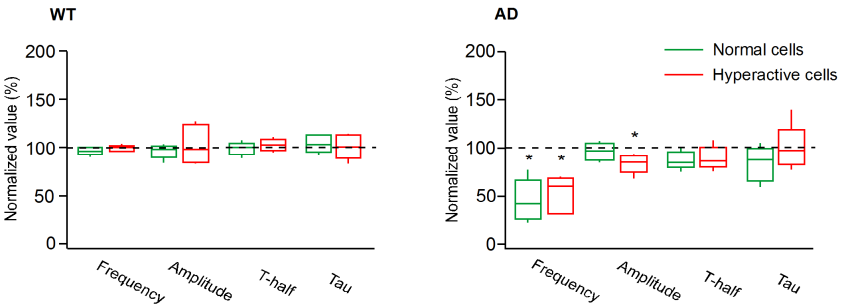

Figure 14. Intracellular Ca^{2+} stores are selectively involved in controlling the ongoing neuronal activity in AD mice. A comparison of median normalized frequency, amplitude, T-half, and tau of spontaneous Ca^{2+} transients of normal and hyperactive neurons in WT (left panel) and AD mice (right panel) (n= 5 mice per group). CPA significantly decreases the frequency of spontaneous Ca^{2+} transients of both normal and hyperactive cells in AD mice (*p<0.05, Wilcoxon Signed-Rank test). The amplitudes of hyperactive cells (*p<0.05; Wilcoxon Signed-Rank test), but not that of normal cells (p>0.05; Wilcoxon Signed-Rank test) are smaller in the presence of CPA. T-half and tau of both cell types are not affected by CPA (p>0.05; Wilcoxon Signed-Rank test). CPA does not influence neither normal nor hyperactive cells in WT mice (p>0.05; Wilcoxon Signed-Rank test). All values measured under CPA are normalized to their respective control values. Dashed help lines are drawn at 100%.

Table 6. Summary of the normalized frequency, amplitude, T-half, and tau of normal and hyperactive cells in WT and AD mice. Data are presented as median ± IQR.

Normalized values (%)	Normal cells		Hyperactive cells	
	WT	AD	WT	AD
Frequency	96 ± 5	45 ± 20 *	100 ± 3	63 ± 33 *
Amplitude	98 ± 4	98 ± 16	98 ± 36	87 ± 8 *
T-half	100 ± 3	86 ± 7	103 ± 5	88 ± 6
Tau	103 ± 13	89 ± 21	100 ± 18	99 ± 10

* Significantly different compared to their respective normalized control values (100%) (p<0.05; Wilcoxon Signed-Rank test).

3.3.2 The role of G384A PS mutation for neuronal hyperactivity

Our data described above revealed a significant contribution of the intracellular Ca^{2+} stores to the AD-mediated neuronal hyperactivity in the plaque vicinity. This hyperactivity might be due to a direct effect of amyloid species [Busche et al., 2008] or, alternatively, to other factors such as proinflammatory substances released from plaque-associated activated microglia and astrocytes [review in Brawek and Garaschuk, 2014]. Another possible factor accounting for this phenomenon could be an AD-associated PS mutation. To understand the mechanisms underlying CPA-sensitive neuronal hyperactivity in AD mice, we repeated the experiments described above in age-matched $PS45^{tg/-}$ and $PS45^{tg/tg}$ mice, which harbor the same PS mutation as APP23xPS45 mice.

3.3.2.1 Neuronal hyperactivity occurs independently of plaque formation and inflammation in PS45 mice

To test whether PS45 mice develop amyloid plaques and/or exhibit any signs of inflammation, we analyzed tissue samples of $PS45^{tg/tg}$ mice by means of immunocytochemistry. Tissue samples of WT and AD mice were used as a negative and a positive control, respectively.

As illustrated in Figure 15A-L, Iba-1 positive microglial cells in $PS45^{tg/tg}$ mice exhibited a typical ramified morphology defined by long thin processes and small somata, similar to microglia cells in WT mice. The CD68 (a marker of phagocytosis, predominantly localizes to lysosomes and endosomes) immunoreactivity of microglial cells in $PS45^{tg/tg}$ was comparable to that of WT mice. Additionally, Thioflavin-S positive amyloid plaques were observed only in AD, but not in $PS45^{tg/tg}$ and WT mice.

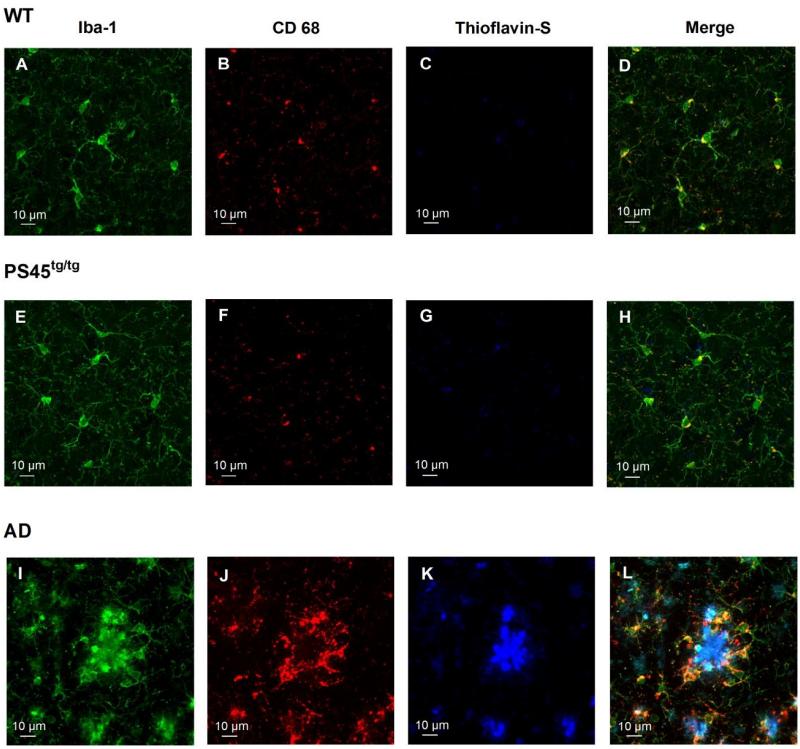

Figure 15. No evidence of microglial activation in PS45$^{tg/tg}$ mice. Sagittal brain sections of WT, PS45$^{tg/tg}$, and AD mice at 10-14 months of age are processed for a triple immunofluorescence staining with Iba-1 antibody for microglia (green, A, E, I), CD68 for marker of activated microglia with phagocytic activity (red, B, F, J), and Thioflavin-S for amyloid plaques (blue, C, G, K). Merged images of the three mouse strains are shown in D, H, and L. The Iba-1 positive microglial cells in PS45$^{tg/tg}$ mice (E) exhibit a typical ramified morphology similar to those in WT mice (A). CD68 immunoreactivity in the PS45$^{tg/tg}$ (F) and WT mice (B) is less intense than in AD mice (J). Microglial cells in AD mice show a hyperthrophic/amoeboid morphology (I) and strong expression of CD68 immunoreactivity (J) in the areas surrounding amyloid plaques (L). In contrast to AD mice, there is no positive staining of amyloid plaques in the PS45$^{tg/tg}$ and WT mice. Data shown in this and the next figure were acquired by Rosa Maria Olmedillas.

In contrast, the CD68-positive microglial cells in AD mice had activated hypertrophic/amoeboid morphology, particularly in the areas surrounding amyloid plaques. Similar results were obtained in 15 sections of 5 mice in each mouse strain.

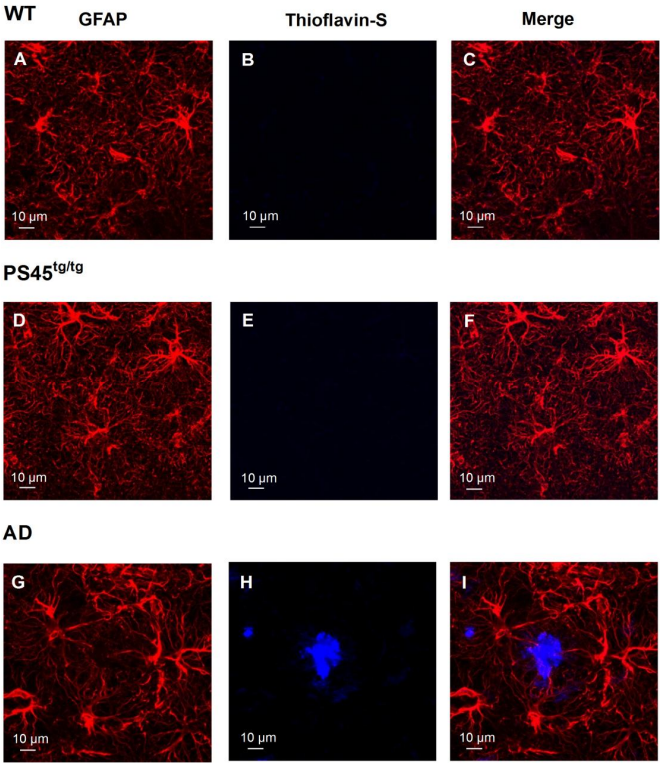

Figure 16. No apparent astrogliosis in PS45$^{tg/tg}$ mice. Sagittal brain sections of WT, PS45$^{tg/tg}$, and AD mice at 10-14 months of age are stained with anti- GFAP antibody for visualization of astrocyte (red, A, D, G) and Thioflavin-S for visualizing amyloid plaques (blue, B, E, H). The merged images of the three mouse strains are shown in C, F, and I. The GFAP-positive astrocytes in PS45$^{tg/tg}$ have a morphology similar to that in WT mice. In AD mice, the reactive astrocytes are found in close proximity to amyloid plaques. Thioflavin-S positive dense-cored compact plaques are observed only in AD mice.

Next, we investigated the astroglial morphology and reactive astrogliosis using an antibody against GFAP, an intermediate filament protein which is expressed by astrocytes and is upregulated upon astrocyte activation. As shown in Figure 16A-I, GFAP-positive astrocytes in PS45$^{tg/tg}$ had morphology similar to that in WT mice. In AD mice, astrocytes with hypertrophy of proximal processes, a characteristic of reactive astrocytes, were apparent in close proximity to amyloid plaques.

Together, these data indicate that PS45$^{tg/tg}$ mice do not develop amyloid plaque depositions. Additionally, there are no signs of microglial activation and reactive astrogliosis in PS45$^{tg/tg}$ mice, indicating that the histological features of inflammation are not observed in this mouse strain. Because of the even lower gene dosage in PS45$^{tg/-}$ mice, we assume that the results obtained above also apply to this mouse strain.

3.3.2.2 Spontaneous network activity in PS45 mice

We first characterized the general features of spontaneous Ca^{2+} transients in PS45$^{tg/-}$ and PS45$^{tg/tg}$ mice. As shown in Figure 17A-D and Table 7, the fraction of silent, normal and hyperactive cells in PS45$^{tg/-}$ (n= 139 cells in 5 mice) and PS45$^{tg/tg}$ mice (n= 141 cells in 5 mice) were indistinguishable from each other (p= 0.34, p=0.29, p=0.52, for silent, normal, and hyperactive cells, respectively; Mann-Whitney test). Additionally, the frequency distribution of spontaneous Ca^{2+} transients appeared similar in both strains (p=0.23; Kolmogorov-Smirnov test).

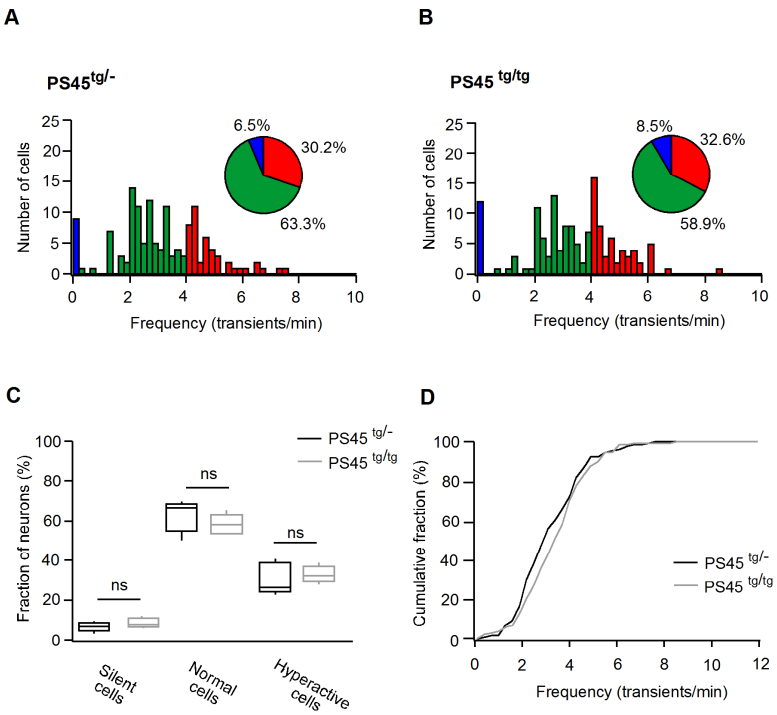

Figure 17. Characterization of spontaneous network activity in PS45$^{tg/-}$ and PS45$^{tg/tg}$ mice. Histograms showing the frequency distributions of spontaneous Ca^{2+} transients in 10-14-month-old PS45$^{tg/-}$ (n= 139 cells in 5 mice) (A) and PS45$^{tg/tg}$ (n = 141 cells in 5 mice) (B) mice. Insets: pie charts showing the relative proportion of silent, normal, and hyperactive cells. (C) Box-and-whisker plots illustrating the median fraction of silent, normal, and hyperactive cells in PS45$^{tg/-}$ and PS45$^{tg/tg}$ mice (n= 5 mice). The fraction of three cell types measured in PS45$^{tg/-}$ are indistinguishable from that measured in PS45$^{tg/tg}$ mice (p>0.05 for all cases; Mann-Whitney test). ns= not significant. (D) The cumulative probability histogram showing similar frequency distribution for spontaneous Ca^{2+} transients recorded in PS45$^{tg/-}$ and PS45$^{tg/tg}$ mice (p= 0.23, Kolmogorov-Smirnov test).

Table 7. Summary of the fractions of silent, normal, and hyperactive cells in PS45$^{tg/-}$ and PS45$^{tg/tg}$ mice. Data are presented as median ± IQR.

	Fraction of neurons (%)	
	PS45 $^{tg/-}$	**PS45 $^{tg/tg}$**
Silent cells	6.70 ± 1.2	7.70 ± 3.2
Normal cells	66.70 ± 7.7	58.30 ± 6.9
Hyperactive cells	26.60 ± 10.9	32.20 ± 3.6

The fractions of three cell types are similar in both strains (p= 0.34, p= 0.29, and p= 0.52 for silent, normal, and hyperactive cells, respectively; Mann-Whitney test).

Next, we analyzed amplitudes, T-half, and tau of spontaneous Ca^{2+} transients in normal and hyperactive cells. For clarity, we compared these parameters in two ways: first –comparison between the two different cell types (normal and hyperactive cells). Second – comparison between the two different mouse strains (PS45$^{tg/-}$ and PS45$^{tg/tg}$). We found that the values measured in normal and hyperactive cells were not significantly different across either cell types or mouse strains (p>0.05 for all cases; Mann-Whitney test) (Figure 18 and Table 8). Thus, all parameters measured in PS45$^{tg/-}$ mice were similar to those obtained in PS45$^{tg/tg}$ mice, indicating that the frequency and the general features of spontaneous Ca^{2+} transients in both strains are independent of mutant PS1 gene dosage.

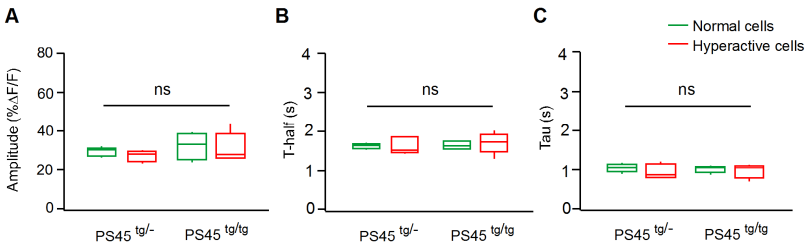

Figure 18. General features of spontaneous Ca^{2+} transients in $PS45^{tg/-}$ and $PS45^{tg/tg}$ mice. A comparison of median amplitude (A), T-half (B), and tau (C) of spontaneous Ca^{2+} transients of normal and hyperactive cells in $PS45^{tg/-}$ and $PS45^{tg/tg}$ mice (n= 5 mice per group) under control conditions. There is no significant difference across either cell types or mouse strains (p>0.05; Mann-Whitney test). ns = not significant.

Table 8. Summary of the amplitude, T-half, and tau of spontaneous Ca^{2+} transients of normal and hyperactive cells in $PS45^{tg/-}$ and $PS45^{tg/tg}$ mice. Data are presented as median ± IQR.

Parameters	Normal cells		Hyperactive cells	
	$PS45^{tg/-}$	$PS45^{tg/tg}$	$PS45^{tg/-}$	$PS45^{tg/tg}$
Amplitude (%ΔF/F)	30 ± 2	33 ± 11	28 ± 3	26 ± 7
T-half (s)	1.66 ± 0.06	1.63 ± 0.13	1.50 ± 0.35	1.75 ± 0.13
Tau (s)	1.06 ± 0.07	1.04 ± 0.05	0.86 ± 0.29	1.06 ± 0.16

There are no significant differences in all values measured in normal and hyperactive cells across either cell types or mouse strains (p>0.05 for all cases; Mann-Whitney test).

3.3.2.3 Characteristics of spontaneous Ca^{2+} transients in WT, $PS45^{tg/-}$, $PS45^{tg/tg}$, and AD mice

To study if the AD-associated PS mutation *per se* has an effect on network activity, we further compared the fractions of the three cell types in $PS45^{tg/-}$ and $PS45^{tg/tg}$ mice to our previous results obtained under control conditions in WT and AD mice. Surprisingly, the fractions of hyperactive cells in both PS45 strains were similar to AD mice (p=0.11 for $PS45^{tg/-}$ and p=0.06 for $PS45^{tg/tg}$ mice; Mann-Whitney test) and these fractions were significantly larger compared to WT mice (*p=0.03 for $PS45^{tg/-}$, *p=0.01 for $PS45^{tg/tg}$ and AD mice; Mann-Whitney test). The fractions of normal cells in both PS45 strains were similar to WT mice (p=0.29 for $PS45^{tg/-}$ and p= 0.09 for $PS45^{tg/tg}$ mice; Mann-Whitney test) and these fractions tended to be larger relative to AD mice (*p=0.04 for $PS45^{tg/-}$ and *p= 0.03 for $PS45^{tg/tg}$ mice; Mann-Whitney test). The fractions of silent cells were similar across the four strains (p>0.05 for all cases; Mann-Whitney test) (Table 9). Next, we compared the general features of spontaneous Ca^{2+} transients (amplitude, T-half, and tau) of normal and hyperactive cells among different mouse strains. As shown in Figure 19 A-C and Table 10, there were no significance differences in all values across either cell types or mouse strains (p>0.05 for all cases; Mann-Whitney test).

Table 9. Summary of the fractions of silent, normal and hyperactive cells in WT, $PS45^{tg/-}$, $PS45^{tg/tg}$, and AD mice. Data are presented as median ± IQR.

	Fraction of neurons (%)			
	WT	**AD**	**PS45 $^{tg/-}$**	**PS45 $^{tg/tg}$**
Silent cells	12.50 ± 1.9	11.10 ± 5.4	6.70 ± 1.2	7.70 ± 3.2
Normal cells	70.40 ± 5.6 *	50 ± 9.3	66.70 ± 7.7 *	58.30 ± 6.9 *
Hyperactive cells	20.80 ± 3.3	40 ± 5.4 †	26.60 ± 10.9 †	32.20 ± 3.6 †

* Significantly different compared to the fraction of normal cells in AD mice (p=0.04 for PS45$^{tg/-}$, p=0.03 for PS45$^{tg/tg}$, and p=0.02 for WT; Mann-Whitney test).

† Significantly different compared to the fraction of hyperactive cells in WT mice (p=0.03 for PS45$^{tg/-}$, p=0.01 for PS45$^{tg/tg}$, and p=0.01 for AD; Mann-Whitney test).

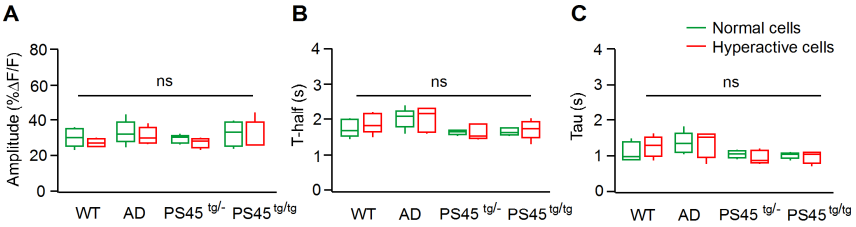

Figure 19. General features of spontaneous Ca^{2+} transients in WT, AD, PS45$^{tg/-}$, and PS45$^{tg/tg}$ mice. A comparison of median amplitude (A), T-half (B), and tau (C) of spontaneous Ca^{2+} transients of normal and hyperactive cells in WT, PS45$^{tg/-}$, PS45$^{tg/tg}$, and AD mice (n= 5 mice per group) under control condition. There are no significant differences in all values measured in normal and hyperactive cells across either cell types or mouse strains (p>0.05 for all cases; Mann-Whitney test). ns = not significant.

Table 10. Summary of the amplitude, T-half, and tau of spontaneous Ca^{2+} transients of normal and hyperactive cells in WT, PS45$^{tg/-}$, PS45$^{tg/tg}$, and AD mice under control condition. Data are presented as median ± IQR.

Parameters	Normal cells			
	WT	AD	PS45 $^{tg/-}$	PS45 $^{tg/tg}$
Amplitude (%ΔF/F)	30 ± 6	32 ± 5	30 ± 2	33 ± 11
T-half (s)	1.69 ± 0.34	2.08 ± 0.12	1.66 ± 0.06	1.63 ± 0.13
Tau (s)	0.95 ± 0.38	1.37 ± 0.24	1.06 ± 0.07	1.04 ± 0.05

Parameters	Hyperactive cells			
	WT	AD	PS45 $^{tg/-}$	PS45 $^{tg/tg}$
Amplitude (%ΔF/F)	27 ± 3	30 ± 6	28 ± 3	26 ± 7
T-half (s)	1.82 ± 0.28	2.14 ± 0.60	1.50 ± 0.35	1.75 ± 0.13
Tau (s)	1.29 ± 0.31	1.51 ± 0.40	0.86 ± 0.29	1.06 ± 0.16

There are no significant differences in all values measured in normal and hyperactive cells across either cell types or mouse strains (p>0.05 for all cases; Mann-Whitney test).

Collectively, these data indicate that a significant increase in the fraction of hyperactive cells can be observed in both PS45 and AD mice, while a prominent reduction in the fraction of normal cells is seen in AD mice only. The fraction of silent cells, however, is similar across all mouse strains. Additionally, the general features of spontaneous Ca^{2+} transients are indistinguishable in all transgenic mice in this study.

3.3.2.4 The contribution of intracellular Ca^{2+} stores to spontaneous neuronal activity in PS45 mice

In the next step, we analyzed the effect of CPA on spontaneous neuronal activity in PS45 mice. Interestingly, the obtained results from either PS45$^{tg/-}$ or PS45$^{tg/tg}$ replicated our findings observed in AD mice (Figure 20A-B and 21A-B). Following 30 min bath application of CPA, there was a striking reduction in the fraction of hyperactive cells (*p<0.05; Wilcoxon Signed-Rank test) and a substantial increase in the fraction of normal cells (*p<0.05; Wilcoxon Signed-Rank test). The fractions of silent cells were unaffected by CPA in both strains (p>0.05; Wilcoxon Signed-Rank test) (Figure 21C-D and Table 11).

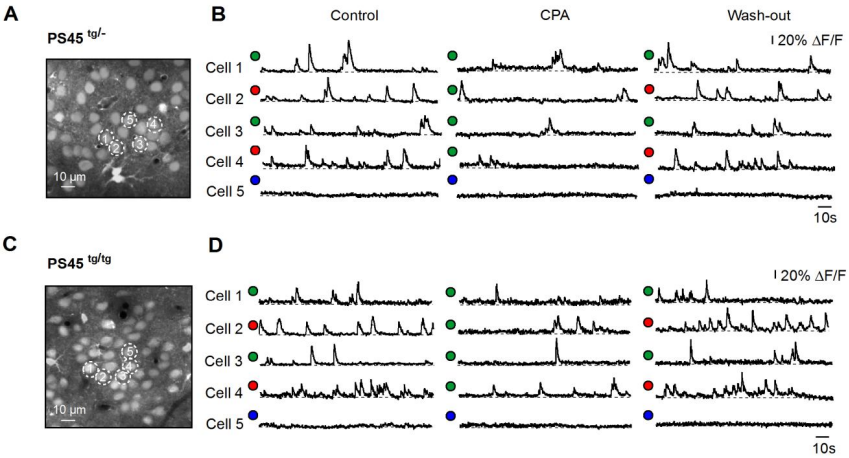

Figure 20. Effect of SERCA blocker CPA on spontaneous Ca^{2+} transients of cortical neurons in $PS45^{tg/-}$ and $PS45^{tg/tg}$ mice. A and C: Maximum intensity projection (158-164 µm ($PS45^{tg/-}$) and 161-167 µm ($PS45^{tg/tg}$) below the dura, step 1 µm) of layer 2/3 neurons of the frontal cortex in a $PS45^{tg/-}$ and a $PS45^{tg/tg}$ mouse, respectively. B and D: Traces are spontaneous Ca^{2+} transients recorded before, during, and after bath application of CPA from neurons marked with respective numbers in A and C. The colored dots indicate the type of neuron (blue, silent; green, normal; and red, hyperactive). Note a remarkable decrease in the frequency of spontaneous Ca^{2+} transients in the presence of CPA in both strains.

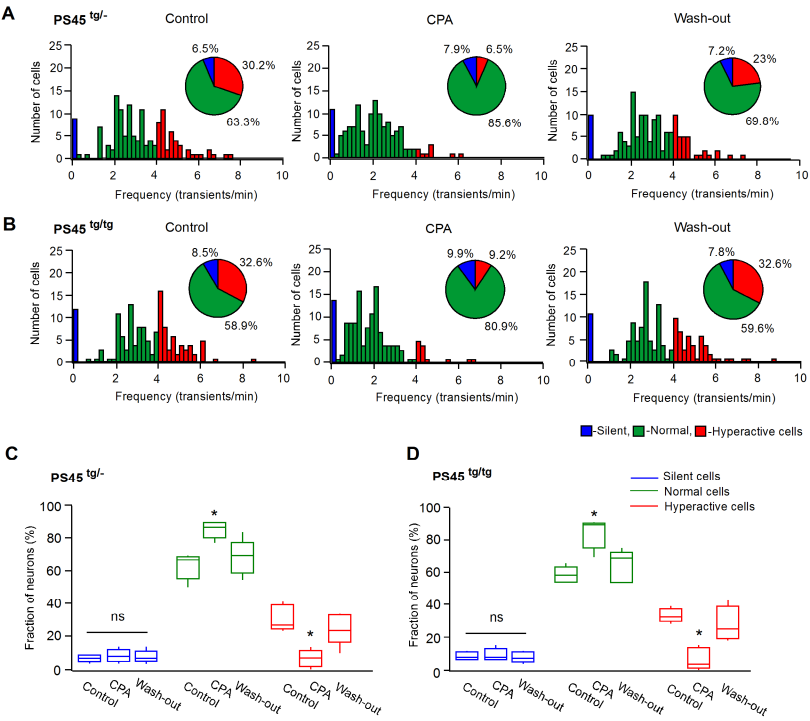

Figure 21. Blocking the Ca^{2+} release from the intracellular stores reduces hyperactivity in PS45 mice. (A and B) Histograms showing the frequency distributions of spontaneous Ca^{2+} transients. Insets: pie charts showing the relative proportion of silent, normal, and hyperactive cells recorded before, during, and after bath application of CPA in $PS45^{tg/-}$ (n= 139 cells in 5 mice) and $PS45^{tg/tg}$ (n = 141 cells in 5 mice) mice. (C and D) Box-and-whisker plots illustrating the median fractions of the three cell types under the three conditions in $PS45^{tg/-}$ and $PS45^{tg/tg}$ mice (n= 5 mice per group). Note a significant decrease in the fraction of hyperactive cells (*p<0.05; Wilcoxon Signed-Rank test) and a proportional increase in the fraction of normal cells (p>0.05; Wilcoxon Signed-Rank test) in the presence of CPA in both mouse strains. The fraction of silent cells is similar across the three conditions (p>0.05; Wilcoxon Signed-Rank test).

Table 11. Summary of the fractions of three cell types under control, CPA, and wash-out condition in PS45$^{tg/-}$ and PS45$^{tg/tg}$ mice. Data are presented as median ± IQR.

Fraction of neurons (%)	Silent cells		Normal cells		Hyperactive cells	
	PS45 $^{tg/-}$	PS45 $^{tg/tg}$	PS45 $^{tg/-}$	PS45 $^{tg/tg}$	PS45 $^{tg/-}$	PS45 $^{tg/tg}$
Control	6.70 ± 1.2	7.70 ± 3.2	66.70 ± 7.7	58.30 ± 6.9	26.60 ± 10.9	32.20 ± 3.6
CPA	7.70 ± 3	7.70 ± 3.2	86.60 ± 5.2 *	89.30 ± 8.9 *	6.70 ± 5.3 *	3.60 ± 8.4 *
Wash-out	6.70 ± 1.2	7.10 ± 4	69.20 ± 6.7	68.70 ± 15.1	23.30 ± 8.8	25 ± 14

* Significantly different compared to their respective control and wash-out values (p<0.05; Wilcoxon Signed-Rank test).

Detailed analyses showed that the frequency of normal and hyperactive cells was significantly reduced by CPA in both mouse strains (*p<0.05; Wilcoxon Signed-Rank test). Likewise, CPA significantly decreased the amplitudes of hyperactive cells (*p<0.05; Wilcoxon Signed-Rank test) but not those of normal cells (p>0.05; Wilcoxon Signed-Rank test). However, T-half and tau of normal and hyperactive cells were not affected by CPA (p>0.05; Wilcoxon Signed-Rank test) (Figure 22 and Table 12). These findings are consistent with our results obtained in AD mice.

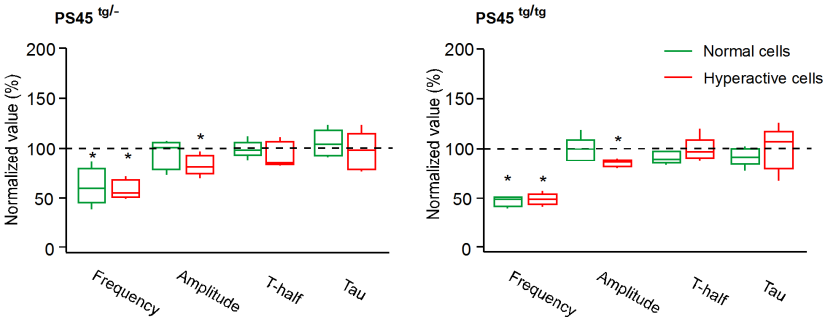

Figure 22. Intracellular Ca^{2+} stores are involved in controlling neuronal activity in $PS45^{tg/-}$ and $PS45^{tg/tg}$ mice. A comparison of median normalized frequency, amplitudes, T-half, and tau of spontaneous Ca^{2+} transients of normal and hyperactive cells in $PS45^{tg/-}$ (left panel) and $PS45^{tg/tg}$ (right panel) mice (n= 5 mice per group). CPA significantly decrease the frequency of both normal and hyperactive cells in $PS45^{tg/-}$ and $PS45^{tg/tg}$ mice (*p<0.05; Wilcoxon Signed-Rank test). The amplitudes of hyperactive cells (*p<0.05; Wilcoxon Signed-Rank test), but not that of normal cells (p>0.05; Wilcoxon Signed-Rank test), in both mouse strains are smaller in the presence of CPA. T-half and tau of normal and hyperactive cells in both mouse strains are not affected by CPA (p>0.05, Wilcoxon Signed-Rank test). All values measured under CPA are normalized to their respective control values. Dashed help lines are drawn at 100%.

Table 12. Summary of the normalized frequency, amplitude, T-half, and tau in $PS45^{tg/-}$ and $PS45^{tg/tg}$ mice. Data are presented as median ± IQR.

Normalized values (%)	Normal cells		Hyperactive cells	
	PS45 $^{tg/-}$	PS45 $^{tg/tg}$	PS45 $^{tg/-}$	PS45 $^{tg/tg}$
Frequency	60 ± 19 *	52 ± 6 *	57 ± 12 *	51 ± 4 *
Amplitude	103 ± 20	100 ± 12	82 ± 9 *	89 ± 4 *
T-half	100	92 ± 10	86 ± 17	100 ± 3
Tau	106 ± 16	94 ± 6	100 ± 25	110 ± 16

* Significantly different compared to the normalized values under control condition (100%) (p<0.05; Wilcoxon Signed-Rank test).

Thus, we concluded that intracellular Ca^{2+} stores influence the frequency of spontaneous activity in both $PS45^{tg/-}$ and $PS45^{tg/tg}$ mice, similar to the situation in AD mice. Furthermore, the store-mediated neuronal hyperactivity occurred in PS45 mice independently of plaque formation and inflammation suggesting that mutation in PS gene represents one of the mechanisms underlying neuronal hyperactivity.

3.3.2.5 Characteristics of spontaneous Ca^{2+} transients in young adult PS45 mice

Our findings raised the question whether the PS mutation-mediated neuronal hyperactivity occurs in an age-dependent manner. To this end, we extended our investigation to young adult PS45 mice at 6-7 months of age. As the results obtained above in $PS45^{tg/-}$ and $PS45^{tg/tg}$ mice were similar, we performed the experiments in $PS45^{tg/-}$ mice only. To investigate the involvement of PS mutation in neuronal activity in young adult mice, we compared the fractions of the three cell types (silent, normal, hyperactive) between young adult $PS45^{tg/-}$ (n= 142 cells in 5 mice) and age-matched WT mice analyzed previously (compared our Figure 23A to Figure 1 in Busche et al. 2008). Interestingly, the fraction of hyperactive cells in young adult $PS45^{tg/-}$ tended to be larger than those in WT mice (9.1% versus 1.2%). A significant difference in the proportion of the three cell types was observed between the mouse strains (**p<0.001, Chi-Square test). Thus, the PS mutation-mediated neuronal hyperactivity is already presented in young adult animals.

We then compared the fraction of the cell types and the frequency distribution of spontaneous Ca^{2+} transients between young adult and aged $PS45^{tg/-}$ mice. As shown in Figure 23A-D and Table 13, there was a significant increase in the fraction of hyperactive cells and a substantial decrease in the fraction of normal cells in aged $PS45^{tg/-}$ compared to young adult mice of the same strain (*p= 0.01 for both cases; Mann-Whitney test). The fraction of silent cells, however, was similar in both age groups (p= 0.34, Mann-Whitney test). Furthermore, the population of imaged neurons in aged $PS45^{tg/-}$ mice showed a higher frequency than in young adult animals as demonstrated by a rightward shift in the cumulative probability histograms (**p<0.001, Kolmogorov-Smirnov test). These results are consistent with our previous data observed in 10-14-month-old WT and AD mice suggesting that the aging process leads to an increase in neuronal hyperactivity.

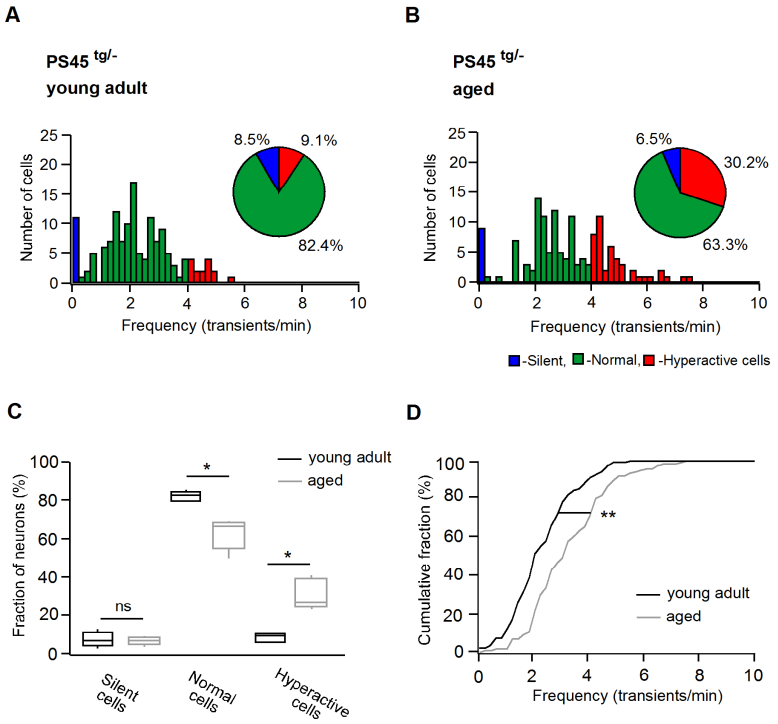

Figure 23. Aging-mediated neuronal hyperactivity in PS45$^{tg/-}$ mice. (A and B) Histograms showing the frequency distributions of spontaneous Ca^{2+} transients in 6-7-month-old (n= 142 cells in 5 mice) and 10-14-month-old PS45$^{tg/-}$ (n= 139 cells in 5 mice, the same data set as the one shown in Figure 17A) mice. Insets: pie charts showing the relative proportion of silent, normal, and hyperactive cells. Note a remarkable increase in the fraction of hyperactive cells in aged PS45$^{tg/-}$ mice. (C and D) Box-and-whisker plots illustrating the median fraction of three cell types in young adult and aged PS45$^{tg/-}$ mice (n= 5 mice per group). There is a prominent increase in the fraction of hyperactive cells and a proportional decrease in the fraction of normal cells in 10-14-month-old PS45$^{tg/-}$ mice compared to young adult animals (*p=0.01 for both cases; Mann-Whitney test). The fraction of silent cells is similar in both age groups (p=0.34; Mann-Whitney test). Cumulative probability histograms showing a higher frequency of spontaneous Ca^{2+} transients in the neuronal population analyzed in aged PS45$^{tg/-}$ than in young adult mice of the same strain (**p< 0.001, Kolmogorov-Smirnov test). ns= not significant.

Table 13. Summary of the fractions of three cell types in young adult and aged PS45 $^{tg/-}$ mice. Data are presented as median ± IQR.

	Fraction of neurons (%)	
	young adult	**aged**
Silent cells	7.70 ± 3.1	6.70 ± 1.2
Normal cells	82.80 ± 2.5	66.70 ± 7.7 *
Hyperactive cells	10.30 ± 3.8	26.60 ± 10.9*

* Significantly different compared to the respective values in young adult PS45 $^{tg/-}$ mice (p=0.01 for both cases; Mann-Whitney test).

Next, we analyzed the general features of spontaneous Ca^{2+} transients in young adult PS45$^{tg/-}$ mice. As illustrated in Figure 24A-C and Table 14, both normal and hyperactive cells had similar amplitudes, T-half, and tau (p>0.05 for all cases, Mann-Whitney test). When comparing the two age groups, there was no significant difference in the amplitudes of normal and hyperactive cells (p>0.05 for all cases, Mann-Whitney test). Interestingly, both normal and hyperactive cells in aged animals exhibited a significantly prolonged T-half (*p= 0.01 for normal and *p= 0.04 for hyperactive cells; Mann-Whitney test) and tau (*p= 0.02 for normal and *p= 0.03 for hyperactive cells; Mann-Whitney test) compared to the values obtained in young adult animals. Our findings indicate that aging also influences the general features of spontaneous neuronal activity in PS45 mice as suggested by prolonged T-half and tau of spontaneous Ca^{2+} transients.

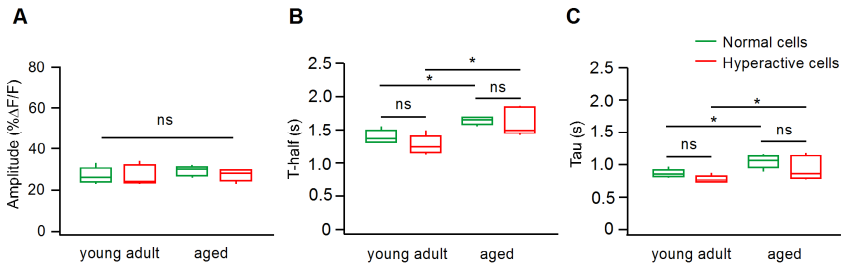

Figure 24. Prolonged spontaneous Ca^{2+} transients in aged $PS45^{tg/-}$ mice. A comparison of amplitude (A), T-half (B), and tau (C) of spontaneous Ca^{2+} transients of normal and hyperactive cells in young adult and aged $PS45^{tg/-}$ mice under control conditions. In young adult $PS45^{tg/-}$ mice, there are no significant differences between normal and hyperactive cells for all parameters tested (p>0.05 for all cases, Mann-Whitney test). When comparing between the two age groups, both normal and hyperactive cells of aged $PS45^{tg/-}$ mice exhibit significantly prolonged T-half (*p= 0.01 for normal and *p= 0.04 for hyperactive cells; Mann- Whitney test) and tau (*p= 0.02 for normal and *p= 0.03 for hyperactive cells; Mann-Whitney test). The amplitudes of both cell types are similar in both age groups (p>0.05 for all cases, Mann-Whitney test). ns= not significant.

Table 14. Summary of the amplitude, T-half, and tau of spontaneous Ca^{2+} transients of normal and hyperactive cells in young adult and aged $PS45^{+/-}$ mice. Data are presented as median ± IQR.

Parameters	Normal cells		Hyperactive cells	
	young adult	aged	young adult	aged
Amplitude (%ΔF/F)	26 ± 3	30 ± 2	24 ± 6	28 ± 3
T-half (s)	1.37 ± 0.09	1.66 ± 0.06 *	1.24 ± 0.11	1.50 ± 0.35 †
Tau (s)	0.86 ± 0.01	1.06 ± 0.07 *	0.76 ± 0.01	0.86 ± 0.29 †

* Significantly different compared to the values measured in normal cells of young adult mice (p=0.01 for T-half and p=0.02 for tau; Mann-Whitney test).

† Significantly different compared to the values measured in hyperactive cell of young adult mice (p=0.04 for T- half and p=0.03 for tau; Mann-Whitney test).

3.3.2.6 Contribution of intracellular Ca^{2+} stores to spontaneous neuronal activity in young adult PS45 mice

Next, we analyzed the effect of CPA on spontaneous neuronal activity in young adult $PS45^{tg/-}$ mice (Figure 25). Upon CPA-induced ER Ca^{2+} depletion, we observed a significant reduction in the fraction of hyperactive cells (*p<0.05, Wilcoxon Signed-Rank test) and a modest increase in the fraction of normal cells, but this did not reach statistical significance (p>0.05, Wilcoxon Signed-Rank test). The fraction of silent cells was not affected by CPA (p>0.05, Wilcoxon Signed-Rank test) (Figure 26A-B and Table 15). To characterize the effect of CPA in more detail, we normalized all values under CPA (frequency, amplitude, T-half, and tau) to their respective control values. CPA significantly decreased the frequency of normal as well as hyperactive cells (*p<0.05 for both cases; Wilcoxon Signed-Rank test). In the presence of CPA, amplitudes were significantly smaller in hyperactive cells (*p<0.05; Wilcoxon Signed-Rank test), but not in normal cells (p>0.05; Wilcoxon Signed-Rank test). T-half and tau of normal and hyperactive cells were unaltered by CPA (p>0.05; Wilcoxon Signed-Rank test) (Figure 26C and Table 16).

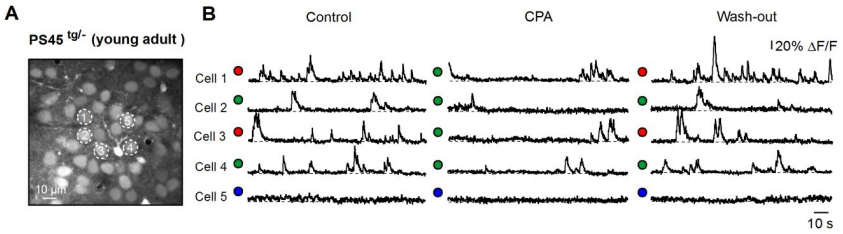

Figure 25. Effect of SERCA blocker CPA on spontaneous Ca^{2+} transients of cortical neurons in young adult $PS45^{tg/-}$ mice. (A) Maximum intensity projection (163-169 µm below the dura, step 1 µm) of layer 2/3 neurons of the frontal cortex in a $PS45^{tg/-}$ mouse at the age of 6 months. (B) Traces are spontaneous Ca^{2+} transients recorded before, during, and after bath application of CPA from neurons marked with respective numbers in (A). The colored dots indicate the type of neuron (blue, silent;

green, normal; and red, hyperactive). Note a remarkable decrease in the frequency of spontaneous Ca^{2+} transients in the presence of CPA.

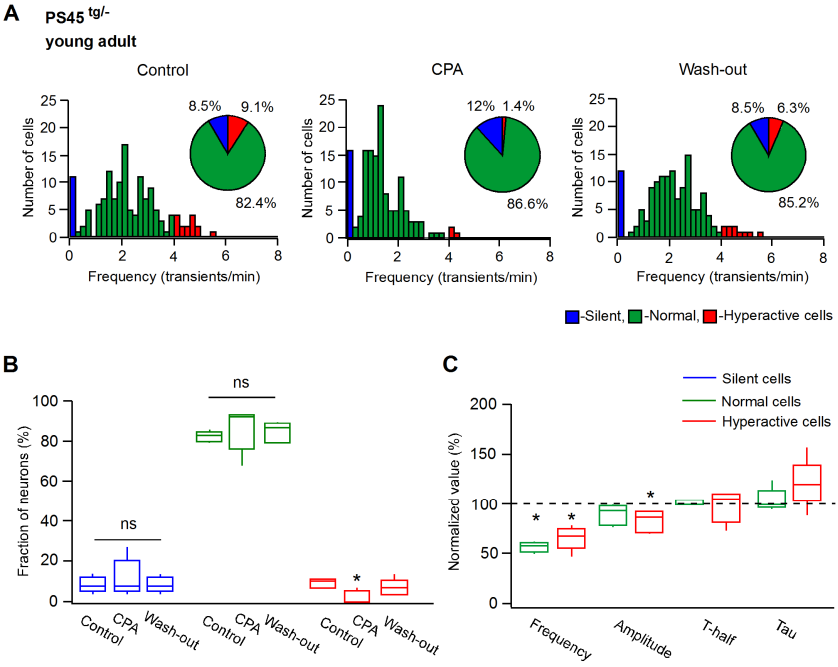

Figure 26. Neuronal hyperactivity in young adult PS45$^{tg/-}$ mice is sensitive to SERCA pump blockade. (A) Histograms showing the frequency distributions of spontaneous Ca^{2+} transients recorded before, during, and after bath application of CPA in young adult PS45$^{tg/-}$ mice (n= 142 cells in 5 mice). Insets: pie charts showing relative proportions of silent, normal, and hyperactive cells and the three conditions (B) Box-and-whisker plots illustrating the median fraction of the three cell types (n= 5 mice). Under CPA there is a small but significant decrease in the fraction of hyperactive cells (*p<0.05; Wilcoxon Signed-Rank test) and a slight increase in the fraction of normal cells, but this does not reach statistical significance (p>0.05; Wilcoxon Signed-Rank test). The fraction of silent cells is not affected by CPA (p>0.05; Wilcoxon Signed-Rank test). (C) The distribution of median normalized frequency, amplitude, T-half, and tau of spontaneous Ca^{2+} transients measured under CPA in normal and hyperactive cells (n= 5 mice). CPA significantly decreases the frequency of both normal and hyperactive cells (*p<0.05 for both cases, Wilcoxon Signed-Rank

test). Amplitudes of hyperactive cells are significantly smaller under CPA (*p<0.05; Wilcoxon Signed-Rank test), but not those of normal cells. T-half and tau of both cell types are unaltered by CPA (p>0.05 for both cases; Wilcoxon Signed-Rank test). All values measured under CPA are normalized to their respective control values. Dashed help lines are drawn at 100%. ns= not significant.

Table 15. Summary of the fractions of silent, normal, and hyperactive cells before, during and after bath application of CPA in young adult PS45$^{tg/-}$ mice. Data are presented as median ± IQR.

Fraction of neurons (%)	PS45 $^{tg/-}$ (young adult)		
	Control	CPA	Wash-out
Silent cells	7.70 ± 3.10	7.70 ± 6.4	7.70 ± 3.10
Normal cells	82.80 ± 2.50	92.30 ± 6.10	86.70 ± 9.20
Hyperactive cells	10.30 ± 3.80	0 ± 3.44 *	6.90 ± 3.30

* Significantly different compared to the respective control value (p<0.05; Wilcoxon Signed-Rank test).

Table 16. Summary of the normalized frequency, amplitude, T-half, and tau of normal and hyperactive cells in young adult PS45$^{tg/-}$ mice. Data are presented as median ± IQR.

Normalized values (%)	PS45 $^{tg/-}$ (young adult)	
	Normal cells	Hyperactive cells
Frequency	58 ± 6 *	68 ± 6 *
Amplitude	94 ± 15	88 ± 19 *
T-half	100 ± 4	105 ± 19
Tau	100 ± 3	120 ± 3

* Significantly different compared to their normalized values under control condition (100%) (p<0.05; Wilcoxon Signed-Rank test).

In summary, blocking Ca^{2+} release from intracellular stores reduced hyperactivity in young adult $PS45^{tg/-}$ mice and normalized the neuronal network activity. These findings are consistent with our results obtained in aged $PS45^{tg/-}$ mice, indicating that in $PS45^{tg/-}$ mice intracellular Ca^{2+} stores are involved in controlling the frequency of spontaneous Ca^{2+} transients in an age-independent manner.

3.3.2.7 Presynaptic Ca^{2+} signals and the role of intracellular Ca^{2+} stores in PS45 mice

Mounting evidence suggests that the presynaptic intracellular Ca^{2+} stores may participate in triggering neurotransmitter release [Llano et al., 2000; Emptage et al., 2001; Bardo et al., 2002; Simkus and Stricker, 2002]. To elucidate whether the store-mediated neuronal hyperactivity in PS45 mice is caused by presynaptic mechanisms, we labeled neurons in layer 5/6 of the motor cortex with AAV-GCaMP6f and analyzed their axonal projections to superficial cortical layer 1 (Figure 27A and B). The spontaneous Ca^{2+} transients in axonal boutons were monitored before, during, and after bath application of CPA (Figure 28A and B), and the frequencies as well as the amplitudes were analyzed across the three conditions.

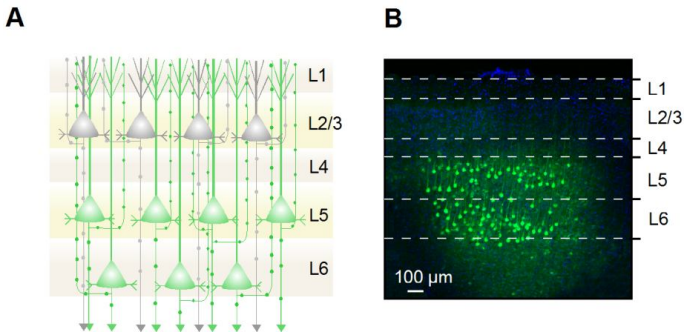

Figure 27. Layer 5/6 cortical neurons in the motor cortex labeled with AAV-GCaMP6f. (A) Schematics showing intracortical connections in the motor cortex. Labeled neurons in L5/6 are colored in green and unlabeled neurons in L2/3 are colored in gray. Thick lines represent dendrites. Axonal branches are depicted by thin lines and filled circles denote axonal boutons. (B) *Post mortem* fixed tissue slice stained with DAPI (blue). Green fluorescence reveals GCaMP6f-labeled neurons. Dashed lines indicate boundaries of the cortical layer. L1, layer 1; L2/3, layer 2/3; L4, layer 4; L5, layer 5; L6, layer 6.

After 30-min exposure to CPA, we observed a small but significant reduction in the frequencies and amplitudes of spontaneous Ca^{2+} transients in axonal boutons (n= 92 boutons in 5 mice) (*p<0.05; Wilcoxon Signed-Rank test) (Figure 28C and Table 17). This effect was reversible upon wash-out of CPA (p>0.05; Wilcoxon Signed-Rank test).

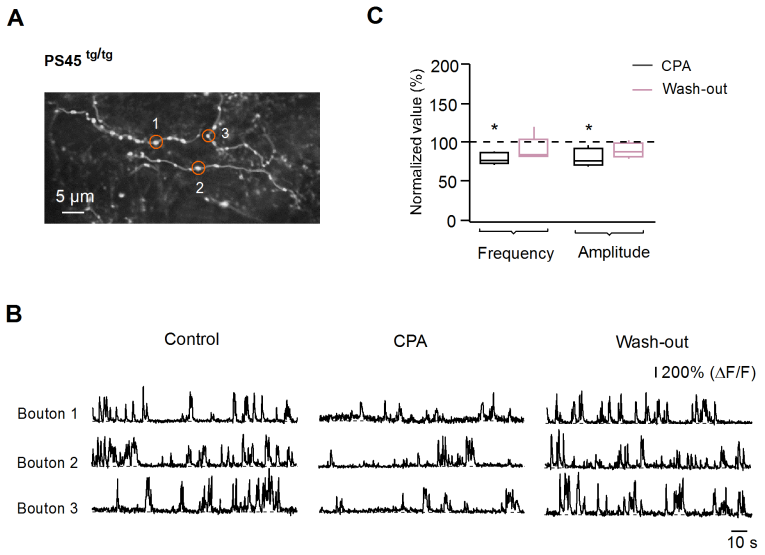

Figure 28. Intracellular Ca^{2+} stores influence the frequency and the amplitude of spontaneous Ca^{2+} transients in axonal boutons in PS45$^{tg/tg}$ mice. (A) Maximum intensity projection (21-25 µm below the dura, step 0.5 µm) of axonal segments and boutons in layer 1 of the motor cortex in a PS45$^{tg/tg}$ mouse. (B) Traces are spontaneous Ca^{2+} transients in axonal boutons recorded before, during, and after bath

application of CPA in axonal boutons marked with orange circles and respective numbers in (A). Note a decrease in the frequency of spontaneous Ca^{2+} transients in axonal boutons in the presence of CPA. (C) Box-and-whisker plots illustrating the median normalized frequencies and amplitudes of spontaneous Ca^{2+} transients in axonal boutons (n= 5 mice). CPA significantly decreased the frequency and amplitude of spontaneous Ca^{2+} transients (*p<0.05; Wilcoxon Singed-Rank test). This effect reverted upon wash-out of CPA (p>0.05 when compared to control condition; Wilcoxon Singed-Rank test). All values measured under CPA are normalized to their respective control values. A dashed help line is drawn at 100%.

Table 17. Summary of the normalized frequency and amplitude of spontaneous Ca^{2+} transients of axonal boutons in $PS45^{tg/tg}$ mice. Data are presented as median ± IQR.

Parameters	CPA	Wash-out
Normalized frequency (%)	77 ± 10*	84 ± 5
Normalized amplitude (%)	80 ± 17*	88 ± 11

* Significantly different compared to their normalized values under control condition (100%) (p<0.05; Wilcoxon Signed-Rank test).

We further investigated whether intracellular Ca^{2+} stores influence the patterns of spontaneous Ca^{2+} transients in axonal boutons. To this end, we classified Ca^{2+} transients in axonal boutons into two groups: *single transients* and *bursts* according to the criteria described in the method section (Figure 29A). Upon CPA treatment, we observed a significant reduction in the frequency of both single transients and bursts (*p<0.05; Wilcoxon Signed-Rank test), but this reduction was of a similar extent (p= 0.75; Mann-Whitney test) (Figure 29D and Table 17). Therefore, the relative fractions of single transients and bursts observed under CPA did not differ from those observed under control conditions (p>0.05 for both cases; Wilcoxon Signed-Rank test) (Figure 29B and C and Table 18).

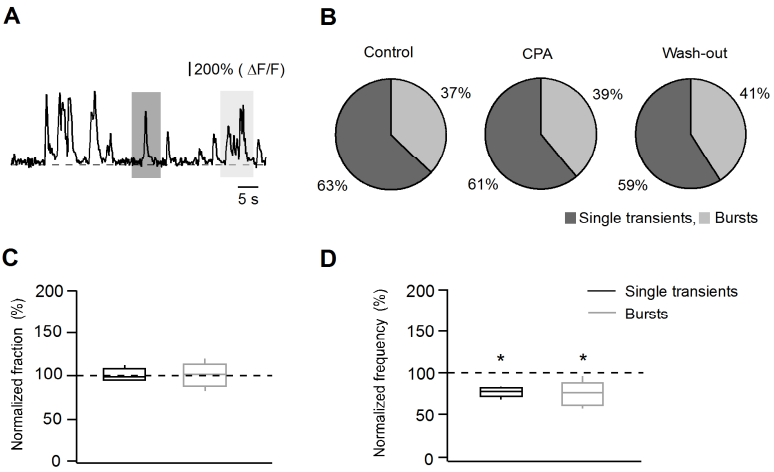

Figure 29. Effect CPA on single transients and bursts in axonal boutons in PS45$^{tg/tg}$ mice. (A) Representative example of spontaneous Ca^{2+} transients in an axonal bouton. A dark gray box indicates a single transient and a light gray box indicates a burst. (B) Pie charts showing the relative proportion of single transients and bursts recorded before, during, and after bath application of CPA (n= 92 boutons in 5 mice). Box-and-whisker plots illustrating the median normalized fraction (C) and frequency (D) of single transients and bursts of spontaneous Ca^{2+} transients in axonal boutons (n= 5 mice). The fractions of both firing patterns are not affected by CPA (p>0.05; Wilcoxon Signed-Rank test), while the frequencies of both firing patterns are significantly decreased in the presence of CPA (*p<0.05; Wilcoxon Singed-Rank test).

Table 18. Summary of the normalized fraction and frequency of single transients and bursts in PS45$^{tg/tg}$ mice. Data are presented as median ± IQR.

Parameters	Single transients	Bursts
Normalized fraction (%)	99 ± 7	101 ± 12
Normalized frequency (%)	79 ± 4*	78 ± 15*

* Significantly different compared to their normalized values under control condition (100%) (p<0.05; Wilcoxon Signed-Rank test).

From the obtained results, we concluded that the intracellular Ca^{2+} stores are involved in controlling Ca^{2+} transients in axonal boutons, but influence the generation of single transients and bursts in a similar manner. We have to mention, however, that in this experimental protocol the craniotomy was performed closed to the viral injection site. Therefore, we cannot exclude that CPA diffuses to layer 5/6 and partially depleted the intracellular Ca^{2+} stores in the somata of these cells.

3.3.2.8 The contribution of presynaptic glutamate release on postsynaptic spontaneous neuronal activity in PS45 mice

To investigate the contribution of presynaptic glutamate release on postsynaptic neuronal activity, the effect of activity-dependent irreversible NMDAR blocker MK-801 on spontaneous somatic Ca^{2+} transients was examined in PS45 mice. As we have not seen any difference neither in the basic properties of spontaneous Ca^{2+} transients in $PS45^{tg/-}$ and $PS45^{tg/tg}$ mice nor in their response to CPA, the experiments were performed in $PS45^{tg/-}$ mice only. In this protocol, spontaneous Ca^{2+} transients were monitored before and every 10 minutes during topical application of 200 µM MK-801. To reach a plateau of the antagonistic effect, MK-801 was applied for a long period of time (~ 2 hr). Following parameters were analyzed in these experiments: the maximum reduction of frequency, the time required to reach a half maximum reduction of frequency, and the amplitudes of spontaneous Ca^{2+} transients.

As shown in Figure 30A, in the presence of MK-801 the frequency of spontaneous Ca^{2+} transients measured in normal and hyperactive cells gradually decreased and finally reached a plateau level. For analysis, we normalized all the recorded values to the respective control values in the absence of MK-801. There was a significant decrease in the frequency of either normal (n = 34 cells in 5 mice) or hyperactive cells (n= 20 cells in 5 mice, normalized frequency 60±26% and 60±23% for

normal and hyperactive cells, respectively, *p<0.05 for both cases; Wilcoxon Signed-Rank test) and the degree of reduction was similar for both cell types (p=0.92; Mann-Whitney test) (Figure 30B). Interestingly, the time required to reach a half maximum reduction of frequency was significantly shorter for hyperactive cells compared to that measured in normal cells (15.50±7 s versus 30±12.75 s, *p=0.02; Mann-Whitney test) (Figure 30C). The amplitudes of spontaneous Ca^{2+} transients measured in both cell types were unaffected by MK-801 (p>0.05; Wilcoxon Signed-Rank test) (Figure 30D). Our results suggest that the frequency of spontaneous Ca^{2+} transients measured in somata of layer 2/3 neurons in $PS45^{tg/-}$ mice depends on activation of postsynaptic NMDA receptors. Furthermore, postsynaptic NMDA receptors in hyperactive cells have higher open probability compared to that in normal cells, which is likely due to an increased presynaptic release probability of respective glutamatergic synapses.

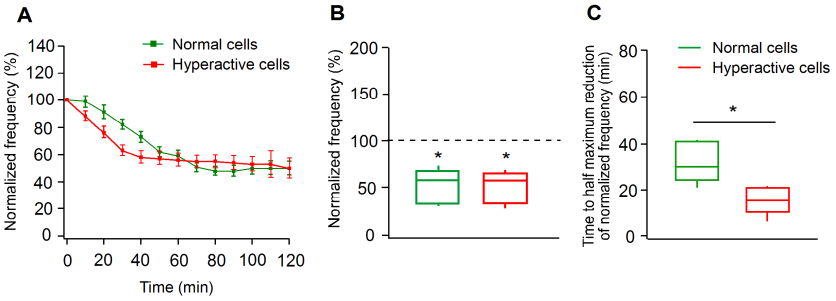

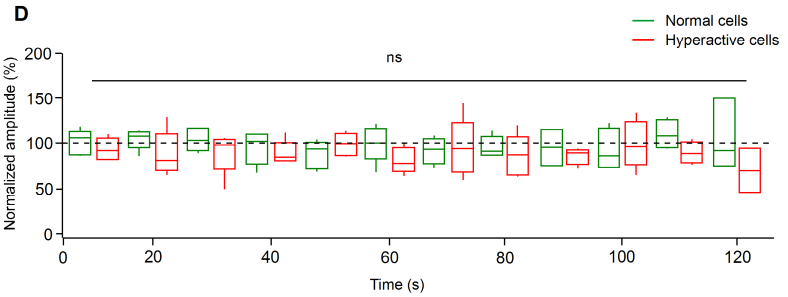

Figure 30. Effect of MK-801 treatment on spontaneous Ca^{2+} transients in $PS45^{tg/-}$ mice. (A) Normalized frequency versus time plot showing the effect of bath-applied MK-801 in normal (green line; n= 34 cells in 5 mice) and hyperactive cells (red line; n= 20 cells in 5 mice). Data are presented as mean±SEM**.** Box-and-whisker plots showing the median maximum reduction in frequency (B), the time to half maximum reduction of frequency (C), and the amplitudes (D) of spontaneous Ca^{2+} transients in the presence of MK-801 (n= 5 mice). There is a significant reduction of frequency for both normal and hyperactive cells (*p<0.05 for both cases, Wilcoxon Signed-Rank test). The time to half maximum reduction of frequency measured in hyperactive cells is significantly shorter compared to that measured in normal cells (*p=0.02; Mann-Whitney test). The amplitudes of both normal and hyperactive cells are not affected by MK-801 (p>0.05; Wilcoxon Signed-Rank test). Dashed help lines are drawn at 100%.

3.3.2.9 The role of intracellular Ca^{2+} stores for spontaneous dendritic Ca^{2+} signals in PS45 mice

Next, we investigated how mutant PS1-mediated dysfunction of Ca^{2+} stores impacts spontaneous dendritic Ca^{2+} transients in $PS45^{tg/-}$ mice. To do so, we examined the effect of CPA on spontaneous Ca^{2+} transients in dendritic branches of layer 2/3 pyramidal neurons, which were loaded with a small molecule Ca^{2+} indicator OGB-1 by means of electroporation (see methods for further details). We first classified the recorded cell as normal or hyperactive by recording the spontaneous somatic Ca^{2+} transients. Then, we switched to recording of spontaneous Ca^{2+} transients in apical dendritic branches. The transients were monitored before, during, and after bath application of CPA, similar to the previous protocols (Figure 31A). Dendritic Ca^{2+} transients obtained

from paired branch recordings were categorized into *local* and *synchronous transients* according to the approach mentioned in the methods section (Figure 31B).

After depletion of intracellular Ca^{2+} stores by CPA, there was a pronounced decrease in the frequency of spontaneous dendritic Ca^{2+} transients measured in either normal (n= 40 branches from 14 cells in 9 mice, normalized frequency 61±8%, $^{**}p<0.01$; Wilcoxon Signed-Rank test) or hyperactive cells (n= 34 branches from 14 cells in 9 mice, 60±24%, $^{**}p<0.01$; Wilcoxon Signed-Rank test) and this decrease was of a similar extent ($p=0.75$, Mann-Whitney test) (Figure 31C). Interestingly, hyperactive cells also exhibited a significant reduction in the amplitudes of local and synchronous dendritic Ca^{2+} transients (n= 26 branches from 9 cells in 6 mice, $^{*}p<0.05$ for both cases; Wilcoxon Signed-Rank test). The reduction in the former was stronger than in the latter ($^{*}p=0.03$; Mann-Whitney test). In normal cells, the amplitudes of local and synchronous dendritic Ca^{2+} transients were not affected by CPA (n= 30 branches from 10 cells in 6 mice, $p>0.05$ for both cases; Wilcoxon Signed-Rank test) (Figure 31D and Table 19). To analyze the effect of CPA in more detail, we compared the fractions of local and synchronous dendritic Ca^{2+} transients across the three conditions. Surprisingly, there was a significant increase in the fraction of local dendritic Ca^{2+} transients and a proportional decrease in the fraction of synchronous dendritic Ca^{2+} transients measured in hyperactive cells ($^{**}p<0.01$; Wilcoxon Signed-Rank test). The values obtained from normal cells exhibited similar trends, but these trends did not reach significance ($p>0.05$ for both cases; Wilcoxon Signed-Rank test) (Figure 32A-B and Table 20).

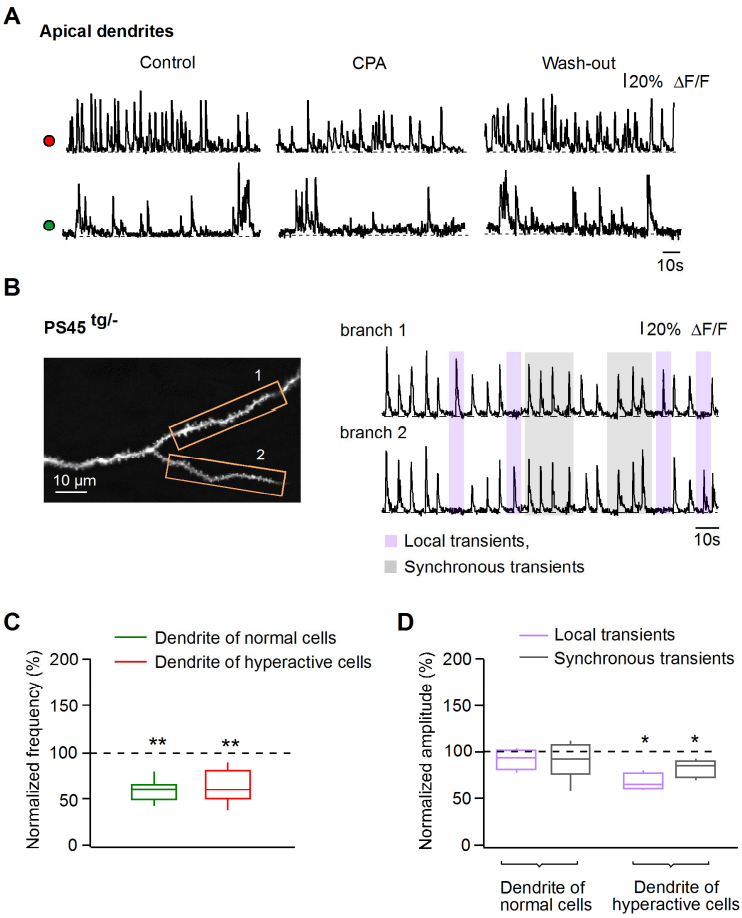

Figure 31. Effect of CPA on spontaneous dendritic Ca^{2+} transients in $PS45^{tg/-}$ mice. (A) Traces are spontaneous dendritic Ca^{2+} transients recorded before, during, and after bath application of CPA. The colored dots indicate the type of neuron (green, normal and red, hyperactive cell). Note a decrease in the frequency of spontaneous dendritic Ca^{2+} transients measured in normal and hyperactive cells in the presence of CPA. (B) Left panel: Maximum intensity projection (153-157 µm below the dura, step 0.5 µm) of apical dendritic branches of an electroporated pyramidal neuron. Orange boxes indicate regions chosen for simultaneous recording of spontaneous Ca^{2+} transients. Traces in the right panel are spontaneous dendritic Ca^{2+} transients recorded from dendritic branches marked with respective numbers in the left panel.

Gray boxes indicate synchronous spontaneous dendritic Ca^{2+} transients occurring in both branches at the same time. Purple boxes indicate local spontaneous dendritic Ca^{2+} transients occurring independently in one of the branches. (C) Box-and-whisker plots illustrating the distribution of median normalized frequency of spontaneous dendritic Ca^{2+} transients measured in normal and hyperactive cells (n= 9 mice). In the presence of CPA, there is a significant decrease in the frequency of spontaneous dendritic Ca^{2+} transients measured in both cell types (**p<0.01; Wilcoxon Signed-Rank test) and these decreases are similar for both cell types (p=0.75; Mann-Whitney test). (D) The distribution of median normalized amplitudes of local and synchronous dendritic Ca^{2+} transients measured in normal and hyperactive cells (n= 6 mice). In hyperactive cells, CPA significantly decreased the amplitudes of local and synchronous dendritic Ca^{2+} transients (*p<0.05; Wilcoxon Signed-Rank test). The reduction of amplitudes in the former was stronger than in the latter (*p=0.03; Mann-Whitney test). There was no change in the amplitudes of local and synchronous spontaneous dendritic Ca^{2+} transients measured in normal cells during CPA treatment (p>0.05; Wilcoxon Signed-Rank test). All values measured under CPA are normalized to their respective control values. Dashed help lines are drawn at 100%.

Table 19. Summary of the normalized amplitude of local and synchronous dendritic Ca^{2+} transients of normal and hyperactive cells measured under CPA in PS45 $^{tg/-}$ mice. Data are presented as median ± IQR.

	Normalized amplitude (%)	
	Dendrite of normal cells	**Dendrite of hyperactive cells**
Local transients	95 ± 14	66 ± 12 *
Synchronous transients	93 ± 19	85 ± 12 *

* Significantly different compared to their respective normalized values under control condition (100%) (p<0.05; Wilcoxon Signed-Rank test).

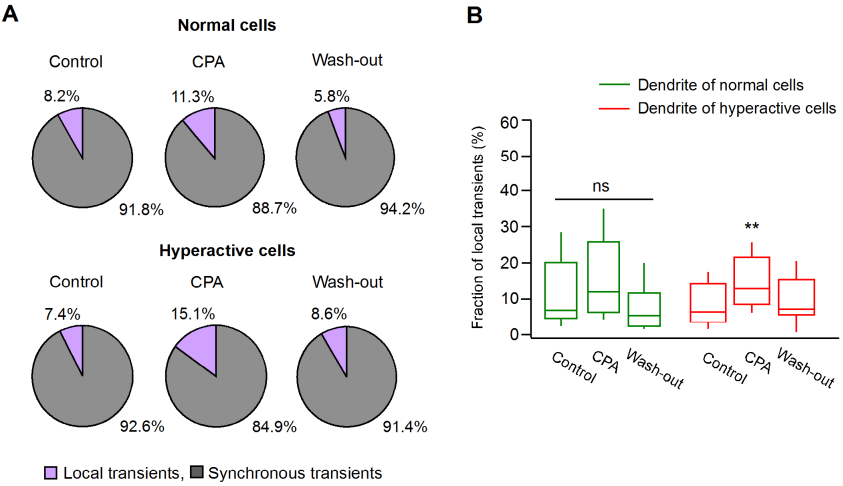

Figure 32. Intracellular Ca^{2+} stores influence the synchronization of spontaneous dendritic Ca^{2+} transients in PS45 $^{tg/-}$ mice. (A) Pie charts showing the relative proportion of local and synchronous dendritic Ca^{2+} transients measured in normal (n= 30 branches from 10 cells in 6 mice) and hyperactive (n= 26 branches from 9 cells in 6 mice) cells before, during and after CPA application. (B) Box-and-whisker plots showing the median fraction of local and synchronous dendritic Ca^{2+} transients measured in normal (n= 9 cells) and hyperactive (n= 9 cells) cells. There is a significant increase in the fraction of local spontaneous Ca^{2+} transients of dendrites measured in hyperactive cells (**p< 0.01; Wilcoxon Signed-Rank test) during CPA application. The values obtained from the dendrites measured in normal cells show similar trends, but these results do not reach the level of significance (p>0.05 for both cases; Wilcoxon Signed-Rank test). ns = not significant.

Table 20. Summary of the fractions of local and synchronous dendritic Ca^{2+} transients measured in normal and hyperactive cells before, during, and after bath application of CPA in PS45 $^{tg/-}$ mice. Data are presented as median ± IQR.

Fraction of transients (%)	Local transients		Synchronous transients	
	Normal cells	Hyperactive cells	Normal cells	Hyperactive cells
Control	7 ± 10.88	6.17 ± 7.58	93 ± 10.88	93.83 ± 7.58
CPA	12 ± 14.60	12.77 ± 7.94**	88 ± 14.60	87.23 ± 7.95**
Wash-out	5.46 ± 5.46	7.48 ± 3.06	94.54 ± 5.46	92.52 ± 3.05

** Significantly different compared to their respective values in control and wash-out conditions (p<0.01; Wilcoxon Signed-Rank test).

Next, we compared the data obtained from dendritic recordings to those from the somatic recordings, obtained previously (see above) in the same mouse strain. As illustrated in Figure 33A-B and Table 21-22, under CPA the spontaneous Ca^{2+} transients of either somata or dendrites measured in normal and hyperactive cells exhibited a significant reduction of the frequency (*p<0.05 for all cases; Wilcoxon Signed-Rank test). Additionally, the amplitudes of the somatic and the dendritic Ca^{2+} transients measured in hyperactive cells were significantly smaller (*p<0.05 for all cases; Wilcoxon Signed-Rank test). In normal cells, CPA did not influence the amplitudes of neither somata nor dendrites (p>0.05 for all cases; Wilcoxon Signed-Rank test). The overall effect of CPA on the spontaneous Ca^{2+} transients in somata and dendrites measured in both cell types was similar to each other (p>0.05 for all cases; Mann-Whitney test).

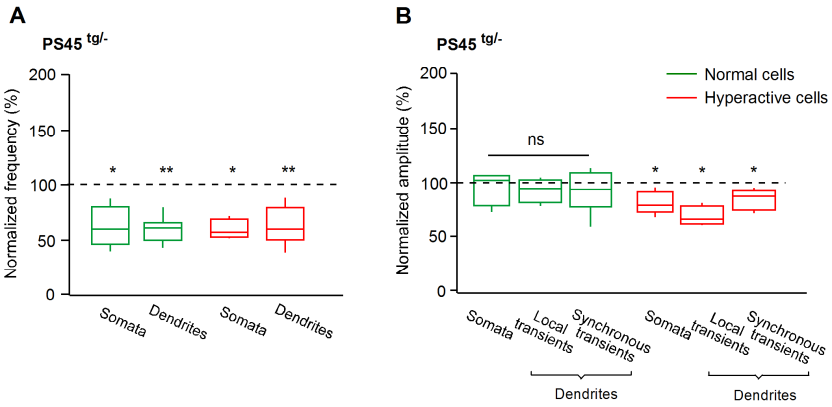

Figure 33. Intracellular Ca^{2+} stores are involved in controlling the spontaneous Ca^{2+} transients in both somata and dendrites in PS45$^{tg/-}$ mice. Box-and-whisker plots illustrating the distribution of median normalized frequencies (A) and amplitudes (B) of spontaneous Ca^{2+} transients of somata and dendrites measured in normal and hyperactive cells during CPA treatment in PS45 $^{tg/-}$ mice. Note that there is a significant reduction in the frequency of either somata or dendrites measured in normal and hyperactive cells (*p<0.05 for all cases; Wilcoxon Signed-Rank test) and the effects on somata and dendrites are similar to each other (p>0.05 for all cases; Mann-Whitney test). In hyperactive cells, CPA significantly decrease the amplitudes both in somata and in dendrites (*p<0.05 for all cases; Wilcoxon Signed-Rank test) and this reduction in the amplitudes is of a similar extent (p>0.05 for all cases; Mann-Whitney test). In normal cells, CPA does not influence the amplitudes neither in somata nor in dendrites (p>0.05 for all cases; Wilcoxon Signed-Rank test) and the effects are similar for soma and dendrites of both cell types (p>0.05 for all cases; Mann-Whitney test). All values measured under CPA are normalized to their respective control values. Dashed help lines are drawn at 100%. ns= not significant.

Table 21. Summary of the normalized frequency of spontaneous Ca^{2+} transients of somata and dendrites measured in normal and hyperactive cells under CPA in PS45 $^{tg/-}$ mice. Data are presented as median ± IQR.

	Normalized frequency (%)	
	Normal cells	**Hyperactive cells**
Somata	60 ± 19 *	57 ± 12 *
Dendrites	61 ± 8 *	60 ± 24 *

* Significantly different compared to their respective normalized values under control condition (100%) (p<0.05; Wilcoxon Signed-Rank test).

Table 22. Summary of the normalized amplitude of spontaneous Ca^{2+} transients of somata and dendrites measured in normal and hyperactive cells under CPA in PS45 $^{tg/-}$ mice. Data are presented as median ± IQR.

	Normalized amplitude (%)	
	Normal cells	**Hyperactive cells**
Somata	103 ± 20	82 ± 9 *
Dendrites		
local transients	95 ± 14	66 ± 12 *
synchronous transients	93 ± 19	85 ± 12 *

* Significantly different compared to their respective normalized values under control condition (100%) (p<0.05; Wilcoxon Signed-Rank test).

In summary, our data demonstrate that intracellular Ca^{2+} stores are involved in controlling the frequency and the synchronization of spontaneous dendritic Ca^{2+} transients. Additionally, the intracellular Ca^{2+} stores play a role in modulating the spontaneous activity of both somata and dendrites in a similar manner.

Chapter 4

Discussion

4.1 Aging-mediated increase in neuronal hyperactivity

The present study describes an alteration of ongoing spontaneous neuronal activity in the frontal cortex of aged mice. Using *in vivo* two-photon Ca^{2+} imaging technique, we observed an increase in the neuronal activity in 10-14-month-old mice as suggested by a robust increase in the fraction of hyperactive cells compared to that in 6-10-month-old animals. Interestingly, this result was observed not only in AD and PS45$^{tg/-}$ mice, but also in WT mice. On average, the fraction of hyperactive cells increased by approximately 20% in aged mice of all three strains, indicating that age progression aggravates neuronal hyperactivity. Obtained results provided additional evidence to support Khachaturian's hypothesis that dysregulation of neuronal Ca^{2+} homeostasis is linked to brain aging in the first place [Khachaturian, 1989]. A previous study using learning tasks with implanted electrodes in hippocampus has demonstrated an abnormal increase in firing rates of CA3 neurons in aged rats (25-27 months old) compared to young adult rats (6-8 months old). Interestingly, in aged rats these hyperactive neurons fail to encode new spatial information and cause a progressive memory impairment [Wilson et al., 2005]. A recent electrophysiological study in hippocampal slices has also shown that CA3 neurons in aged rats (29-32 months old) exhibit higher action potential firing rates and faster action potential repolarizations than CA3 neurons in young adult rats (2-5 months old). These results are mediated by enhanced expression of A-type potassium channels (Kv4.2/Kv4.30) [Simkin et al., 2015]. Our results expand the above findings and show that aging-mediated increase in neuronal hyperactivity is a widespread phenomenon which also affects neuronal network in the frontal cortex.

Given the results obtained from three different mouse strains in this study, a common denominator is the aging processes. One can think about three possible mechanisms of aging-mediated increase in neuronal hyperactivity. The first possible explanation is a slight depolarization of the cell membrane. It is generally accepted that aging

is associated with an increased amount of oxidative stress and a progressive decline in the antioxidant defense [Zaidi, 2010]. The imbalance of these mechanisms leads to an excessive production of free radicals which damage various biomolecules such as lipids, proteins, and DNA [Uttara et al., 2009]. Age-related oxidative stress occurs in multiple organ systems, including the brain [Mattson, 2007; Supnet and Bezprozvanny, 2010]. The free radical-mediated lipid peroxidation of the neuronal membrane will eventually promote membrane-associated oxidative stress (MAOS). MAOS disrupts neuronal energy metabolism and ion homeostasis by impairing the function of ion- motive ATPases, glutamate and glucose transporters. These changes promote membrane depolarization and Ca^{2+} influx through NMDA receptors and VGCC which further increase the Ca^{2+} accumulation within neurons [Mattson MP, 2004, 2007; Stranahan and Mattson, 2012]. The second explanation is an increase in presynaptic spontaneous transmitter release. The perturbation in Ca^{2+} homeostasis, glucose or energy deprivation, and oxidative stress occurring in aged neurons can interfere with ER function and promote ER stress [Brown and Naidoo, 2012]. The result of a study using cultured hippocampal neurons has reported the impact of ER stress on synaptic transmission. The mentioned above depolarization-induced increase in $[Ca^{2+}]_i$ as well as ER stress-mediated increase in Ca^{2+} sensitivity of the presynaptic spontaneous transmitter release machinery [Nosyreva and Kavalali, 2010] increase the amount of neurotransmitter release from excitatory synapses. The third explanation is a low-grade inflammation-mediated neuronal excitability. The aging process in the brain also causes a dysregulation of the immune system which is characterized by immunosenescence and a chronic low-grade inflammation [Jurgens and Johnson, 2012; Gabuzda and Yankner, 2013; Deleide et al., 2015]. Studies in the brain of normal aged mice have illustrated an overall increase in the levels of proinflammatory cytokines, including interleukin-1 beta (IL-1β), interleukin-6 (IL-6), and tumor necrosis factor alpha (TNF-α) [Godbout et al., 2005; Chen et al., 2008; Dugan et al., 2009; Baron et al., 2014]. Several studies have provided evidence for a link between

proinflammatory cytokines and neuronal excitability. For example, in a study on cultured hippocampal neurons, IL-1β increased NMDA receptor function through activation of tyrosine kinase 2 and subsequent NR2A/B subunit phosphorylation, thereby enhancing NMDA receptor-mediated Ca^{2+} influx [Viviani et al., 2003]. A more recent study using electrophysiological approaches reported that TNF-α increases surface localization of NMDA receptor NR1 subunits [Wheeler et al., 2009]. Furthermore, TNF-α preferentially increases synaptic expression of GluR2-lacking AMPA receptors. This is important as AMPA receptors lacking this subunit become permeable to Ca^{2+} [Jonas et al., 1994]. There is also evidence for a TNF-α-mediated increase in the frequency of spontaneous miniature postsynaptic currents in cultured hippocampal neurons [Grassi et al., 1994]. In addition, it has been reported that IL-1β and TNF-α impair the synaptic excitation-inhibition balance. One likely mechanism for this is a TNF-α- or IL-1β-mediated inhibition of astrocyte glutamate uptake [Hu et al., 2000; Ye et al., 1996]. Another possible mechanism is that TNF-α causes an endocytosis of $GABA_A$ receptors [Stellwagen et al., 2005]. We incorporate these age-associated changes into a model of aging-mediated increase in neuronal hyperactivity (Figure 34).

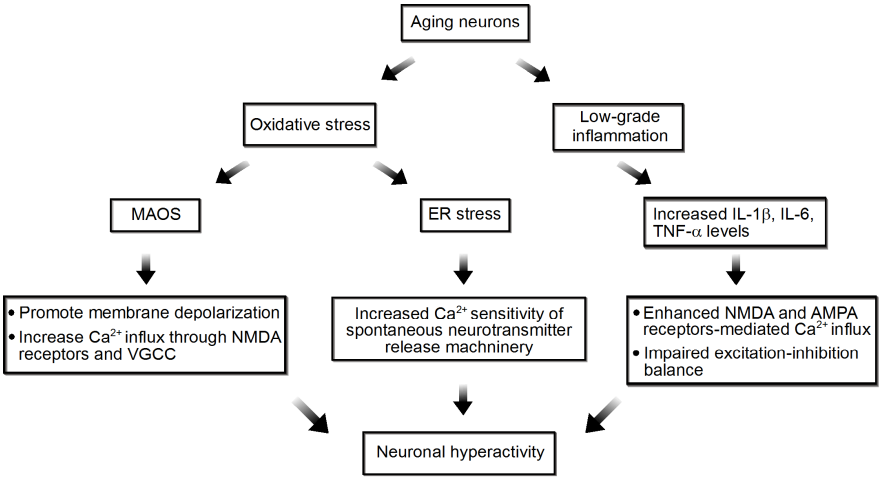

Figure 34. A schematic drawing of the proposed mechanisms of aging-mediated increase in neuronal hyperactivity. MAOS, membrane-associated oxidative stress; ER, endoplasmic reticulum; IL-1β, interleukin-1 beta; IL-6, interleukin-6; TNF-α, tumor necrosis factor alpha; NMDA, N-methyl-D-aspartate; AMPA, α-amino-3-hydroxy-5-methyl-4-isoxazolepropionic acid; VGCC, voltage-gated Ca^{2+} channels.

4.2 Enhanced caffeine-induced Ca^{2+} release from intracellular stores in amyloid-depositing mice

We have first established a technique that enables the *in vivo* study of the function of intracellular Ca^{2+} stores. Using this new technique, our data revealed that application of RyR agonist caffeine results in a greater Ca^{2+} release from the intracellular stores in AD compared to WT mice. This statement is substantiated by the following findings: (i) a prolonged sustained phase of elevated $[Ca^{2+}]_i$, as indicated by increased T-half and tau of caffeine-induced Ca^{2+} transients, (ii) an increase in unitary caffeine-evoked responses, as suggested by the increased AUC ratio. We also observed a trend toward increased amplitude of caffeine-induced Ca^{2+} transients in AD compared to WT mice, but this difference

did not reach the level of statistical significance (Figure 8). Considering responses of the three different cell types in AD mice (i.e. silent, normal, and hyperactive cells), the enhancement of caffeine-induced Ca^{2+} transients was most pronounced in hyperactive cells (Figure 10). Our findings confirmed and extended previous *in vitro* observations which reported exaggerated caffeine-induced Ca^{2+} signals in several AD models. Studies using primary neuronal cultures and acute brain slice preparations obtained from 3xTg AD mice and PS1-M146V KI mice have demonstrated large increases in caffeine-induced Ca^{2+} responses. [Chan et al., 2000; Smith et al., 2005; Stutzmann et al., 2006; Chakroborty et al., 2009; Zhang et al., 2010]. Similar alterations have also been observed in APP_{swe} and APP_{695}- expressing SH-SY5Y neuroblastoma cells [Oules et al., 2012]. Thus, our results reinforce the notion that aberrant Ca^{2+} signaling contribute to AD pathology and provide for the first time *in vivo* evidence for the dysregulation of ER Ca^{2+} homeostasis.

Exacerbated caffeine-induced Ca^{2+} signals observed here could simply be due to an elevated ER Ca^{2+} accumulation. Indeed, our AD mouse model carries the PS1-G384A mutation which has been proposed to cause a disruption of the function of ER Ca^{2+} leak channels, thereby leading to overloaded ER Ca^{2+} stores [Tu et al., 2006; Nelson et al., 2007]. Another possible explanation is an alteration in the function and/or expression of RyR in AD mice. Several studies have demonstrated an increase in RyR expression levels in different AD models and its link to APP and/or PS mutations. The previous studies reported that RyR isoform 3 is upregulated in mutant PS expressing PC12 cells, hippocampal neurons from PS1-M146V KI mice [Chan et al., 2000], and cortical neurons from $APP_{swe/ind}$ mice [Supnet et al., 2006; Supnet et al., 2010]. Additionally, an upregulation of RyR isoform 2 has been reported in the hippocampal tissue of 3xTg AD mice [Chakroborty et al., 2009]. Based on our present findings and those of previous studies, we propose a mechanism accounting for an enhanced caffeine-induced Ca^{2+} release from intracellular stores in the intact cerebral

cortex of AD mice (Figure 35). We hypothesize that the PS-mediated passive ER Ca^{2+} leakage in WT mice exhibits normal function and therefore provides the proper control of ER Ca^{2+} levels. In AD mice, the passive ER Ca^{2+} leakage is disrupted by PS mutation and thus ER Ca^{2+} levels are enhanced. Furthermore, the RyR expression is elevated in AD compared to WT mice, which leads to an enhanced amount of Ca^{2+} released in response to an agonist application. These mechanisms result in an exacerbated caffeine-induced Ca^{2+} signals in AD mice.

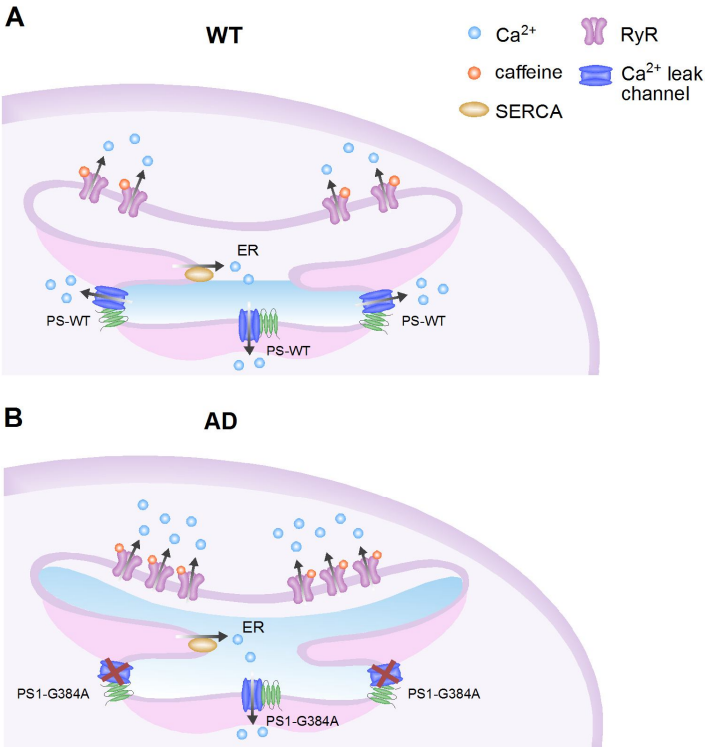

Figure 35. A proposed mechanism for an enhanced caffeine-induced Ca^{2+} release from intracellular stores in AD mice. (A) The PS-mediated passive ER Ca^{2+} leak channels in WT mice show normal function. These channels provide the proper control of ER Ca^{2+} levels. (B) In AD mice, the ER Ca^{2+} leak activity of PS is impaired, which in turn, leads to overloaded ER Ca^{2+} stores. Additionally, the RyR expression levels are upregulated. Therefore, the application of RyR agonist caffeine results in exacerbated caffeine-induced Ca^{2+} signals in AD compared to WT mice. Note the ER Ca^{2+} levels are represented by the blue area. Arrows indicate the direction of Ca^{2+} flux. ER, endoplasmic reticulum; RyR, ryanodine receptor; SERCA, sarcoplasmic / endoplasmic Ca^{2+}-ATPase; PS, presenilin. Not all receptors are shown.

The dysregulation of ER Ca^{2+} homeostasis may have a detrimental effect on neuronal survival and may contribute to AD pathology. It has been reported, for example, that overloaded ER Ca^{2+} stores enhance the vulnerability of cells to apoptosis [LaFerla, 2002]. The perturbation of ER Ca^{2+} signals disrupts protein folding and eventually leads to ER stress [Brown and Naidoo, 2012]. Additionally, an increase in ER Ca^{2+} release can further trigger increased Aβ formation and increased hyperphosphorylated tau [Querfurth and Selkoe, 1994]. Furthermore, the synaptic dysfunction and cognitive deficits can be affected by aberrant ER Ca^{2+} signaling [Chakroborty et al., 2009; Peng et al., 2012; Oules et al., 2012].

4.3 NMDA receptor activation-mediated CICR in amyloid-depositing mice

Our results reveal that *in vivo* NMDA-mediated Ca^{2+} entry triggers local Ca^{2+} release from intracellular Ca^{2+} stores in AD mice. This finding is consistent with previous *in vitro* studies which reported that the activation of NMDA receptors contributed to CICR in the acute brain slice preparations from 3xTg AD mice [Goussakov et al., 2010]. In our experiments, NMDA-mediated CICR is most profound in hyperactive cells compared to that in silent and normal cells (Figure 11). These data correlate with our observation that the pronounced response of caffeine-

induced Ca^{2+} transients was also observed in hyperactive cells, indicating that in AD mice hyperactive cells exhibit a stronger overfilling of intracellular Ca^{2+} stores relative to silent and normal cells in AD mice.

4.4 Store depletion normalizes pathological activity patterns in amyloid-depositing mice

So far, the underlying causes of neuronal network hyperactivity in AD pathology are not entirely clear. It has been proposed that this phenomenon might be due to the direct effect of Aβ species [Busche et al., 2008; Grienberger et al., 2012; Busche et al., 2012], the relative decrease in synaptic inhibition [Busche et al., 2008], and proinflammatory substances released from plaque-associated glial cells [review in Brawek and Garaschuk, 2014]. In this study, we demonstrate that emptying of intracellular Ca^{2+} stores though CPA treatment normalizes pathological activity patterns in AD mice (Figure 13). This is due to a remarkable decrease in the frequency of spontaneous somatic Ca^{2+} transients of both normal and hyperactive cells in AD, but not in WT mice. Among different cell types in AD mice, a reduction in the amplitudes of spontaneous somatic Ca^{2+} transients upon CPA treatment was observed only in hyperactive cells (Figure 14). This indicates that the contribution of Ca^{2+} release from intracellular stores to the amplitudes of spontaneous somatic Ca^{2+} transients is stronger in hyperactive cells than in normal cells. Thus, our results provide evidence that important mechanism underlying the neuronal network hyperactivity in AD mice may be related to Ca^{2+} release from intracellular stores. In WT mice, however, the neuronal network hyperactivity was insensitive to store depletion, suggesting that there may be another mechanism underlying this phenomenon.

4.5 PS1 mutation-mediated neuronal network hyperactivity

We report here for the first time that the FAD-linked PS1 G384A mutation can cause the neuronal network hyperactivity in the frontal cortex of PS45 mice. We observed a striking increase in the fraction of hyperactive cells and a proportional decrease in the fraction of normal cells in 10-14-month-old $PS45^{tg/-}$ and $PS45^{tg/tg}$ mice when compared to age-matched WT mice (Figure 17). Interestingly, we found that the fractions of three cell types (silent, normal, and hyperactive cells), the frequency distributions, and the general features of spontaneous somatic Ca^{2+} transients were similar in both $PS45^{tg/-}$ and $PS45^{tg/tg}$ mouse strains (Figure 18). This suggests that the mutant PS1 gene dosage does not influence the frequency pattern and the characteristics of spontaneous somatic Ca^{2+} transients. The results of immunohistochemical stainings demonstrate that aged $PS45^{tg/tg}$ mice do not develop amyloid plaque depositions. Furthermore, there were neither signs of microglial activation nor reactive astrogliosis (Figure 15-16), indicating that the neuronal hyperactivity in PS45 mice occurs independently of plaque formation and inflammation. We further investigated the effect of intracellular Ca^{2+} stores on neuronal network hyperactivity in PS45 mice. Under CPA, there was a pronounced decrease in the frequency, but not in the T-half and tau, of both normal and hyperactive cells. Additionally, a selective reduction in the amplitudes of spontaneous somatic Ca^{2+} transients was observed in hyperactive cells. Interestingly, blocking Ca^{2+} release from intracellular Ca^{2+} stores reduced hyperactivity of both PS45 strains in a similar manner to that observed in AD mice (Figure 21 and 22). Therefore, the PS1 G384A mutation alone is sufficient to mediate neuronal network hyperactivity.

To investigate whether the PS mutation-mediated neuronal hyperactivity occurs in an age-specific manner, we extended our observation to young adult $PS45^{tg/-}$ mice at 6-7 months of age. Interestingly, the fraction of hyperactive cells in young adult $PS45^{tg/-}$ mice tended to be larger than

that in age-matched WT mice analyzed previously [Busche et al., 2008]. Hence, neuronal hyperactivity occurs already in young adult PS45$^{tg/-}$ mice. Furthermore, blocking Ca^{2+} release from intracellular stores reduced hyperactivity and normalized the neuronal network activity in young adult PS45$^{tg/-}$ mice. A reduction in the amplitudes of spontaneous somatic Ca^{2+} transients was observed in hyperactive cells, but not in normal cells (Figure 26). These findings are consistent with our results obtained in aged PS45$^{tg/-}$ mice, indicating that in PS45$^{tg/-}$ mice the intracellular Ca^{2+} stores are involved in controlling the frequency and amplitudes (in hyperactive cells) of spontaneous somatic Ca^{2+} transients in an age-independent manner. Surprisingly, different results were observed when we compared our findings in young adult PS45$^{tg/-}$ mice with a previous study [Grienberger et al., 2012] using a similar technique. Their results have shown that the fraction of hyperactive cells in the visual cortex in 8-10-month-old PS45 mice was similar to that in age-matched WT mice. The cause of this discrepancy remains unknown, but the different intracortical wiring in the visual and frontal cortex may be a contributing factor.

When comparing general features of spontaneous somatic Ca^{2+} transients between young adult and aged PS45$^{tg/-}$ mice, we found that both normal and hyperactive cells in aged animals exhibited a delay in $[Ca^{2+}]_i$ recovery as suggested by prolonged T-half and tau of spontaneous somatic Ca^{2+} transients (Figure 24). Generally, the duration of elevated $[Ca^{2+}]_i$ following neuronal excitation is determined by the clearance of cytosolic Ca^{2+} and the capacity of cytosolic Ca^{2+} binding proteins, e.g. calmodulin and calbindin [Toescu and Verkhratsky, 2000]. We speculate that the prolonged spontaneous somatic Ca^{2+} transients in aged neurons might be related to the following mechanisms. First, an age-dependent decrease in the effectiveness of plasma membrane Ca^{2+} extrusion pathways like PMCA and NCX. Previous studies have demonstrated a decrease in PMCA pumping activity and the expression level of PMCA in aged rat brains. It has been proposed that a suppression of PMCA activity is associated

with conformational changes of PMCA induced by oxidative modifications [Zaidi et al., 1998; Zaidi and Michaelis, 1999; Zaidi, 2010; Zaidi et al., 2015]. A progressive decline in the effectiveness of calmodulin in stimulating PMCA activity has also been reported in aged rat brains. This effect is related to oxidative modifications of methionine residues leading to a loss of structural stability of calmodulin [Zaidi et al., 1998; Gao et al., 1999]. Additionally, a decline of NCX activity due to a reduction in its affinity for Ca^{2+} transport has been observed in aged rats [Gomez-Villafuertes et al., 2007]. Second, the prolonged spontaneous Ca^{2+} transients may be caused by a reduction of cytoplasmic Ca^{2+} buffer capacity. Studies in aged rat brains have reported a reduction in the number of calbindin-immunoreactive neurons in several brain regions, including hippocampus and perirhinal cortex [Toescu and Verkhratsky, 2000; Moyer et al., 2011]. Thus, an age-related decline in the function of PMCA and NCX together with a reduction in capacity of cytosolic Ca^{2+} binding may result in the prolonged decay phase of spontaneous somatic Ca^{2+} transients in aged $PS45^{tg/-}$ mice.

4.6 The contribution of intracellular Ca^{2+} stores to pre- and postsynaptic Ca^{2+} signals in PS45 mice

Our results prompted us to further investigate whether store-mediated neuronal network hyperactivity in PS45 mice is caused by pre- or postsynaptic mechanisms. The investigations of the presynaptic compartment provided two major evidences. First, our findings show a significant decrease in the frequency and amplitudes of spontaneous Ca^{2+} transients in axonal boutons in the presence of CPA (Figure 28 and 29), implying that the presynaptic intracellular Ca^{2+} stores influence the transmitter release. This evidence is in close agreement with previous studies in the acute brain slice preparation and the hippocampal slice culture, which also demonstrated a role of presynaptic intracellular Ca^{2+} stores in modulating spontaneous and evoked transmitter release [Llano

et al., 2000; Bardo et al., 2002; Emptage et al., 2001; Simkus and Stricker, 2002; Galante and Marty, 2003]. However, we could only observe little effect on the distribution of single transients and burst, implying that the pattern of spontaneous Ca^{2+} transients in axonal boutons occurs independently of presynaptic intracellular Ca^{2+} stores. Second, we found a significant reduction in the frequency of spontaneous somatic Ca^{2+} transients of both normal and hyperactive cells during MK-801 treatment, indicating an influence of presynaptic glutamate release on the frequency of spontaneous somatic Ca^{2+} transients. Furthermore, the time required to reach a half maximum reduction of frequency was significantly shorter in hyperactive cells compared to normal cells. This result implies that the synapses on hyperactive cells exhibit higher open probability of the postsynaptic NMDA receptors than that in normal cells which is likely due to the higher probability of presynaptic glutamate release (Figure 30).

The analyses of postsynaptic dendritic compartments provide the following conclusions. First, intracellular Ca^{2+} stores are involved in controlling the frequency of spontaneous dendritic Ca^{2+} transients in normal and hyperactive cells. This notion comes from the finding that the depletion of intracellular Ca^{2+} stores significantly reduced the frequency of spontaneous dendritic Ca^{2+} transients in normal and hyperactive cells (Figure 31A and B). Our results are consistent with previous studies in the CA1 region of rat hippocampal slice [Manita and Ross, 2009]. Their results described the role of Ca^{2+} release from intracellular stores in modulating the frequency of spontaneous Ca^{2+} events in dendritic branches in pyramidal neurons. Second, we observed a selective reduction in the amplitudes of local and synchronous dendritic Ca^{2+} transients in hyperactive cells, but not in normal cells, upon emptying of intracellular Ca^{2+} stores, indicating that the amplitudes of spontaneous dendritic Ca^{2+} transients in hyperactive cells are amplified by Ca^{2+} release from intracellular stores (Figure 31). Third, intracellular Ca^{2+} stores are at least in part responsible for the synchronization of spontaneous dendritic Ca^{2+} transients and this synchronization is slightly

more pronounced in hyperactive cells. Our findings are in agreement with previous studies in rat hippocampal slice which demonstrated that Ca^{2+} release from intracellular stores contributes to the propagation of Ca^{2+} transients in apical dendrites of pyramidal neurons. Additionally, the initiation of dendritic Ca^{2+} transients occurs at branch points where IP_3R and RyR accumulated [Manita and Ross, 2009; Ross, 2012]. Based on this evidence, we assume that the synchronization of paired dendritic branches arises from the store-mediated propagation of spontaneous dendritic Ca^{2+} transients. Blocking Ca^{2+} release from intracellular stores leads to a reduction of the propagation which can be detected as an increase in the fraction of local transients and a proportional decrease in the fraction of synchronous transients (Figure 32).

4.7 Possible mechanisms underlying intracellular Ca^{2+} store-mediated neuronal hyperactivity in PS45 mice

Based on the results of the present study, we propose a model to account for the neuronal network hyperactivity in PS45 mice. We hypothesize that the hyperactivity may be related to an increased probability of transmitter release from presynaptic terminals. In this model, an increase of Ca^{2+} liberation from presynaptic intracellular Ca^{2+} stores through RyR and IP_3R causes an increase in $[Ca^{2+}]_i$, which in turn, triggers the fusion of synaptic vesicles with the plasma membrane of presynaptic terminals. This enhances the transmitter release and subsequently increases the frequency of postsynaptic Ca^{2+} transients. The emptying of intracellular Ca^{2+} stores with CPA reduces Ca^{2+} release from intracellular Ca^{2+} stores, thereby decreasing the $[Ca^{2+}]_i$ in the presynaptic terminal. This decreases the synaptic vesicle release which eventually leads to a reduction in the frequency of postsynaptic spontaneous Ca^{2+} transients (Figure 36).

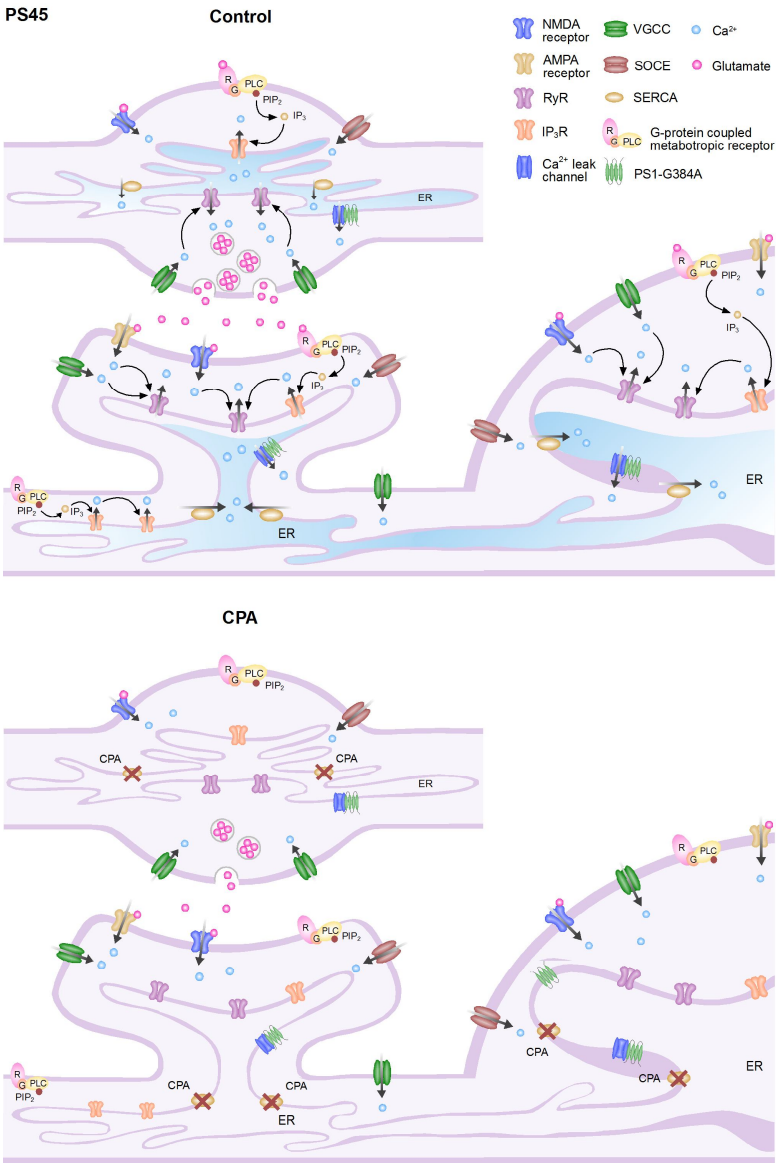
PS45
Control
NMDA receptor
VGCC
Ca2+
AMPA receptor
SOCE
Glutamate
RyR
SERCA
IP3R
G-protein coupled metabotropic receptor
Ca2+ leak channel
PS1-G384A
ER
CPA

Figure 36. A propose mechanism for intracellular Ca^{2+} stores-mediated increase in a probability of transmitter release from presynaptic terminals in PS45 mice. Schematic illustration of the experimental condition under control (upper panel) and during CPA treatment (lower panel) in PS45 mice. Note the ER Ca^{2+} levels are represented by the blue area. Arrows indicate direction of ion flux. ER, endoplasmic reticulum; RyR, ryanodine receptor; IP_3R, inositol triphosphate receptor; IP_3, inositol 1,4,5-trisphosphate; PIP_2, phosphatidylinositol 4,5-bisphosphate; SERCA, sarcoplasmic / endoplasmic Ca^{2+}-ATPase; NMDA, N-methyl-D-aspartate; AMPA, α-amino-3-hydroxy-5-methyl-4-isoxazolepropionic acid; VGCC, voltage-gated Ca^{2+} channels; PLC, phospholipase C; SOCE, store-operated Ca^{2+} entry. Not all receptors are shown.

Additionally, a decrease in transmitter release from presynaptic terminal likely also leads to a reduction in the amplitude of postsynaptic Ca^{2+} transients in hyperactive cells. Furthermore, a reduction in CICR in the postsynaptic compartment might contribute to the reduced amplitudes of postsynaptic Ca^{2+} transients as well as to the de-synchronization of postsynaptic Ca^{2+} transients between the dendritic branches.

4.8 Clinical implications

Several studies suggest the detrimental consequences of aberrant neuronal hyperactivity on neuronal network function. The first consequence would be a sustained increase of $[Ca^{2+}]_i$ which can further activates protein phosphatase calcineurin [Kuchibhotla et al., 2008]. The excessive calcineurin activity has been proposed to cause dendritic degeneration, including dendritic beading and spine loss [Zeng et al., 2007]. Second, the neuronal hyperactivity may contribute to behavioral and memory deficits. Studies using task-related functional magnetic resonance imaging (fMRI) have reported an involvement of hippocampal hyperactivity in performance deficits in patient with amnestic mild cognitive impairment (aMCI) [Bakker et al., 2012, Yassa et al., 2010]. Third, evidence from an fMRI study in nondemented aged human has shown that the hippocampal hyperactivity is associated with progressive

cortical atrophy [Putcha et al., 2011]. Fourth, there are several lines of evidence demonstrating the neuronal activity-dependent regulation of Aβ secretion [Cirrito et al., 2005; Bero et al., 2011]. In rat hippocampal slices treated with Aβ oligomers, the neuronal hyperactivity results in enhanced synaptic release of Aβ and its oligomerization at synaptic sites [Deshpande et al., 2009]. This result is consistent with *in vivo* study in transgenic mice overexpressing APP with Swedish and Austrain mutation, which has shown that the optogenetically induced neuronal hyperactivity upregulates Aβ production and increases Aβ release from presynaptic terminals [Yamamoto et al., 2015].

A recent work using a new technology called chemogenetic approach which allows selective activation or inhibition of affected neurons has demonstrated that a chronic attenuation of neuronal hyperactivity *in vivo* reduces a degree of amyloid deposition and synaptic pathology associated with amyloid plaques in 5xFAD and APP_{swe}/PS1deltaE9 mice [Yuan and Grutzendler, 2016]. Several studies raise the possibility that an attenuation of aberrant neuronal network hyperactivity might be a potential therapeutic for AD. Studies in patients and animal models have described an effect of an antiepileptic drug levetiracetam on neuronal hyperactivity. A treatment with low dose levetiracetam normalizes hippocampal hyperactivity and improves memory performance during a cognitive task in patient with aMCI [Bakker et al., 2012]. Furthermore, evidence from $APP_{swe/ind}$ mice has indicated that long-term treatment with levetiracetam reduces epileptiform activity, improves memory performance, and reverses synaptic deficits and plasticity [Sanchez et al., 2012]. Consistent with these findings, a protective effect of levetiracetam on behavioral deficits has been reported in APP_{swe}/PS1deltaE9 mice [Shi et al., 2013]. In addition, a high dose treatment of valproic acid, an antiepileptic drug with Na^+ channel blocking property, has been shown to reduce the frequency of epileptiform discharges in APP_{swe}/PS1deltaE9 mice [Ziyatdinova et al., 2011]. Another recent study has reported that an acute treatment with the γ-secretase inhibitor completely reverses neuronal hyperactivity and

reduces soluble Aβ levels in APP23/PS45 mice [Busche et al., 2012]. Additionally, it was found that a genetic ablation of gene encoding tau in $APP_{swe/ind}$ mice normalizes neuronal hyperactivity, ameliorates the severity of the seizure phenotype, and prevents behavioral deficits [Roberson et al., 2007, 2011].

To date, the only available therapeutic for AD is symptomatic treatment which can temporarily ameliorate the symptoms and improve quality of life for patients [Selkoe, 2013]. There are two types of drugs which have been approved for AD treatment: acetylcholinesterase inhibitors and NMDA receptor agonists. However, there is no existing preventative and curative therapy that effectively reverses or stops AD progression. Current researches in AD drug development focus mainly on modulation of amyloid deposition, for example anti-amyloid aggregation agents, Aβ immunotherapy, β-secretase inhibitors, γ-secretase inhibitors, and α-secretase potentiation. Additionally, drugs interfering with tau deposition and anti-inflammatory agents have been identified [Selkoe, 2013; Yiannopoulou and Papageorgiou, 2013]. Our results reveal that blocking the Ca^{2+} release from intracellular stores through CPA treatment normalizes neuronal network hyperactivity associated with FAD-linked PS1 mutation. Therefore, we propose that normalizing Ca^{2+} release from ER might be an effective strategy to slow down pathological progression of AD. Although CPA has been approved for research purpose only, a RyR inhibitor dantrolene might be an attractive drug since it is approved by the Food and Drug Administration (FDA) for clinical treatment. Besides its potential therapeutic benefit for malignant hyperthermia and muscle spasticity, dantrolene also has a neuroprotective effect [Muehlschlegel and Sims, 2009; Liang and Wei, 2015]. Recent works have reported beneficial effects of dantrolene treatment in AD mouse models. *In vivo* long-term dantrolene treatment (11 months) starting prior to the onset of amyloid deposition improves learning ability and decreases amyloid plaque burden in the hippocampus in 3xTg AD mice [Peng et al., 2012]. Chronic dantrolene treatment (3 months) also restores cognitive function in aged APP_{swe}

mice. Additionally, dantrolene reduces a production of C99 fragment from APP and extracellular Aβ load in primary cultured neurons isolated from APP_{swe} mice [Oules et al., 2012]. Another study has described the beneficial effects of sub-chronically short term (4 weeks) dantrolene treatment. This short-term treatment regimen normalizes expression levels of RyR2 and restores synaptic transmission and plasticity homeostasis in 3xTg AD mice. In addition, the amyloid plaque deposition within the cortex and hippocampus is reduced in dantrolene-treated APP_{swe}/PS1-M146V mice [Chakrobotry et al., 2012].

Conclusion

Our data reveal that the function of intracellular Ca^{2+} stores is altered in the intact cerebral cortex of AD mice as suggested by exacerbated RyR-mediated Ca^{2+} release signals. Additionally, hyperactive cells in AD mice exhibit a stronger overfilling of their intracellular Ca^{2+} stores as indicated by a most pronounced CICR via NMDA-mediated Ca^{2+} influx. Furthermore, our study demonstrates an abnormal increase in neuronal hyperactivity in the frontal cortex in aged AD, $PS45^{tg/-}$, and WT mice compared to that in young adult animals, implicating that age progression aggravates neuronal hyperactivity. As shown in store depletion experiments, this hyperactivity has a store-independent (in WT mice) as well as an additional store-dependent (in AD and PS45 mice) component. Consistently, the store depletion normalizes pathological activity patterns in amyloid-depositing mice. Obtained results from PS45 mice provide the evidence that FAD-linked PS1 G384A mutation alone is sufficient to mediate neuronal hyperactivity. Interestingly, this phenomenon is independent of gene dosage, plaques formation, and inflammation, but rather dependent on Ca^{2+} release from intracellular Ca^{2+} stores. In addition, intracellular Ca^{2+} stores are critically involved in controlling the frequency of pre-and postsynaptic Ca^{2+} signals as well as the synchronization of spontaneous dendritic Ca^{2+} transients in PS45 mice. This suggests the contribution of intracellular Ca^{2+} stores to

network-driven spontaneous Ca^{2+} transients. These results further strengthen the relevance of dysregulation of Ca^{2+} homeostasis in AD pathology. Thus, we propose that modulation of neuronal network hyperactivity by reducing Ca^{2+} release from intracellular Ca^{2+} stores may serve as a feasible therapeutic strategy for treating AD.

References

Alberdi E, Sanchez-Gomez MV, Cavaliere F, Perez-Samartin A, Zugaza JL, Trullas R, Domercq M, and Matute C (2010) Amyloid Beta Oligomers Induce Ca^{2+} Dysregulation and Neuronal Death through Activation of Ionotropic Glutamate Receptors. *Cell Calcium* 47(3): 264-72.

Amatniek JC, Hauser WA, DelCastillo-Castaneda C, Jacobs DM, Marder K, Bell K, Albert M, Brandt J, and Stern Y (2006) Incidence and Predictors of Seizures in Patients with Alzheimer's Disease. *Epilepsia* 47(5): 867-72.

Almeida CG, Tampellini D, Takahashi RH, Greengard P, M. T. Lin MT, Snyder EM, and Gouras GK (2005) Beta-Amyloid Accumulation in App Mutant Neurons Reduces Psd-95 and Glur1 in Synapses *Neurobiol Dis* 20(2): 187-98.

Annunziato L, Pignataro G, and Di Renzo GF (2004) Pharmacology of Brain Na^{+}/Ca^{2+} Exchanger: From Molecular Biology to Therapeutic Perspectives. *Pharmacol Rev* 56(4): 633-54.

Arispe N, Pollard HB, and Rojas E (1993) Giant Multilevel Cation Channels Formed by Alzheimer Disease Amyloid Beta-Protein [a Beta P-(1-40)] in Bilayer Membranes. *Proc Natl Acad Sci U S A* 90(22): 10573-7.

Auffret A, Gautheron V, Mattson MP, Mariani J, and Rovira C (2010) Progressive Age-Related Impairment of the Late Long-Term Potentiation in Alzheimer's Disease Presenilin-1 Mutant Knock-in Mice. *J Alzheimers Dis* 19(3): 1021-33.

Bakker A, Krauss GL, Albert MS, Speck CL, Jones LR, Stark CE, Yassa MA, Bassett SS, Shelton AL, and Gallagher M (2012) Reduction of Hippocampal Hyperactivity Improves Cognition in Amnestic Mild Cognitive Impairment. *Neuron* 74(3): 467-74.

Ballard C, Gauthier S, Corbett A, Brayne C, Aarsland D, and Jones E (2011) Alzheimer's Disease. *Lancet* 377(9770): 1019-31.

Bardo S, Robertson B, and Stephens GJ (2002) Presynaptic Internal Ca^{2+} Stores Contribute to Inhibitory Neurotransmitter Release onto Mouse Cerebellar Purkinje Cells. *Br J Pharmacol* 137(4): 529-37.

Bardo S, Cavazzini MG, and Emptage N (2006) The Role of the Endoplasmic Reticulum Ca^{2+} Store in the Plasticity of Central Neurons. *Trends Pharmacol Sci* 27(2): 78-84.

Baron R, Babcock AA, Nemirovsky A, Finsen B, and Monsonego A (2014) Accelerated Microglial Pathology Is Associated with Abeta Plaques in Mouse Models of Alzheimer's Disease. *Aging Cell* 13(4): 584-95.

Bero AW, Yan P, Roh JH, Cirrito JR, Stewart FR, Raichle ME, Lee JM, and Holtzman DM (2011) Neuronal Activity Regulates the Regional Vulnerability to Amyloid-Beta Deposition. *Nat Neurosci* 14(6): 750-6.

Berridge MJ (1998) Neuronal Calcium Signaling. *Neuron* 21(1): 13-26.

Berridge MJ (2002) The Endoplasmic Reticulum: A Multifunctional Signaling Organelle. *Cell Calcium* 32(5-6): 235-49.

Berridge MJ, Bootman MD, and Roderick HL (2003) Calcium Signalling: Dynamics, Homeostasis and Remodelling. *Nat Rev Mol Cell Biol* 4(7): 517-29.

Berridge MJ (2010) Calcium Hypothesis of Alzheimer's Disease. *Pflugers Arch* 459(3): 441-9.

Bertram L and Tanzi RE. (2008) Thirty Years of Alzheimer's Disease Genetics: The Implications of Systematic Meta-Analyses. *Nat Rev Neurosci* 9(10): 768-78.

Bezprozvanny I and Mattson MP (2008) Neuronal Calcium Mishandling and the Pathogenesis of Alzheimer's Disease. *Trends Neurosci* 31(9): 454-63.

Bojarski L, Pomorski P, Szybinska A, Drab M, Skibinska-Kijek A, Gruszczynska-Biegala J, and Kuznicki J (2009) Presenilin-Dependent Expression of STIM Proteins and Dysregulation of Capacitative Ca^{2+} Entry in Familial Alzheimer's Disease. *Biochim Biophys Acta* 6(7): 6.

Brawek B and Garaschuk O (2014) Network-Wide Dysregulation of Calcium Homeostasis in Alzheimer's Disease. *Cell Tissue Res* 357(2): 427-38.

Brion JP (1998) Neurofibrillary Tangles and Alzheimer's Disease. *Eur Neurol* 40(3): 130-40.

Brown MK and Naidoo N (2012) The Endoplasmic Reticulum Stress Response in Aging and Age-Related Diseases. *Front Physiol* 3(263).

Bruno AM, Huang JY, Bennett DA, Marr RA, Hastings ML, and Stutzmann GE (2012) Altered Ryanodine Receptor Expression in Mild Cognitive Impairment and Alzheimer's Disease. *Neurobiol Aging* 33(5): 30.

Busche MA, Eichhoff G, Adelsberger H, Abramowski D, Wiederhold KH, Haass C, Staufenbiel M, Konnerth A, and Garaschuk O (2008) Clusters of Hyperactive Neurons near Amyloid Plaques in a Mouse Model of Alzheimer's Disease. *Science* 321(5896): 1686-9.

Busche MA, Chen X, Henning HA, Reichwald J, Staufenbiel M, Sakmann B, and Konnerth A (2012) Critical Role of Soluble Amyloid-Beta for Early

Hippocampal Hyperactivity in a Mouse Model of Alzheimer's Disease. *Proc Natl Acad Sci U S A* 109(22): 8740-5.

Cedazo-Minguez A, Popescu BO, Ankarcrona M, Nishimura T, and Cowburn RF (2002) The Presenilin 1 DeltaE9 Mutation Gives Enhanced Basal Phospholipase C Activity and a Resultant Increase in Intracellular Calcium Concentrations. *J Biol Chem* 277(39): 36646-55.

Celsi F, Pizzo P, Brini M, Leo S, Fotino C, Pinton P, and Rizzuto R (2009) Mitochondria, Calcium and Cell Death: A Deadly Triad in Neurodegeneration. *Biochim Biophys Acta* 5: 335-44.

Chakroborty S, Goussakov I, Miller MB, and Stutzmann GE (2009) Deviant Ryanodine Receptor-Mediated Calcium Release Resets Synaptic Homeostasis in Presymptomatic 3xTg-AD Mice. *J Neurosci* 29(30): 9458-70.

Chakroborty S, Briggs C, Miller MB, Goussakov I, Schneider C, Kim J, Wicks J, Richardson JC, Conklin V, Cameransi BG, and Stutzmann GE (2012) Stabilizing ER Ca^{2+} Channel Function as an Early Preventative Strategy for Alzheimer's Disease. *PLoS One* 7(12): 21.

Chan SL, Mayne M, Holden CP, Geiger JD, and Mattson MP (2000) Presenilin-1 Mutations Increase Levels of Ryanodine Receptors and Calcium Release in PC12 Cells and Cortical Neurons. *J Biol Chem* 275(24): 18195-200.

Chang EH, Savage MJ, Flood DG, Thomas JM, Levy RB, Mahadomrongkul V, Shirao T, Aoki C, and Huerta PT (2006) AMPA receptor downscaling at the onset of Alzheimer's disease pathology in double knockin mice. *Proc Natl Acad Sci USA* 103(9): 3410-3415.

Chen J, Buchanan JB, Sparkman NL, Godbout JP, Freund GG, and Johnson RW (2008) Neuroinflammation and Disruption in Working Memory in Aged Mice after Acute Stimulation of the Peripheral Innate Immune System. *Brain Behav Immun* 22(3): 301-11.

Cheung KH, Shineman D, Muller M, Cardenas C, Mei L, Yang J, Tomita T, Iwatsubo T, Lee VM, and Foskett JK (2008) Mechanism of Ca^{2+} Disruption in Alzheimer's Disease by Presenilin Regulation of InsP3 Receptor Channel Gating. *Neuron* 58(6): 871-83.

Cheung KH, Mei L, Mak DO, Hayashi I, Iwatsubo T, Kang DE, and Foskett JK (2010) Gain-of-Function Enhancement of IP3 Receptor Modal Gating by Familial Alzheimer's Disease-Linked Presenilin Mutants in Human Cells and Mouse Neurons. *Sci Signal* 3(114): 2000818.

Cirrito JR, Yamada KA, Finn MB, Sloviter RS, Bales KR, May PC, Schoepp DD, Paul SM, Mennerick S, and Holtzman DM (2005) Synaptic Activity Regulates Interstitial Fluid Amyloid-Beta Levels in Vivo. *Neuron* 48(6): 913-22.

Cleary JP, Walsh DM , Hofmeister JJ, Shankar GM, Kuskowski MA, Selkoe DJ, and Ashe KH (2005) Natural Oligomers of the Amyloid-Beta Protein Specifically Disrupt Cognitive Function. *Nat Neurosci* 8 (1): 79-84.

Deleidi M, Jaggle M, and Rubino G (2015) Immune Aging, Dysmetabolism, and Inflammation in Neurological Diseases. *Front Neurosci* 9(172).

De Paola V, Holtmaat A, Knott G, Song S, Wilbrecht L, Caroni P, and Svoboda K (2006) Cell Type-Specific Structural Plasticity of Axonal Branches and Boutons in the Adult Neocortex. *Neuron*, 49(6): 861-75.

De Strooper B Iwatsubo T, and Wolfe MS (2012) Presenilins and Gamma-Secretase: Structure, Function, and Role in Alzheimer Disease. *Cold Spring Harb Perspect Med* 2(1).

Demuro A, Mina E, Kayed R, Milton SC, Parker I, and Glabe CG (2005) Calcium Dysregulation and Membrane Disruption as a Ubiquitous Neurotoxic Mechanism of Soluble Amyloid Oligomers. *J Biol Chem* 280(17): 17294-300.

Deshpande A, Kawai H, Metherate R, Glabe CG, and Busciglio J (2009) A Role for Synaptic Zinc in Activity-Dependent Abeta Oligomer Formation and Accumulation at Excitatory Synapses. *J Neurosci* 29(13): 4004-15.

Dickerson BC, Salat DH, Greve DN, Chua EF, Rand-Giovannetti E, Rentz DM, Bertram L, Mullin K, Tanzi RE, Blacker D, Albert MS, and Sperling RA (2005) Increased Hippocampal Activation in Mild Cognitive Impairment Compared to Normal Aging and AD. *Neurology* 65(3): 404-11.

Dugan LL, Ali SS, Shekhtman G, Roberts AJ, Lucero J, Quick KL, and Behrens MM (2009) IL-6 Mediated Degeneration of Forebrain Gabaergic Interneurons and Cognitive Impairment in Aged Mice through Activation of Neuronal Nadph Oxidase. *PLoS One* 4(5): 13.

Elston GN, Rosa MG, and Calford MB(1996) Comparison of Dendritic Fields of Layer III Pyramidal Neurons in Striate and Extrastriate Visual Areas of the Marmoset: A Lucifer Yellow Intracellular Injection. *Cereb Cortex* 6(6): 807-13.

Emptage N, Bliss TV, and Fine A (1999) Single Synaptic Events Evoke NMDA Receptor-Mediated Release of Calcium from Internal Stores in Hippocampal Dendritic Spines. *Neuron* 22(1): 115-24.

Ekinci FJ, Malik KU, and Shea TB (1999) Activation of the L Voltage-Sensitive Calcium Channel by Mitogen-Activated Protein (MAP) Kinase Following Exposure of Neuronal Cells to Beta-Amyloid. MAP Kinase Mediates Beta-Amyloid-Induced Neurodegeneration. *J Biol Chem* 274(42): 30322-7.

Ferreiro E, Oliveira CR, and Pereira C (2004) Involvement of Endoplasmic Reticulum Ca^{2+} Release through Ryanodine and Inositol 1,4,5-Triphosphate

Receptors in the Neurotoxic Effects Induced by the Amyloid-Beta Peptide. *J Neurosci Res* 76(6): 872-80.

Feske S, Gwack Y, Prakriya M, S. Srikanth S, Puppel SH, Tanasa B, Hogan PG, Lewis RS, Daly M, and Rao A (2006) A Mutation in Orai1 Causes Immune Deficiency by Abrogating CRAC Channel Function. *Nature* 441(7090): 179-85.

Gabuzda, D., and B. A. Yankner (2013) Physiology: Inflammation Links Ageing to the Brain. *Nature* 497(7448): 197-8.

Galante M, and Marty A (2003) Presynaptic Ryanodine-Sensitive Calcium Stores Contribute to Evoked Neurotransmitter Release at the Basket Cell-Purkinje Cell Synapse. *J Neurosci* 23 (35): 11229-34.

Gao J, Yin D, Yao Y, Williams TD, and Squier TC (1998) Progressive Decline in the Ability of Calmodulin Isolated from Aged Brain to Activate the Plasma Membrane Ca-ATPase. *Biochemistry* 37(26): 9536-48.

Garaschuk O, Yaari Z, and Konnerth A (1997) Release and Sequestration of Calcium by Ryanodine-Sensitive Stores in Rat Hippocampal Neurones. *J Physiol* 502(1): 13-30.

Garaschuk O, Milos RI, and Konnerth A (2006) Targeted Bulk-Loading of Fluorescent Indicators for Two-Photon Brain Imaging *in vivo*. *Nat Protoc* 1(1): 380-6.

Garaschuk O, Milos RI, Grienberger C, Marandi N, Adelsberger H, and Konnerth A (2006) Optical Monitoring of Brain Function *in vivo*: From Neurons to Networks. *Pflugers Arch* 453(3): 385-96.

Garaschuk O (2013) Imaging Microcircuit Function in Healthy and Diseased Brain. *Exp Neurol* 242 : 41-9.

Ghosh A and Greenberg ME (1995) Calcium Signaling in Neurons: Molecular Mechanisms and Cellular Consequences. *Science* 268(5208): 239-47.

Giorgi C, Agnoletto C, Bononi A, Bonora M, De Marchi E, Marchi S, Missiroli S, Patergnani S, Poletti F, Rimessi A, Suski JM, Wieckowski MR, and Pinton P (2012) Mitochondrial Calcium Homeostasis as Potential Target for Mitochondrial Medicine. *Mitochondrion* 12(1): 77-85.

Godbout JP, Chen J, Abraham J, Richwine AF, Berg BM, Kelley KW, and Johnson RW (2005) Exaggerated Neuroinflammation and Sickness Behavior in Aged Mice Following Activation of the Peripheral Innate Immune System. *Faseb J* 19(10): 1329-31.

Goedert M, Klug A, and Crowther RA (2006) Tau Protein, the Paired Helical Filament and Alzheimer's Disease. *J Alzheimers Dis* 9(3): 195-207.

Gomez-Tortosa E, Barquero S, Baron M, Gil-Neciga E, Castellanos F, Zurdo M, Manzano S, Munoz DG, Jimenez-Huete A, Rabano A, Sainz MJ, Guerrero R, Gobernado I, Perez-Perez J, and Jimenez-Escrig A (2010) Clinical-Genetic Correlations in Familial Alzheimer's Disease Caused by Presenilin 1 Mutations. *J Alzheimers Dis* 19(3): 873-84.

Gomez-Villafuertes R, Mellstrom B, and Naranjo JR (2007) Searching for a Role of NCX/NCKX Exchangers in Neurodegeneration. *Mol Neurobiol* 35(2): 195-202.

Goussakov I, Miller MB, and Stutzmann GE (2010) NMDA-Mediated Ca^{2+} Influx Drives Aberrant Ryanodine Receptor Activation in Dendrites of Young Alzheimer's Disease Mice. *J Neurosci* 30(36): 12128-37.

Grassi F, Mileo AM, L. Monaco L, Punturieri A, Santoni A, and Eusebi F (1994) TNF-Alpha Increases the Frequency of Spontaneous Miniature Synaptic Currents in Cultured Rat Hippocampal Neurons. *Brain Res* 659(1-2): 226-30.

Green KN, Demuro A, Akbari Y, Hitt BD, Smith IF, Parker I, and LaFerla FM (2008) SERCA Pump Activity Is Physiologically Regulated by Presenilin and Regulates Amyloid Beta Production. *J Cell Biol* 181(7): 1107-16.

Grienberger C and Konnerth A (2012) Imaging Calcium in Neurons. *Neuron* 73(5): 862-85.

Grienberger C, Rochefort NL, Adelsberger H, Henning HA, Hill DN, Reichwald J, Staufenbiel M, and Konnerth A (2012) Staged Decline of Neuronal Function *in vivo* in an Animal Model of Alzheimer's Disease. *Nat Commun* 3(774).

Hensley K, Carney JM, Mattson MP, Aksenova M, Harris M, Wu JF, Floyd RA, and Butterfield DA (1994) A Model for Beta-Amyloid Aggregation and Neurotoxicity Based on Free Radical Generation by the Peptide: Relevance to Alzheimer Disease. *Proc Natl Acad Sci U S A* 91(8): 3270-4.

Hermes M, Eichhoff G, and Garaschuk O (2010) Intracellular Calcium Signalling in Alzheimer's Disease. *J Cell Mol Med* 14(1-2): 30-41.

Hirase H, Qian L, Bartho P, and Buzsaki G (2004) Calcium Dynamics of Cortical Astrocytic Networks *in vivo*. *PLoS Biol* 2(4): 13.

Ho A and Shen J (2011) Presenilins in Synaptic Function and Disease. *Trends Mol Med* 17(11): 617-24.

Hu S, Sheng WS, Ehrlich LC, Peterson PK, and Chao CC (2000) Cytokine Effects on Glutamate Uptake by Human Astrocytes. *Neuroimmunomodulation* 7(3): 153-9.

Inoue S (2008) In Situ Abeta Pores in AD Brain Are Cylindrical Assembly of Abeta Protofilaments. *Amyloid* 15(4): 223-33.

Jayadev S, Leverenz JB, Steinbart E, Stahl J, Klunk W, Yu CE, and Bird TD (2010) Alzheimer's Disease Phenotypes and Genotypes Associated with Mutations in Presenilin 2. *Brain* 133(4): 1143-54.

Jin H, Sanjo N, Uchihara T, Watabe K, St George-Hyslop P, Fraser PE, and Mizusawa H (2010) Presenilin-1 Holoprotein Is an Interacting Partner of Sarco Endoplasmic Reticulum Calcium-ATPase and Confers Resistance to Endoplasmic Reticulum Stress. *J Alzheimers Dis* 20(1): 261-73.

Jonas P, Racca C, Sakmann B, Seeburg PH, and Monyer H (1994) Differences in Ca^{2+} Permeability of AMPA-Type Glutamate Receptor Channels in Neocortical Neurons Caused by Differential GluR-B Subunit Expression. *Neuron* 12(6): 1281-9.

Jurgens HA and Johnson RW (2012) Dysregulated Neuronal-Microglial Cross-Talk During Aging, Stress and Inflammation. *Exp Neurol* 233(1): 40-8.

Kamenetz F, Tomita T, Hsieh H, Seabrook G, Borchelt D, Iwatsubo T, Sisodia S, and Mlinow R (2003) APP Processing and Synaptic Function. *Neuron* 37(6): 925-937.

Katayama TK, Imaizumi TK, Manabe T, Hitomi J, Kudo T, and Tohyama M (2004) Induction of Neuronal Death by ER Stress in Alzheimer's Disease. *J Chem Neuroanat* 28(1-2): 67-78.

Keller JN, Guo Q, Holtsberg FW, Bruce-Keller AJ, and Mattson MP (1998) Increased Sensitivity to Mitochondrial Toxin-Induced Apoptosis in Neural Cells Expressing Mutant Presenilin-1 Is Linked to Perturbed Calcium Homeostasis and Enhanced Oxyradical Production. *J Neurosci* 18(12): 4439-50.

Khachaturian ZS (1989) Calcium, Membranes, Aging, and Alzheimer's Disease. Introduction and Overview. *Ann N Y Acad Sci* 568: 1-4.

Kleizen B and Braakman I (2004) Protein Folding and Quality Control in the Endoplasmic Reticulum. *Curr Opin Cell Biol* 16(4): 343-9.

Kolarova, M., F. Garcia-Sierra, A. Bartos, J. Ricny, and D. Ripova (2012) Structure and Pathology of Tau Protein in Alzheimer Disease. *Int J Alzheimers Dis* 731526(10): 29.

Korkotian E and Segal M (1998) Fast Confocal Imaging of Calcium Released from Stores in Dendritic Spines. *Eur J Neurosci* 10(6): 2076-84.

Kuchibhotla KV, Goldman ST, Lattarulo CR, Wu HY, Hyman BT, and Bacskai BJ (2008) Abeta Plaques Lead to Aberrant Regulation of Calcium Homeostasis *in vivo* Resulting in Structural and Functional Disruption of Neuronal Networks. *Neuron* 59(2): 214-25.

Kunz PA, Roberts AC, and Philpot BD (2013) Presynaptic NMDA Receptor Mechanisms for Enhancing Spontaneous Neurotransmitter Release. *J Neurosci* 33(18): 7762-9.

LaFerla FM (2002) Calcium Dyshomeostasis and Intracellular Signalling in Alzheimer's Disease. *Nat Rev Neurosci* 3(11): 862-72.

Leissring MA, Paul BA, Parker I, Cotman CW, and LaFerla FM (1999a) Alzheimer's Presenilin-1 Mutation Potentiates Inositol 1,4,5-Trisphosphate-Mediated Calcium Signaling in Xenopus Oocytes. *J Neurochem* 72(3): 1061-8.

Leissring MA, Parker I, and LaFerla FM (1999b) Presenilin-2 Mutations Modulate Amplitude and Kinetics of Inositol 1, 4,5-Trisphosphate-Mediated Calcium Signals. *J Biol Chem* 274(46): 32535-8.

Leissring MA, Akbari Y, Fanger CM, Cahalan MD, Mattson MP, and LaFerla FM (2000) Capacitative Calcium Entry Deficits and Elevated Luminal Calcium Content in Mutant Presenilin-1 Knockin Mice. *J Cell Biol* 149(4): 793-8.

Liang L and Wei H (2015) Dantrolene, a Treatment for Alzheimer Disease? *Alzheimer Dis Assoc Disord* 29(1): 1-5.

Liou J, Fivaz M, Inoue T, and Meyer T (2007) Live-Cell Imaging Reveals Sequential Oligomerization and Local Plasma Membrane Targeting of Stromal Interaction Molecule 1 after Ca^{2+} Store Depletion. *Proc Natl Acad Sci U S A* 104(22): 9301-6.

Liou J, Kim ML, Heo WD, Jones JT, Myers JW, Ferrell JE, and Meyer T (2005) STIM Is a Ca^{2+} Sensor Essential for Ca^{2+}-Store-Depletion-Triggered Ca^{2+} Influx. *Curr Biol* 15(13): 1235-41.

Llano I, Gonzalez J, Caputo C, Lai FA, Blayney LM, Tan YP, and Marty A (2000) Presynaptic Calcium Stores Underlie Large-Amplitude Miniature IPSCs and Spontaneous Calcium Transients. *Nat Neurosci* 3(12): 1256-65.

Mak DO and Foskett JK (2015) Inositol 1,4,5-Trisphosphate Receptors in the Endoplasmic Reticulum: A Single-Channel Point of View. *Cell Calcium* 58(1): 67-78.

Manita S and Ross WN (2009) Synaptic Activation and Membrane Potential Changes Modulate the Frequency of Spontaneous Elementary Ca^{2+} Release Events in the Dendrites of Pyramidal Neurons. *J Neurosci* 29(24): 7833-45.

Mann DM, Pickering-Brown SM, Takeuchi A, and Iwatsubo T (2001) Amyloid Angiopathy and Variability in Amyloid Beta Deposition Is Determined by Mutation Position in Presenilin-1-Linked Alzheimer's Disease. *Am J Pathol* 158(6): 2165-75.

Mattson MP (2004) Metal-Catalyzed Disruption of Membrane Protein and Lipid Signaling in the Pathogenesis of Neurodegenerative Disorders. *Ann N Y Acad Sci* : 37-50.

Mattson MP (2007) Calcium and Neurodegeneration. *Aging Cell* 6(3): 337-50.

Mattson MP (2010) ER Calcium and Alzheimer's Disease: In a State of Flux. *Sci Signal* 3(114).

Mayeux R (2003) Epidemiology of Neurodegeneration. *Annu Rev Neurosci* 26: 81-104.

Mayeux R and Stern Y (2012) Epidemiology of Alzheimer disease. *Cold Spring Harb Perspect Med* 2.

McGuinness L, Taylor C, Taylor RD, Yau C, Langenhan T, Hart ML, Christian H, P. W. Tynan PW, P. Donnelly P, and N. J. Emptage NJ (2010) Presynaptic NMDARs in the Hippocampus Facilitate Transmitter Release at Theta Frequency. *Neuron* 68(6): 1109-27.

Mellstrom B and Naranjo JR (2001) Mechanisms of Ca^{2+}-Dependent Transcription. *Curr Opin Neurobiol* 11(3): 312-9.

Minkeviciene R, Rheims S, Dobszay MB, Zilberter M, Hartikainen J, Fulop L, B. Penke, Zilberter Y, Harkany T, Pitkanen A, and Tanila H (2009) Amyloid Beta-Induced Neuronal Hyperexcitability Triggers Progressive Epilepsy. *J Neurosci* 29(11): 3453-62.

Moehlmann T, Winkler E, Xia X, Edbauer D, Murrell J, Capell A, Kaether C, Zheng H, Ghetti B, Haass C, and Steiner H (2002) Presenilin-1 Mutations of Leucine 166 Equally Affect the Generation of the Notch and APP Intracellular Domains Independent of Their Effect on Abeta 42 Production. *Proc Natl Acad Sci U S A* 99(12): 8025-30.

Moyer JR Jr, Furtak SC, McGann JP, and Brown TH (2011) Aging-Related Changes in Calcium-Binding Proteins in Rat Perirhinal Cortex. *Neurobiol Aging* 32(9): 1693-706.

Muehlschlegel S and Sims JR (2012) Dantrolene: Mechanisms of Neuroprotection and Possible Clinical Applications in the Neurointensive Care Unit. *Neurocrit Care* 10(1): 103-15.

Nelson O, Tu H, Lei T, Bentahir M, De Strooper B, and Bezprozvanny I (2007) Familial Alzheimer Disease-Linked Mutations Specifically Disrupt Ca^{2+} Leak Function of Presenilin 1. *J Clin Invest* 117(5): 1230-9.

Nelson O, Supnet C, Liu H, and Bezprozvanny I (2010) Familial Alzheimer's Disease Mutations in Presenilins: Effects on Endoplasmic Reticulum Calcium

Homeostasis and Correlation with Clinical Phenotypes. *J Alzheimers Dis* 21(3): 781-93.

Nevian T and Helmchen F (2007) Calcium Indicator Loading of Neurons Using Single-Cell Electroporation. *Pflugers Arch* 454(4): 675-88.

Nosyreva E and Kavalali ET (2010) Activity-Dependent Augmentation of Spontaneous Neurotransmission During Endoplasmic Reticulum Stress. *J Neurosci* 30(21): 7358-68.

Oddo S, Caccamo A, Shepherd JD, Murphy MP, Golde TE, Kayed R, Metherate R, Mattson MP, Akbari Y, and LaFerla FM (2003) Triple-Transgenic Model of Alzheimer's Disease with Plaques and Tangles: Intracellular Abeta and Synaptic Dysfunction. *Neuron* 39 (3): 409-21.

Oules B, Del Prete D, Greco B, Zhang X, Lauritzen I, Sevalle J, Moreno S, Paterlini-Brechot P, Trebak M, Checler F, Benfenati F, and Chami M (2012) Ryanodine Receptor Blockade Reduces Amyloid-Beta Load and Memory Impairments in Tg2576 Mouse Model of Alzheimer Disease. *J Neurosci* 32(34): 11820-34.

Palop JJ, Chin J, Roberson ED, Wang J, Thwin MT, Bien-Ly N, Yoo J, Ho KO, Yu GQ, Kreitzer A, Finkbeiner S, Noebels JL, and Mucke L (2007) Aberrant Excitatory Neuronal Activity and Compensatory Remodeling of Inhibitory Hippocampal Circuits in Mouse Models of Alzheimer's Disease. *Neuron* 55(5): 697-711.

Palop JJ and Mucke L (2009) Epilepsy and Cognitive Impairments in Alzheimer Disease. *Arch Neurol* 66(4): 435-40.

Peng J, Liang G, S. Inan S, Wu Z, Joseph DJ, Meng Q, Peng Y, Eckenhoff MF, and Wei H (2012) Dantrolene Ameliorates Cognitive Decline and Neuropathology in Alzheimer Triple Transgenic Mice. *Neurosci Lett* 516(2): 274-9.

Phillis JW and O'Regan MH (2004) A Potentially Critical Role of Phospholipases in Central Nervous System Ischemic, Traumatic, and Neurodegenerative Disorders. *Brain Res Brain Res Rev* 44(1): 13-47.

Pollard HB, Rojas E, and Arispe N (1993) A New Hypothesis for the Mechanism of Amyloid Toxicity, Based on the Calcium Channel Activity of Amyloid Beta Protein (A beta P) in Phospholipid Bilayer Membranes. *Ann N Y Acad Sci* 695: 165-8.

Popescu BO, Cedazo-Minguez A, Benedikz E, Nishimura T, Winblad B, Ankarcrona M, and Cowburn RF (2004) Gamma-Secretase Activity of Presenilin 1 Regulates Acetylcholine Muscarinic Receptor-Mediated Signal Transduction. *J Biol Chem* 279(8): 6455-64.

Putcha D, Brickhouse M, O'Keefe K, Sullivan C, Rentz D, Marshall G, Dickerson B, and Sperling R (2011) Hippocampal Hyperactivation Associated with Cortical Thinning in Alzheimer's Disease Signature Regions in Non-Demented Elderly Adults. *J Neurosci* 31(48): 17680-8.

Querfurth HW and Selkoe DJ (1994) Calcium Ionophore Increases Amyloid Beta Peptide Production by Cultured Cells. *Biochemistry* 33(15): 4550-61.

Quist A, Doudevski I, Lin H, Azimova R, D. Ng D, Frangione B, Kagan B, Ghiso J, and Lal R (2005) Amyloid Ion Channels: A Common Structural Link for Protein-Misfolding Disease. *Proc Natl Acad Sci U S A* 102(30): 10427-32.

Ramirez OA and Couve A (2011) The Endoplasmic Reticulum and Protein Trafficking in Dendrites and Axons. *Trends Cell Biol* 21(4): 219-27.

Rizzuto R, De Stefani D, Raffaello A, and Mammucari C (2012) Mitochondria as Sensors and Regulators of Calcium Signalling. *Nat Rev Mol Cell Biol* 13(9): 566-78.

Roberson ED, Scearce-Levie K, Palop JJ, Yan F, Cheng IH, Wu T, Gerstein H, Yu GQ, and Mucke L (2007) Reducing Endogenous Tau Ameliorates Amyloid Beta-Induced Deficits in an Alzheimer's Disease Mouse Model. *Science* 316(5825): 750-4.

Roberson ED, Halabisky B, Yoo JW, Yao J, Chin J, Yan F, Wu T, Hamto P, Devidze N, Yu GQ, Palop JJ, Noebels JL, and Mucke L (2011) Amyloid-Beta/Fyn-Induced Synaptic, Network, and Cognitive Impairments Depend on Tau Levels in Multiple Mouse Models of Alzheimer's Disease. *J Neurosci* 31(2): 700-11.

Roos JP, DiGregorio J, Yeromin AV, Ohlsen K, Lioudyno M, Zhang S, Safrina O, Kozak JA, Wagner SL, Cahalan MD, Velicelebi G, and Stauderman KA (2005) STIM1, an Essential and Conserved Component of Store-Operated Ca^{2+} Channel Function. *J Cell Biol* 169(3): 435-45.

Ross WN (2012) Understanding Calcium Waves and Sparks in Central Neurons. *Nat Rev Neurosci* 13(3): 157-68.

Salminen A, Kauppinen A, Suuronen T, Kaarniranta K, and Ojala J (2009) ER Stress in Alzheimer's Disease: A Novel Neuronal Trigger for Inflammation and Alzheimer's Pathology. *J Neuroinflammation* 6(41): 1742-2094.

Sanchez PE, Zhu L, Verret L, Vossel KA, Orr AG, Cirrito JR, Devidze N, Ho K, Yu GQ, Palop JJ, and Mucke L (2012) Levetiracetam Suppresses Neuronal Network Dysfunction and Reverses Synaptic and Cognitive Deficits in an Alzheimer's Disease Model. *Proc Natl Acad Sci U S A* 109(42): 6.

Sandler VM and Barbara JG (1999) Calcium-Induced Calcium Release Contributes to Action Potential-Evoked Calcium Transients in Hippocampal CA1 Pyramidal Neurons. *J Neurosci* 19(11): 4325-36.

Scharfman HE (2012) Untangling Alzheimer's Disease and Epilepsy. *Epilepsy Curr* 12(5): 178-83.

Schneider I, Reverse D, Dewachter I, Ris L, Caluwaerts N, Kuiperi C, Gilis M, Geerts H, Kretzschmar H, Godaux E, Moechars D, Van Leuven F, and Herms J (2001) Mutant Presenilins Disturb Neuronal Calcium Homeostasis in the Brain of Transgenic Mice, Decreasing the Threshold for Excitotoxicity and Facilitating Long-Term Potentiation. *J Biol Chem* 276(15): 11539-44.

Schwaller B (2010) Cytosolic Ca^{2+} Buffers. *Cold Spring Harb Perspect Biol* 2(11): 13.

Selkoe DJ (2004) Cell Biology of Protein Misfolding: The Examples of Alzheimer's and Parkinson's Diseases. *Nat Cell Biol* 6(11): 1054-61.

Selkoe DJ (2013) The Therapeutics of Alzheimer's Disease: Where We Stand and Where We Are Heading. *Ann Neurol* 74(3): 328-36.

Shankar GM, Li S, Mehta TH, Garcia-Munoz A, Shepardson NE, Smith I, Brett FM, Farrell MA, Rowan MJ, Lemere CA, Regan CM, Walsh DM, Sabatini BL, and Selkoe DJ (2008) Amyloid-Beta Protein Dimers Isolated Directly from Alzheimer's Brains Impair Synaptic Plasticity and Memory. *Nat Med* 14(8): 837-42.

Shenoda B (2015) The Role of Na^{+}/Ca^{2+} Exchanger Subtypes in Neuronal Ischemic Injury. *Transl Stroke Res* 6(3): 181-90.

Sheng M, Sabatini BL, Südhof T (2012) Synapses and Alzheimer's Disease. Cold Spring Harb Persepct Biol 4(5): 1-17.

Shepherd GM, Raastad M, and Andersen P (2002) General and Variable Features of Varicosity Spacing Along Unmyelinated Axons in the Hippocampus and Cerebellum. *Proc Natl Acad Sci U S A* 99(9): 6340-5.

Shepherd GM, Stepanyants A, Bureau I, Chklovskii D, and Svoboda K (2005) Geometric and Functional Organization of Cortical Circuits. *Nat Neurosci* 8(6): 782-90.

Shi JQ, Wang BR, Tian YY, Xu J, Gao L, Zhao SL, Jiang T, Xie HG, and Zhang YD (2013) Antiepileptics Topiramate and Levetiracetam Alleviate Behavioral Deficits and Reduce Neuropathology in APPswe/PS1dE9 Transgenic Mice. *CNS Neurosci Ther* 19(11): 871-81.

Simkin D, Hattori S, Ybarra N, Musial TF, Buss EW, Richter H, Oh MM, Nicholson DA, and Disterhoft JF (2015) Aging-Related Hyperexcitability in CA3

Pyramidal Neurons Is Mediated by Enhanced a-Type K^+ Channel Function and Expression. *J Neurosci* 35(38): 13206-18.

Simkus CR and Stricker C (2002) The Contribution of Intracellular Calcium Stores to mEPSCs Recorded in Layer II Neurones of Rat Barrel Cortex. *J Physiol* 545(2): 521-35.

Smith IF, Hitt B, Green KN, S. Oddo S, and LaFerla FM (2005) Enhanced Caffeine-Induced Ca^{2+} Release in the 3xTg-AD Mouse Model of Alzheimer's Disease. *J Neurochem* 94(6): 1711-8.

Snyder EM, Nong Y, Almeida CG, Paul S, Moran T, Choi EY, Nairn AC, Salter MW, Lombroso PJ, Gouras GK, and Greengard P (2005) Regulation of Nmda Receptor Trafficking by Amyloid-Beta. *Nat Neurosci* 8(8): 1051-8.

Sperling RA, Dickerson BC, Pihlajamaki M, Vannini P, LaViolette PS, Vitolo OV, Hedden T, Becker JA, Rentz DM, Selkoe DJ, and Johnson KA (2010) Functional Alterations in Memory Networks in Early Alzheimer's Disease. *Neuromolecular Med* 12(1): 27-43.

Spruston N (2008) Pyramidal Neurons: Dendritic Structure and Synaptic Integration. *Nat Rev Neurosci* 9(3): 206-21.

Stellwagen DE, Beattie C, Seo JY, and Malenka RC (2005) Differential Regulation of AMPA Receptor and GABA Receptor Trafficking by Tumor Necrosis Factor-Alpha. *J Neurosci* 25(12): 3219-28.

Stettler DD, Yamahachi H, Li W, Denk W, and Gilbert CD (2006) Axons and Synaptic Boutons Are Highly Dynamic in Adult Visual Cortex. *Neuron* 49(6): 877-87.

Stosiek C, Garaschuk O, Holthoff K, and Konnerth A (2003) *In vivo* Two-Photon Calcium Imaging of Neuronal Networks. *Proc Natl Acad Sci U S A* 100(12): 7319-24.

Stranahan AM and Mattson MP (2012) Recruiting Adaptive Cellular Stress Responses for Successful Brain Ageing. *Nat Rev Neurosci* 13(3): 209-16.

Strehler EE, Caride AJ, Filoteo AG, Xiong Y, Penniston JT, and Enyedi A. (2007) Plasma Membrane Ca^{2+} ATPases as Dynamic Regulators of Cellular Calcium Handling. *Ann N Y Acad Sci*: 226-36.

Stutzmann GE, LaFerla FM, and Parker I (2003) Ca^{2+} Signaling in Mouse Cortical Neurons Studied by Two-Photon Imaging and Photoreleased Inositol Triphosphate. *J Neurosci* 23(3): 758-65.

Stutzmann GE, Caccamo A, LaFerla FM, and Parker I (2004) Dysregulated IP3 Signaling in Cortical Neurons of Knock-in Mice Expressing an Alzheimer's-

Linked Mutation in Presenilin1 Results in Exaggerated Ca^{2+} Signals and Altered Membrane Excitability. *J Neurosci* 24(2): 508-13.

Stutzmann GE, Smith I, Caccamo A, Oddo S, Laferla FM, and Parker I (2006) Enhanced Ryanodine Receptor Recruitment Contributes to Ca^{2+} Disruptions in Young, Adult, and Aged Alzheimer's Disease Mice. *J Neurosci* 26(19): 5180-9.

Stutzmann GE and Mattson MP (2011) Endoplasmic Reticulum Ca^{2+} Handling in Excitable Cells in Health and Disease. *Pharmacol Rev* 63(3): 700-27.

Sun, X., V. Beglopoulos, M. P. Mattson, and J. Shen (2005). Hippocampal Spatial Memory Impairments Caused by the Familial Alzheimer's Disease-Linked Presenilin 1 M146v Mutation *Neurodegener Dis* 2 (1): 6-15.

Sun S, Zhang H, Liu J, Popugaeva E, Xu NJ, Feske S, White CL, and Bezprozvanny I (2014) Reduced Synaptic STIM2 Expression and Impaired Store-Operated Calcium Entry Cause Destabilization of Mature Spines in Mutant Presenilin Mice. *Neuron* 82(1): 79-93.

Supnet C, Grant J, Kong H, Westaway D, and Mayne M (2006) Amyloid-Beta-(1-42) Increases Ryanodine Receptor-3 Expression and Function in Neurons of TgCRND8 Mice. *J Biol Chem* 281(50): 38440-7.

Supnet C and Bezprozvanny I (2010) The Dysregulation of Intracellular Calcium in Alzheimer Disease. *Cell Calcium* 47(2): 183-9.

Supnet C, Noonan C, Richard K, Bradley J, and Mayne M (2010) Up-Regulation of the Type 3 Ryanodine Receptor Is Neuroprotective in the TgCRND8 Mouse Model of Alzheimer's Disease. *J Neurochem* 112(2): 356-65.

Tabaton M and Tamagno E (2007) The Molecular Link between Beta- and Gamma-Secretase Activity on the Amyloid Beta Precursor Protein. *Cell Mol Life Sci* 64(17): 2211-8.

Takasugi N, Tomita T, Hayashi I, Tsuruoka M, Niimura M, Takahashi Y, Thinakaran G, and Iwatsubo T (2003) The Role of Presenilin Cofactors in the Gamma-Secretase Complex. *Nature* 422(6930): 438-41.

Toescu EC and Verkhratsky A (2006) Parameters of Calcium Homeostasis in Normal Neuronal Ageing. *J Anat* 4: 563-9.

Thomson AM and Bannister AP (2003) Interlaminar Connections in the Neocortex. *Cereb Cortex* 13(1): 5-14.

Tu H, Nelson O, Bezprozvanny A, Wang Z, Lee SF, Hao YH, Serneels L, De Strooper B, Yu G, and I. Bezprozvanny I (2006) Presenilins Form ER Ca^{2+} Leak Channels, a Function Disrupted by Familial Alzheimer's Disease-Linked Mutations. *Cell* 126(5): 981-93.

Uttara B, Singh AV, Zamboni P, and Mahajan RT (2009) Oxidative Stress and Neurodegenerative Diseases: A Review of Upstream and Downstream Antioxidant Therapeutic Options. *Curr Neuropharmacol* 7(1): 65-74.

Velez-Pardo C, Arellano JI, Cardona-Gomez P, Jimenez Del Rio M, Lopera F, and De Felipe J (2004) CA1 Hippocampal Neuronal Loss in Familial Alzheimer's Disease Presenilin-1 E280a Mutation Is Related to Epilepsy. *Epilepsia* 45(7): 751-6.

Verkhratsky A and Petersen OH (2002) The Endoplasmic Reticulum as an Integrating Signalling Organelle: From Neuronal Signalling to Neuronal Death. *Eur J Pharmacol* 447(2-3): 141-54.

Viviani B, Bartesaghi S, Gardoni F, Vezzani A, Behrens MM, Bartfai T, Binaglia M, Corsini E, Di Luca M, Galli CL, and M. Marinovich M (2003) Interleukin-1beta Enhances NMDA Receptor-Mediated Intracellular Calcium Increase through Activation of the Src Family of Kinases. *J Neurosci* 23(25): 8692-700.

Wang R, Dineley KT, Sweatt JD, and Zheng H (2004) Presenilin 1 Familial Alzheimer's Disease Mutation Leads to Defective Associative Learning and Impaired Adult Neurogenesis. *Neuroscience* 126 (2): 305-12.

Wang Y and Mandelkow E (2016) Tau in Physiology and Pathology. *Nat Rev Neurosci* 17(1): 22- 35.

Walsh DM, Klyubin I, Fadeeva JV, Cullen WK, Anwyl R, Wolfe MS, Rowan MJ, and Selkoe DJ (2002) Naturally secreted oligomers of amyloid β protein potently inhibit hippocampal long-term potentiation *in vivo*. *Nature* 416(6880): 535-539.

Wheeler D, Knapp E, Bandaru VV, Wang Y, Knorr D, Poirier C, Mattson MP, Geiger JD, and N. J. Haughey (2009) Tumor Necrosis Factor-Alpha-Induced Neutral Sphingomyelinase-2 Modulates Synaptic Plasticity by Controlling the Membrane Insertion of NMDA Receptors. *J Neurochem* 109(5): 1237-49.

Wilson IA, Ikonen S, Gallagher M, Eichenbaum H, and Tanila H (2005) Age-Associated Alterations of Hippocampal Place Cells Are Subregion Specific. *J Neurosci* 25(29): 6877-86.

Xia D, Watanabe H, Wu B, Lee SH, Li Y, Tsvetkov E, Bolshakov VY, Shen J, and Kelleher RJ (2015) Presenilin-1 Knockin Mice Reveal Loss-of-Function Mechanism for Familial Alzheimer's Disease. *Neuron* 85(5): 967-81.

Yamamoto K, Tanei Z, Hashimoto T, Wakabayashi T, Okuno H, Naka Y, Yizhar O, Fenno LE, Fukayama M, Bito H, Cirrito JR, Holtzman DM, Deisseroth K, and Iwatsubo T (2015) Chronic Optogenetic Activation Augments Abeta Pathology in a Mouse Model of Alzheimer Disease. *Cell Rep* 11(6): 859-65.

Yassa MA, Stark SM, Bakker A, Albert MS, Gallagher M, and Stark CE (2010) High- Resolution Structural and Functional MRI of Hippocampal CA3 and Dentate Gyrus in Patients with Amnestic Mild Cognitive Impairment. *Neuroimage* 51(3): 1242-52.

Ye ZC and Sontheimer H (1996) Cytokine Modulation of Glial Glutamate Uptake: A Possible Involvement of Nitric Oxide. *Neuroreport* 7(13): 2181-5.

Yiannopoulou KG and Papageorgiou SG (2013) Current and Future Treatments for Alzheimer's Disease. *Ther Adv Neurol Disord* 6(1): 19-33.

Yoo AS, Cheng I, Chung S, Grenfell TZ, Lee H, Pack-Chung E, Handler M, Shen J, Xia W, Tesco G, Saunders AJ, Ding K, Frosch MP, Tanzi RE, and Kim TW (2000) Presenilin-Mediated Modulation of Capacitative Calcium Entry. *Neuron* 27(3): 561-72.

Yuan P and Grutzendler J (2016) Attenuation of Beta-Amyloid Deposition and Neurotoxicity by Chemogenetic Modulation of Neural Activity. *J Neurosci* 36(2): 632-41.

Zaidi A, Gao J, Squier TC, and Michaelis ML (1998) Age-Related Decrease in Brain Synaptic Membrane Ca^{2+}-ATPase in F344/BNF1 Rats. *Neurobiol Aging* 19(5): 487-95.

Zaidi A and Michaelis ML (1999) Effects of Reactive Oxygen Species on Brain Synaptic Plasma Membrane Ca^{2+}-ATPase. *Free Radic Biol Med* 27(7-8): 810-21.

Zaidi A (2010) Plasma membrane Ca^{2+}- ATPases: Targets of oxidative stress in brain aging and neurodegeneration. *World j Biol Chem* 1(9): 271-280.

Zeng LH, Xu L, Rensing NR, Sinatra PM, Rothman SM, and Wong M (2007) Kainate Seizures Cause Acute Dendritic Injury and Actin Depolymerization *in vivo*. *J Neurosci* 2(43): 11604-13.

Zhang H, Sun S, Herreman A, De Strooper B, and Bezprozvanny I (2010) Role of Presenilins in Neuronal Calcium Homeostasis. *J Neurosci* 30(25): 8566-80.

Zhang SL, Yeromin AV, Zhang XH, Yu Y, Safrina O, Penna A, Roos J, Stauderman KA, and Cahalan MD (2006) Genome-Wide RNAi Screen of Ca^{2+} Influx Identifies Genes That Regulate Ca^{2+} Release-Activated Ca^{2+} Channel Activity. *Proc Natl Acad Sci U S A* 103(24): 9357-62.

Zhang XZ, Li XJ, and Zhang HY (2010) Valproic Acid as a Promising Agent to Combat Alzheimer's Disease. *Brain Res Bull* 81(1): 3-6.

Ziyatdinova S, Gurevicius K, Kutchiashvili N, Bolkvadze T, Nissinen J, Tanila H, and Pitkanen A (2011) Spontaneous Epileptiform Discharges in a Mouse

Model of Alzheimer's Disease Are Suppressed by Antiepileptic Drugs That Block Sodium Channels. *Epilepsy Res* 94(1-2): 75-85.